University of Southampton

Faculty of Engineering and Physical Sciences

School of Chemistry

Biochemical Studies of the Radical SAM Enzyme HydG

by

Nicola Claire Yaxley

Thesis for the degree of Master of Philosophy

January 2022

University of Southampton

Abstract

Faculty of Engineering and Physical Sciences

School of Chemistry

Master of Philosophy

Biochemical Studies of the Radical SAM Enzyme HydG

by

Nicola Claire Yaxley

Radical SAM (RSAM) enzymes are a large family of enzymes which catalyse the reductive cleavage of S-adenosylmethionine, bound at the unique iron of a [4Fe-4S] cluster, to generate a highly reactive deoxyadenosyl radical. This highly reactive intermediate abstracts a hydrogen atom from a substrate to initiate a diverse range of radical mechanisms.

RSAM enzymes are responsible for the formation of many organic cofactors, nucleic acid modification, such as methylation of aromatic carbon centres, formation of antibiotics, DNA dimer repair/isomerisation and metallocofactor assembly in the maturation of [FeFe]-hydrogenase enzymes. RSAM enzymes share structural similarities, such as a C-terminal [4Fe-4S] cluster, coordinated by three protein derived cysteine residues (denoted by the CxxxCxxC sequence motif) and at the active site a triose-phosphate isomerase barrel fold. Despite the many thousands of RSAM enzyme sequences, comparatively few have been characterised and the majority possess unknown structures and functions.

This project aims to further characterise the RSAM enzyme HydG, one of three maturase enzymes involved in the assembly of the [FeFe] hydrogenase H-cluster. HydG is the most investigated of the maturase enzymes with its substrates and structure well resolved, the product of HydG, proposed to be a $[Fe^{II}(CO)_2(CN)Cys]^-$ metallosynthon has been observed spectroscopically bound to the enzyme auxiliary cluster, and synthesised to become an active substrate of HydE but not been characterised upon release from HydG. In this work *Thermoanaerobacter italicus* derived HydG has been heterologously expressed, purified, and chemically reconstituted to produce active enzyme. HydG activity assays have been optimised and co-crystallisation screening experiments explored.

Table of Contents

Table of Tables

Table of Figures

Research Thesis: Declaration of Authorship

Print name: Nicola Claire Yaxley

Title of thesis: Biochemical Studies of the Radical SAM Enzyme HydG

I declare that this thesis and the work presented in it are my own and has been generated by me as the result of my own original research.

I confirm that:

1. This work was done wholly or mainly while in candidature for a research degree at this University;
2. Where any part of this thesis has previously been submitted for a degree or any other qualification at this University or any other institution, this has been clearly stated;
3. Where I have consulted the published work of others, this is always clearly attributed;
4. Where I have quoted from the work of others, the source is always given. With the exception of such quotations, this thesis is entirely my own work;
5. I have acknowledged all main sources of help;
6. Where the thesis is based on work done by myself jointly with others, I have made clear exactly what was done by others and what I have contributed myself;
7. None of this work has been published before submission

Signature: Date:

Acknowledgements

First, I would like to thank my supervisor Prof Peter Roach for giving me the opportunity to take on this challenging and interesting project, and for your infectious enthusiasm, and support along this rather bumpy road. I've gained a lot of experiences which I'm truly grateful for.

A huge thank you to Dr Matthias Baud, you're support over the final few months of this project was sincerely appreciated.

A special thank you to Dr Josh Prince for introducing me to the lab, your patience, wisdom, and support. Big thanks to my lab buddy Dr David Wheatley for the mental support and pragmatism. I'd like to thank Dr Khaled Mohammed and the Tavassoli group for your patience and practical help. I would also like to thank Dr Lukas Karst (University of Freiburg) your visit and practical support proved invaluable to the progress of this project. I'd like to thank summer student Roshny Saji, your motivation, hard work and cheerfulness really helped focus parts of this project.

Thanks also goes to Aran Amin, Sam Forbes, Jake Lawrie-Ashton, Jo Fish and Josh Prince for excessive tea breaks and group therapy.

Last but by no means least, I'd like to thank my partner Tom for your endless support, kindness, humour, and pep talks during times of doubt. It's been a difficult time, but I wouldn't want to have shared it with anyone else. A final thanks go to Ted, the greatest emotional support dog/best friend around.

Definitions and Abbreviations

BioB	Biotin synthase
C.hydrogenoformans	*Carboxudothermus hydrogenoformans*
Cys	Cysteine
DI	Deionised
DOA	5'-Deoxyadenosine
DTT	Dithiothreitol
E.coli	*Escherichia coli*
ENDOR	Electron-nuclear double resonance
EPR	Electron paramagnetic resonance
EXAFS	Extended X-ray absorption fine structure
FTIR	Fourier transform infrared spectroscopy
His	Histidine
HSL	Homoserine lactone
QM	Quantum mechanical
LAM	Lysine-2,3-aminomutase
LipA	Lipoyl synthase
Met	Methionine
MM	Molecular mechanical
MTA	5'-methylthioadenosine
MTAN	5'-methylthioadenosine nucleosidase
MTR	5'-methylthioribose
NADPH	Nicotinamide adenine dinucleotide phosphate
NrdG	Anaerobic ribonucleotide reductase
p-cresol	*Para*-cresol
PEG	Polyethylene glycol
RSAM	Radical SAM
SAH	*S*-adenosyl-L-homocysteine
SAM	S-adenosyl methionine
TIM	Triose phosphate isomerase
ThiH	Tyrosine lyase
Ti	*Thermoanaerobacter italicus*
Txy	*Thermoanaerobacterium xylanolyticum*
Tl	*Thermotoga lettingae*
Tmar	*Thermotoga maritima*
UV-vis	Ultraviolet-visible
XAS	X-ray absorption spectroscopy

Chapter 1 Introduction

1.1 Radical SAM Superfamily

1.1.1 Discovery of the Radical SAM Superfamily

S-adenosyl methionine (SAM) was first described as a catalytic substrate in 1965, for the enzyme pyruvate formate-lyase (PFL-AE) [1, 2]. Another early SAM utilising enzyme described is lysine-2,3-aminomutase (LAM) [3]. Early LAM experiments involving catalysis of radiolabelled SAM identified the substrate as the source of a highly reactive 5'-deoxyadenosine (DOA) radical [4], which is transferred to a metal cofactor [5]. It was noted in these works the similarity between this mechanism and the role of the adenosyl cobalamin derived DOA radical in B_{12}-coenzyme dependent catalysis [4, 6]. Fe^{2+} and S^{2-} dependent activity of Radical SAM (RSAM) enzymes was also first observed in activity assays of LAM and the presence of Fe-S clusters as electron transfer cofactors proposed [7].

In the 1990's studies on a number of enzymes were published, the enzymes described catalysed diverse reactions, but all had two cofactors in common; SAM and Fe-S clusters. A review of these observations was published in 2001 by Cheek and Broderick, first identifying this emerging group of SAM dependent Fe-S enzymes [2, 8].

The first 5 RSAM enzymes to be grouped containing Fe-S clusters were PFL-AE, LAM, biotin synthase (BioB), lipoic acid synthase (LipA), and anaerobic ribonucleotide reductase (NrdG) [2, 8, 9]. The reaction mechanisms catalysed by these enzymes is shown below in Figure 1.1.

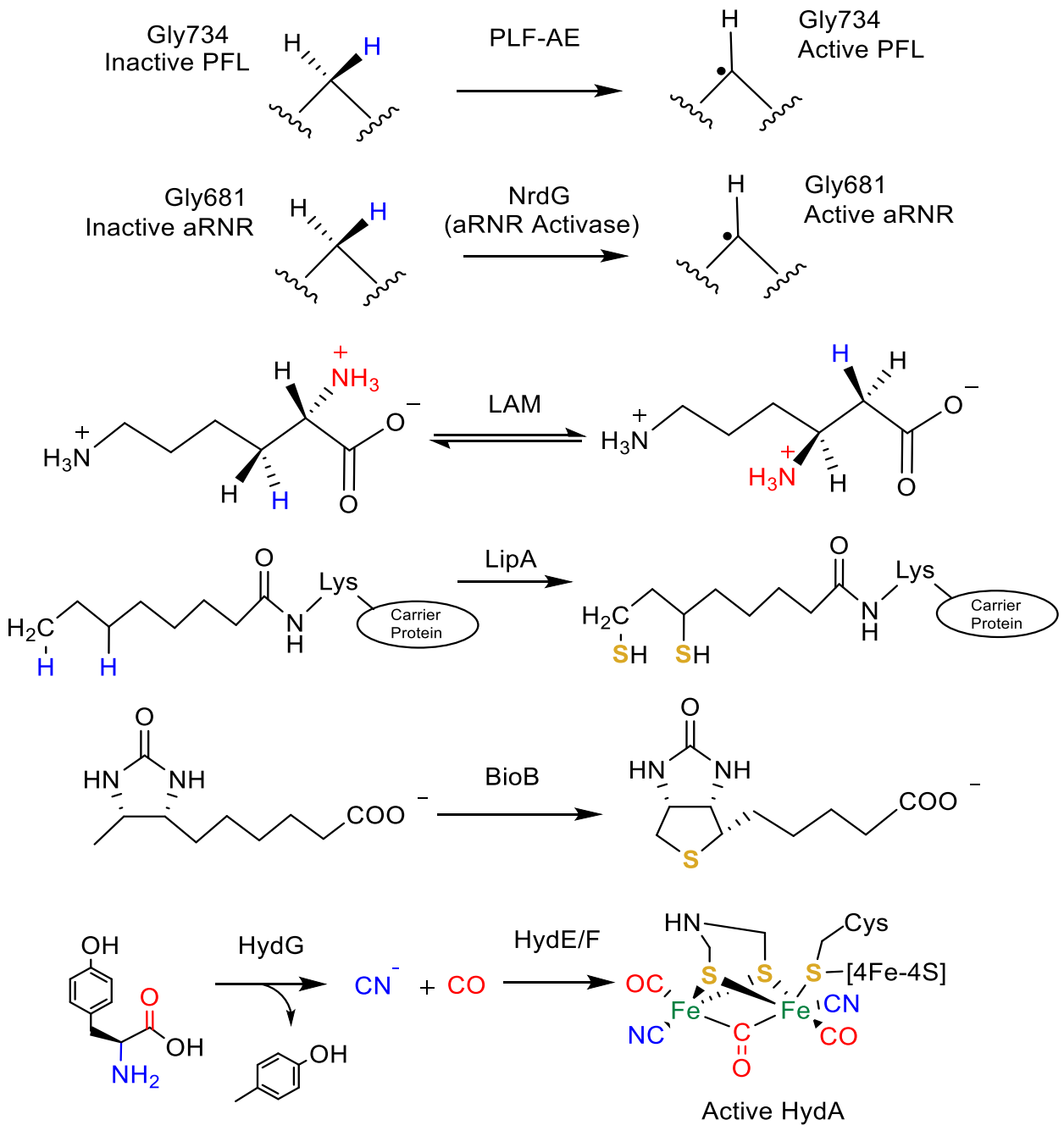

Figure 1.1 Radical SAM enzyme catalysed reactions, PFL-AE [10] , NrdG [11, 12], LAM [13], LipA [12], BioB [12, 13] and HydG [13].

The discovery that all the enzymes which reductively cleave SAM to generate a highly reactive radical contain Fe-S clusters motivated bioinformatics analysis by Sofia *et al.* published in 2001 [9]. This enabled the further identification of over 600 enzymes which catalyse a wide array of reactions but share distant sequence conservation and nearly all contained the exact CxxxCxxC Fe-S cluster consensus motif (Figure 1.2), a small proportion have an increased distance between cysteine pairs, ranging from 3 to 22 [14]. The enzymes

were said to be members of the RSAM superfamily [2, 9]. Now of course the number of members of the RSAM superfamily is over a hundred thousand and their functions are known to range from metabolism, nucleic acid modification and cofactor assembly [14].

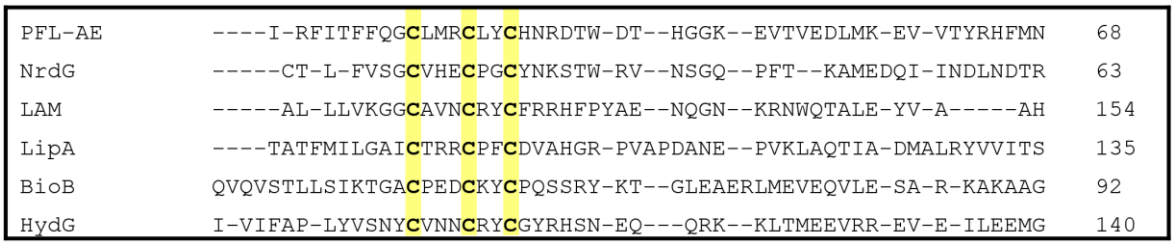

Figure 1.2 Sequence alignment of the conserved Fe-S cluster motif in the RSAM enzymes pyruvate formate lyase activating enzyme (PFL-AE), anaerobic ribonucleotide reductase (NrdG), lysine 2,3-aminomutase (LAM), lipoic acid synthase (LipA), Biotin synthase (BioB) from *E.coli* and the FeFe hydrogenase maturase enzyme HydG from *Thermoanaerobacter italicus*. The CxxxCxxC motif is highlighted yellow.

1.1.2 Functions of the Radical SAM Superfamily

Members of the RSAM superfamily catalyse a highly diverse array of biochemical mechanisms, a small number of which are shown above in Figure 1.1.

RSAM enzymes are responsible for the formation of many organic cofactors such as biotin (BioB) [15, 16], lipoic acid (LipA) [17], menaquinone (MK, vitamin K_2) [18], tyrosine lyase (ThiH) [19, 20] and MoaA [21, 22]. They are also involved in nucleic acid modification, such as methylation of aromatic carbon centres in the cases of RlmN and Cfr [23, 24], formation of antibiotics (Nosiheptide by RSAM NosN [25]), DNA dimer repair/isomerisation in spore photoproduct lyase (SPL) [26] and LAM [5] and metallocofactor assembly in the maturation of [FeFe]-hydrogenase enzymes [27, 28].

Only a relatively small number of RSAM superfamily enzymes have been experimentally described, many are included as members of the superfamily based on the core CxxxCxxC Fe-S cluster consensus motif alone and remain otherwise uncharacterised [13, 14]. More recent work linking understood and unknown RSAM enzymes by sequence similarity and those with known function points to significant sequence variability between RSAM enzymes with similar function, creating challenges for function prediction for those

enzymes yet to be experimentally characterised [14]. Although this is a useful tool it highlights the need for experimental validation in this area to continue and strongly suggests there will be new reactions to be discovered [14].

1.1.3 Radical SAM Enzyme Active Site and SAM Binding

Members of the RSAM Superfamily have very limited sequence similarity and this is reflected in little commonality between their overall structures, the exception to this is the structure and local environment of the RSAM active site which is highly conserved [12]. The majority of the RSAM superfamily members which have been characterised by X-ray crystallography share a common fold structure for radical generation, consisting of a complete $(\beta\alpha)_8$ or partial $(\beta\alpha)_6$ triose phosphate isomerase (TIM) barrel [12]. BioB [29], ThiC [30], PlyB [31], HydE [28]and HydG [32, 33] all contain a complete $(\beta\alpha)_8$ TIM barrel fold [12], while smaller RSAM enzymes such as PFL-AE [34] and CteB contain partial $(\beta\alpha)_6$ folds [35]. The openness of the barrel positively correlates to the size of the substrate and the RSAM active site is located near the top of the barrel buried within loop regions to protect the highly anaerobic centre [12].

At the RSAM active site centre is an oxygen sensitive [4Fe-4S] cluster coordinated by the three cysteine residues of the CxxxCxxC motif. The RSAM active site of *Thermoanaerobacter italicus* (*Ti*) HydG is shown below in Figure 1.3 [32, 36]. The uncoordinated iron of the [4Fe-4S] cluster, commonly referred to as the unique or labile iron, has been well established as the site of SAM binding via its α-amino-nitrogen and α-carboxyl oxygen forming a five-member chelate ring [36-41]. In addition to the conserved CxxxCxxC motif, members of the RSAM superfamily also contain a glycine-rich region (GGE motif) involved in coordinating SAM binding via H-bonds [9, 12, 36, 42].

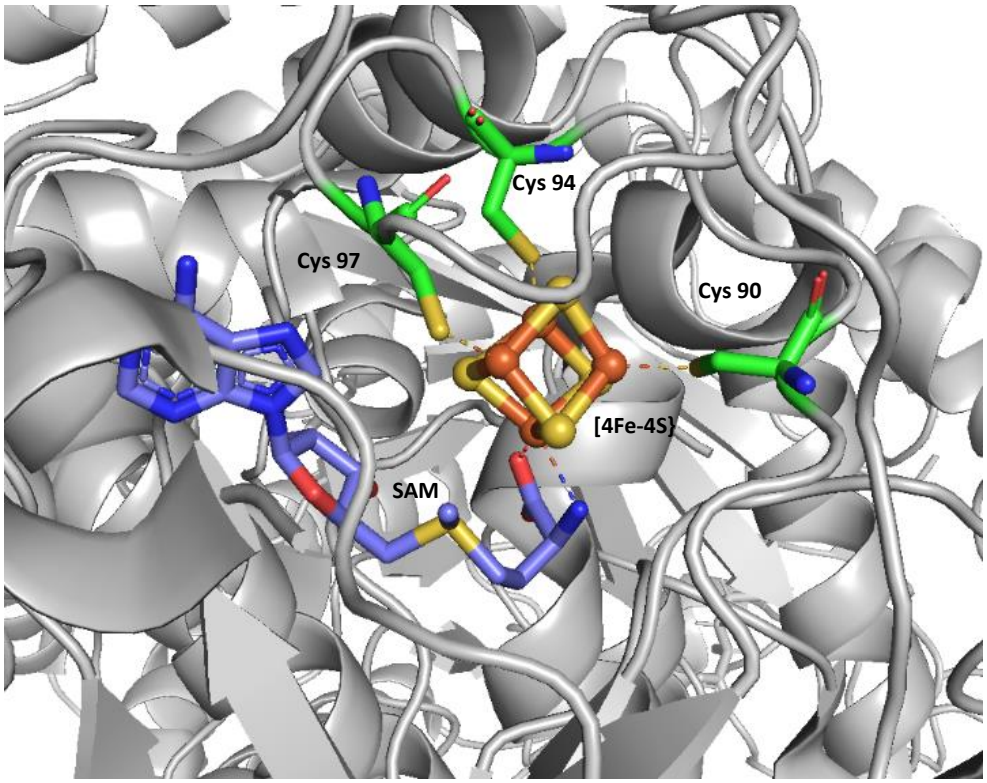

Figure 1.3 RSAM [4Fe-4S] cluster active site of *Ti* HydG coloured in yellow and rust, SAM is shown in purple and coordinating CxxxCxxC motif cysteine residues shown in green (PDB ID 4WCX) [32].

The first experimental evidence for SAM binding to the [4Fe-4S] cluster came from studies of LAM and PFL-AE [37, 38, 40]. Selenium K-edge X-ray absorption spectroscopy (XAS) of the RSAM enzyme LAM and the selenium derivative of SAM (Se-SAM) revealed a 2.7 Å FT peak corresponding to a selenium-iron interaction as a result of Se-SAM cleavage to Se-Met which associates with the Fe-S cluster. These experiments established the need for lysine or *trans*-4,5-dehydrolysine and a reductant for cleavage of Se-SAM [37]. Detailed Mössbauer and electron-nuclear double resonance (ENDOR) spectroscopic studies on PFL-AE first revealed the direct interaction of SAM with the unique iron of the [4Fe-4S] cluster [38, 39]. Mössbauer spectroscopy was used to measure isomer shift changes of [4Fe-4S] clusters where the unique iron site had been reconstituted with ^{57}Fe. Upon incubation with SAM the shift changes observed to at the unique iron site were concordant with direct coordination of SAM [38]. ENDOR experiments measuring hyperfine coupling of isotope labelled SAM provided proof of this interaction [39, 40]. Further ENDOR studies of LAM also confirmed this coordination [43].

These early spectroscopic observations were later confirmed by X-ray crystal structures of SAM bound RSAM enzymes [2, 29, 44]

1.1.4 Reductive Cleavage of SAM

The common catalytic feature among Radical SAM enzymes that enables the generation of the highly reactive radical derived from SAM is a [4Fe-4S] cluster. The $[4Fe\text{-}4S]^{+}$ is an electron donor and the unique iron atom of the cluster is the site of SAM binding [13]. The resulting $[4Fe\text{-}4S]^{2+}$ cluster is reduced by either an external reductant, where SAM is a co-substrate, or where SAM is a cofactor the electron produced from reformation of SAM [2]. Typically *in vivo* the cluster is reduced by flavodoxin (or other single electron donor) and by dithionite *in vitro* [12].

The publication of multiple high resolution crystal structures of the RSAM enzyme HydE: bound to *S*-adenosyl-L-homocysteine (SAH) (1.35 Å) [28], SAM, and DOA + methionine (1.62 Å and 1.25 Å respectively) by Nicolet *et al.* provided the basis for detailed computational studies on the mechanism of SAM cleavage [45].

The calculated activation barrier and free energy of radical formation were 54 kJ mol^{-1-} and 46 kJ mol^{-1} respectively, similar to the experimentally derived values for SAM cleavage by LAM [13, 46]. Hybrid quantum mechanical (QM)/molecular mechanical (MM) methods were implemented alongside the resolved crystal structures of HydE to model SAM cleavage [45]. The reaction energy profile calculated, where the energy of the transition state structure (TS) and radical product are very close points to a concerted reaction that can reverse easily reforming SAM. When SAM is bound to the unique iron it was noted that the unique iron and sulfonium iron of SAM share the same orbital energy, enabling electron transfer between the two atoms [45]. This is contradictory to the previously suggested mechanism of electron transfer proposed between sulfonium of the $[4Fe\text{-}4S]^{+}$ cluster and the SAM sulfonium atom for PFL-AE [10, 39, 47, 48]. However the inferences of this work are based on $[4Fe\text{-}4S]^{+}$ clusters coordinated by four cysteine residues where there is no proposed unique iron as is the case for RSAM enzymes [45, 48]. The findings described for HydE are in agreement with models proposed from studies on LAM [46]. Based on the HydE bound DOA + methionine structure it was also proposed the released methionine can at least briefly bind to the [4Fe-4S] cluster and the affinity of the cluster for these products or

SAM determines whether SAM acts as a cofactor or substrate rather than the mechanism of cleavage [45]. The reaction mechanism is shown below in Figure 1.4.

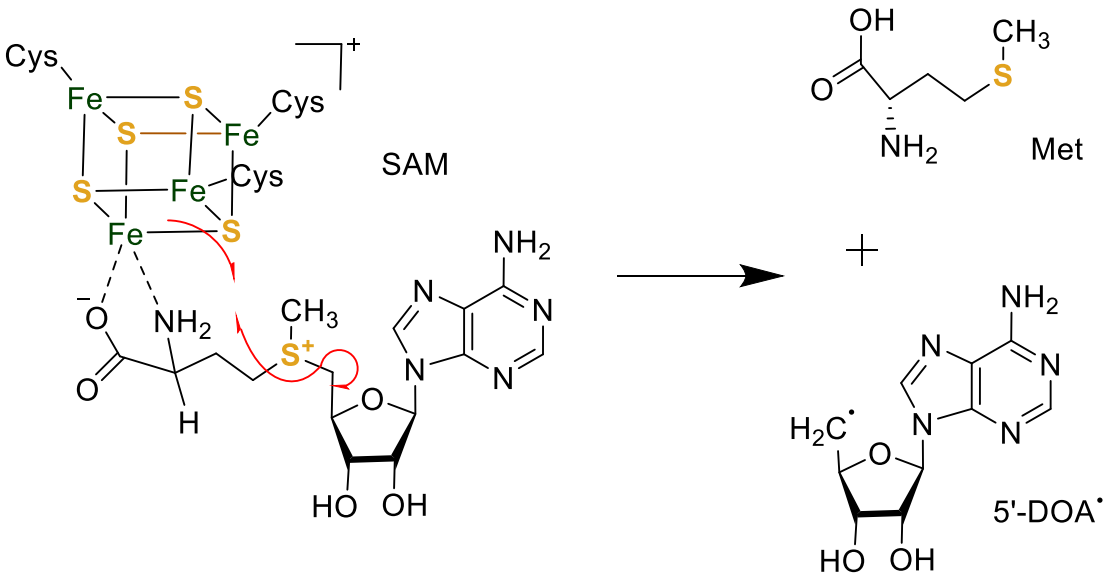

Figure 1.4 Mechanism for the reductive cleavage of SAM resulting in the production of methionine and 5-DOA. reproduced from [1].

In summary, the shared mechanism of RSAM enzyme catalysis involves SAM bound to the reduced $[4Fe\text{-}4S]^{+}$ cluster at the unique iron. The transfer of an electron from $[4Fe\text{-}4S]^{+}$ to SAM homolytically cleaves the S-C 5' bond producing methionine and DOA· [12].

For a long time, due to the instability of DOA, it had not been observed spectroscopically. Synthesis of the SAM allylic analogue S-3',4'-anhydroadenosyl-L-methionine provided early compelling analogous experimental evidence to support the proposed reductive cleavage mechanism of SAM [49, 50]. More recently, EPR and ENDOR experiments involving cryogenic photoinduced electron transfer of the RSAM enzyme PFL-AE have finally characterised the DOA· radical and reduced $[4Fe\text{-}4S]^{+}$ cluster in the absence of PFL substrate [51]. In the quest to characterise DOA· an organometallic catalytic intermediate was observed by EPR, the intermediate is a SAM-derived deoxyadenosyl moiety bound at the unique iron of the [4Fe-4S] via 5'-C of SAM [52]. This is similar to the organometallic intermediate observed in the process by which B_{12} radical enzymes generate DOA· [53]. In the context of RSAM enzymes, in the presence of substrate, DOA· has not been freely observed, and in the experiments above where DOA· has been characterised, photon

energy is utilised to overcome reductive energy barriers, where this otherwise may be achieved by the organometallic intermediate [51].

A recent publication by Impano *et al*. investigating cryogenic photoinduced SAM S-C bond cleavage of RSAM enzymes has revealed regioselectivity of the cleavage event resulting in either DOA· or CH_3· [54]. RSAM enzymes were classified based on the radical product, which was proposed to be a result of the SAM ribose conformation upon binding to the $[4Fe\text{-}4S]^+$ cluster, either 2'-endo/axial C4'-C5' bond or 3'endo/equatorial C4'-C5' bond and not the position of the sulfonium centre [54]. It appears all three sulfonium bonds of SAM can be cleaved under restricted conditions and interactions between SAM and active site residues determine the selectivity of enzymatic catalysis *in vivo*, also providing further evidence for the formation of the SAM-derived deoxyadenosyl organometallic intermediate [52, 54].

1.2 Hydrogenases

1.2.1 Classification of Hydrogenase enzymes

Hydrogenase enzymes catalyse the reversible oxidation of molecular hydrogen to protons and electrons [55, 56] :

$$H_2 \rightleftharpoons 2H^+ + 2e^-$$

Equation 1 Hydrogenase catalysed reversible oxidation of molecular hydrogen.

Hydrogenases are found in bacteria, archaea and less commonly eukarya and have a vital role in cellmotifabolism. Most hydrogenases are capable of performing either reaction *in vitro*, however, *in vivo* they usually function in only one direction depending on the requirements of the cell [55]. They can be soluble, or membrane bound and are capable of distinct functions; for example, membrane bound hydrogenases can function to establish transmembrane proton gradients. All hydrogenases contain a metal ion active site, the composition of which determines which one of three classes they belong to; [FeFe], [NiFe] or [Fe] [55, 56].

[Fe] Hydrogenases are found exclusively in methane producing archaea, they exist alongside four [NiFe] hydrogenases and in reduced nickel conditions [Fe] hydrogenase gene

expression is upregulated [56]. The enzymes catalyse the reduction of methenyl tetrahydro methanoprotein (methenyl-H4MPT+) with molecular hydrogen to methylene-H4MPT and H+. The enzyme differs from [NiFe] and [FeFe] hydrogenases as it does not contain Fe-S clusters, and instead uses Fe-guanylylpyrodinol (Fe-GP) as its unique cofactor [56, 57]. Both when the [Fe] cofactor is bound to the enzyme and when it is free the Fe(II) is complexed by pyridone, two carbon monoxide molecules and cysteine. Pyridone may be the functional equivalent to cyanide in [FeFe] and [NiFe] hydrogenases [57].

[NiFe] hydrogenases are found in archaea and bacteria but not eukarya, they are thought to be the most common hydrogenases [58]. They can be grouped in terms of how they have evolved to function and are the most understood hydrogenases. The four classes of [NiFe] hydrogenases are; 1, membrane-bound, which perform H_2 oxidation; 2, H_2 oxidation and sensory/regulatory enzymes; 3, hydrogenases which can perform oxidation and reduction, as well as NAD(P)+ and F420 reducing and 4, membrane-associated hydrogenlyase complexes (energy-converting) [56, 59]. Most commonly [NiFe] hydrogenases perform oxidation of H_2 and are reversibly inhibited by oxygen, however there are a select group of unusual oxygen tolerant enzymes [59]. Although evolutionary unrelated, [NiFe] and [FeFe] hydrogenases have similarly structured active sites where carbon monoxide and cyanide both coordinate the iron ions (see Figure 1.5). In some [NiFe] hydrogenases instead of two terminal cys residues, one is a replaced by a selenocysteine, these are known as [NiFeSe] hydrogenases [58].

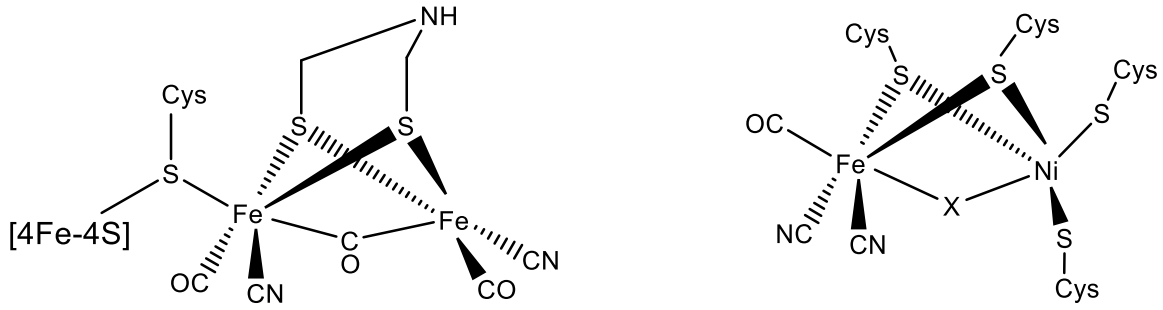

Figure 1.5 [FeFe] and [NiFe] Hydrogenase active sites, reproduced from [56].

[FeFe] hydrogenases are found only in anaerobic bacteria and eukarya and most commonly perform the reverse reaction (Equation 1); reducing protons to generate molecular hydrogen at approximately $(10^4 s^{-1})^8$ [58, 60].

The [FeFe] hydrogenase active site is known as the H-cluster and is well conserved amongst [FeFe] hydrogenases. It can be identified in protein sequences by the presence of three discrete binding motifs named L1 (TSCCPxW), L2 (MPCxxKxxE), and L3 (ExMACxxGCxxGGGxP) [55]. The H-cluster is comprised of a [4Fe-4S] sub cluster which bridges via a cysteine residue to a [2Fe] cluster. This cluster is coordinated by three carbon monoxides, two cyanides and an azadithiolate ligand and is thought to be the site where catalysis occurs (Figure 1.5) [27, 61, 62].

1.2.1.1 Hydrogenases as a source of bioenergy

Generating energy through renewable and sustainable means and decreasing the worlds reliance on finite fossil fuels to combat climate change is one of the most significant problems facing society today [63, 64]. Renewable hydrogen production technology is thought to be a key component in the future of energy, improving the efficiency of renewable hydrogen production is required before it can compete with H_2 production utilising fossil fuels [65].

[FeFe] Hydrogenase enzymes are capable of producing thousands of H_2 molecules per second [66, 67] harnessing this potential has made hydrogenase enzymes the focus of significant research in the field of renewable H_2 production [61, 68]. Recent advances include photosynthetic hydrogen production by [NiFe] and [FeFe] hydrogenase enzymes fused with photosystem I, with photosystem II delivering protons and electrons to the complex from H_2O splitting [69, 70]. These systems provide a proof-of-concept method for photoH_2 production and undoubtedly further optimisation and developments will be made [70].

1.2.2 Maturation of [FeFe] Hydrogenases

The catalytic centre of [Fe-Fe] hydrogenase (HydA) is comprised of a [4Fe-4S] subcluster linked to a [2Fe] subcluster by a single-bridging cysteine thiolate (Figure 1.5), collectively known as the H-cluster [71].

In vivo the cubane [4Fe-4S] subcluster is assembled by house-keeping Fe-S cluster machinery proteins, such as those encoded by the *isc* or *suf* operons [60, 71-73]. Whereas synthesis and assembly of the [2Fe] cluster is coordinated by the three maturase enzymes

HydG, HydE and HydF (expressed in all organisms containing [FeFe] hydrogenases) [27, 56, 71, 74, 75]. Without both subclusters the hydrogenase enzyme is inactive [71, 76].

HydG and HydE have a very high sequence homology [56] and are both members of the RSAM enzyme superfamily. RSAM enzymes all contain an $[4Fe\text{-}4S]^{+}$ which is required for binding (via the unique iron) and reductively cleaving SAM, HydG (and it is proposed HydE) form a DOA radical and methionine as a result of reductive cleavage [77]. Both maturase enzymes HydG and HydE contain an N-terminal [4Fe-4S] cluster and an open binding site for SAM cofactor. At their C-terminal is a second FeS cluster binding motif which in HydG is another cubane cluster. Spectroscopic studies of *Thermatoga maritima* HydE have shown its second cluster to be highly unstable as it has been observed as both a diiron cluster [28] and a cubane cluster [78]. Mutagenesis studies on the conserved cysteine residues of the second cluster, which result in proteins lacking the second cluster are still capable of producing an active [FeFe] hydrogenase *in E.coli*, indicating this second HydE cluster may not play a significant role in the maturation process [28].

Unlike HydG and HydE, HydF is a GTPase. HydF has been identified as performing the final step of the maturation process where it acts as a scaffold and carrier of the final H-cluster precursor. The [2Fe] cluster precursor is assembled by HydG and HydE, whereby HydG generates the metallosynthon that HydE rearranges and dimerises to be transferred to HydF before final assembly at HydA [79-81]. The process is illustrated in Figure 1.6 below [81]. HydF is a homodimer with each monomer comprised of three domains; a GTPase domain located at the N-terminus; [4Fe-4S] cluster binding domain at the C-terminus, and a dimerization domain [82] . Unlike HydG and HydE, the overall protein fold is not globular, but open with the [4Fe-4S] highly exposed [74]. A crystal structure of HydF from *Thermotoga neapolitana* lacking an intact [4Fe-4S] cluster has been described [82].

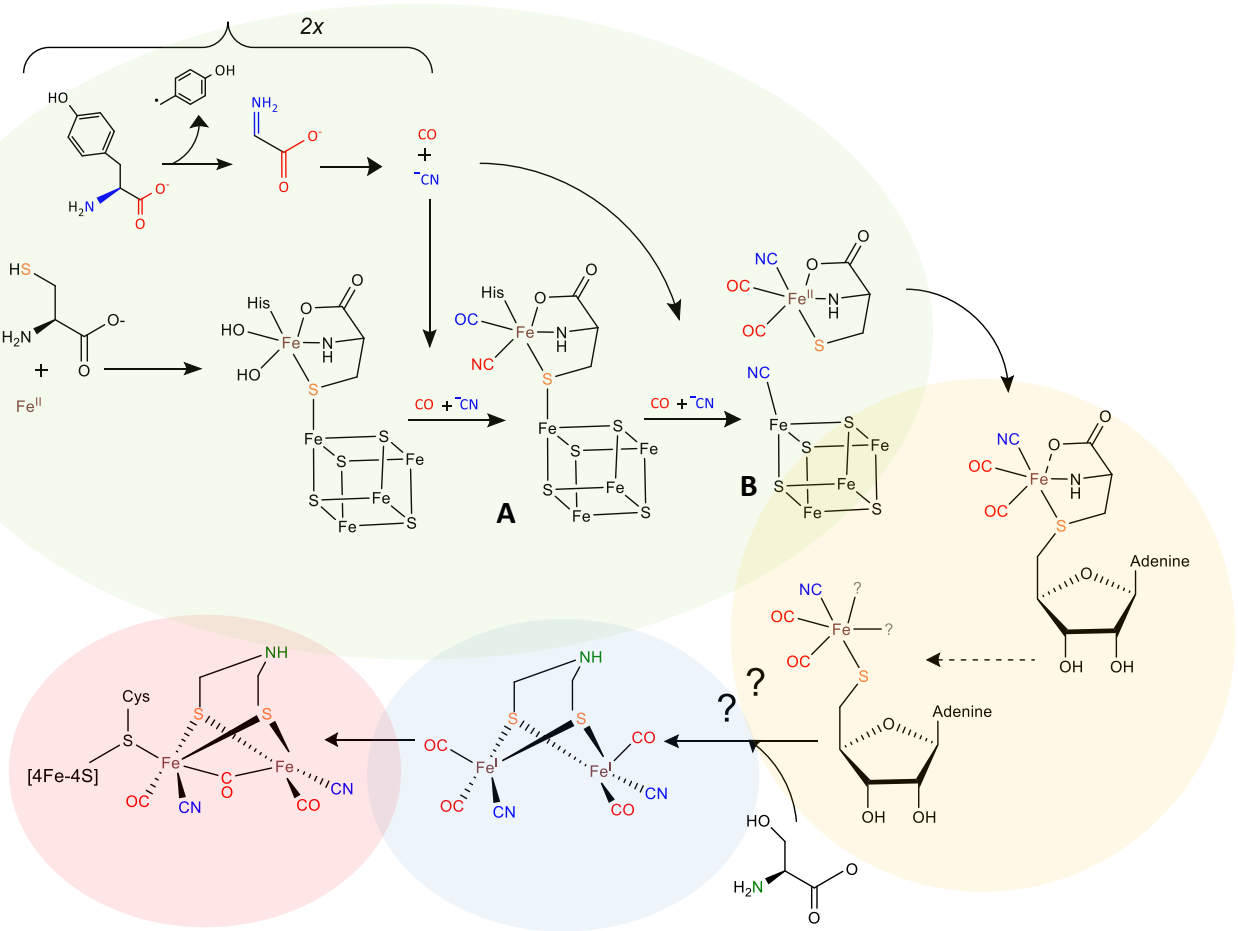

Figure 1.6 Proposed biosynthesis of the [2Fe] subcluster of the H-cluster reproduced from [81]. Green area depicts the stages of HydG maturation, yellow HydE, blue HydF and red represents the formed H-cluster at HydA.

1.2.3 *In vitro* Assembly of Hydrogenases

Cell free *in vitro* assembly of [FeFe] hydrogenase was first investigated by Kuchenreuther *et al.* [83]. This work resulted in a huge step forward in better understanding the roles of the individual maturase enzymes HyG, HydE and HydF in the assembly of active HydA. The key findings from this initial study were that maturation can occur without the enzymes HydE, HydF and in the absence of exogenous tyrosine. It was proposed HydG was responsible for the synthesis of an $[Fe(CO)_x(CN)_x]$ complex which is a precursor to the [2Fe] subcluster [83]. *In vitro* assembly is an incredibly important tool in studying these enzymes as it gives unparalleled control of the reaction allowing the introduction of isotopic labels,

analogous substrates or synthetic enzyme products which, when exploited by relevant spectroscopic techniques, produce highly significant discoveries [61, 84].

In vitro studies by Rao *et al.* have recently demonstrated by EPR and ENDOR spectroscopy, a radiolabelled synthetic [Fe(Cys)$(CO)_2$(CN)] carrier (in the absence of HydG) is capable of maturation of HydA resulting in activity equal to native enzyme. This work also enabled investigation of the biosynthetic sources of the sulfur (cysteine), carbon and nitrogen atoms (serine) of the azadithiolate ligand [85, 86].

1.3 Radical SAM enzyme HydG

1.3.1 Early studies on the role of HydG in the maturation of FeFe Hydrogenases

HydG is the most extensively studied and understood of the three maturase enzymes involved in H cluster assembly. HydG is a RSAM enzyme whose role in the maturation process is to generate the [Fe(II)$(CO)_2$(CN)(Cys)] organometallic synthon which functions as a substrate for the RSAM enzyme HydE (Figure 1.6) [77, 80, 81, 87-89].

The initial identification of the substrates and products of HydG resulted from its high sequence homology (27%) with the RSAM enzyme ThiH [20, 90]. ThiH lyses tyrosine to produce dehydroglycine and *p*-cresol, and it transpired that HydG also utilises tyrosine as its substrate via a similar cleavage reaction. Early studies identified *p*-cresol and dehydroglycine as a product and this pair of products was later expanded to include tyrosine derived CN^- and CO (Figure 1.7) [87, 90, 91].

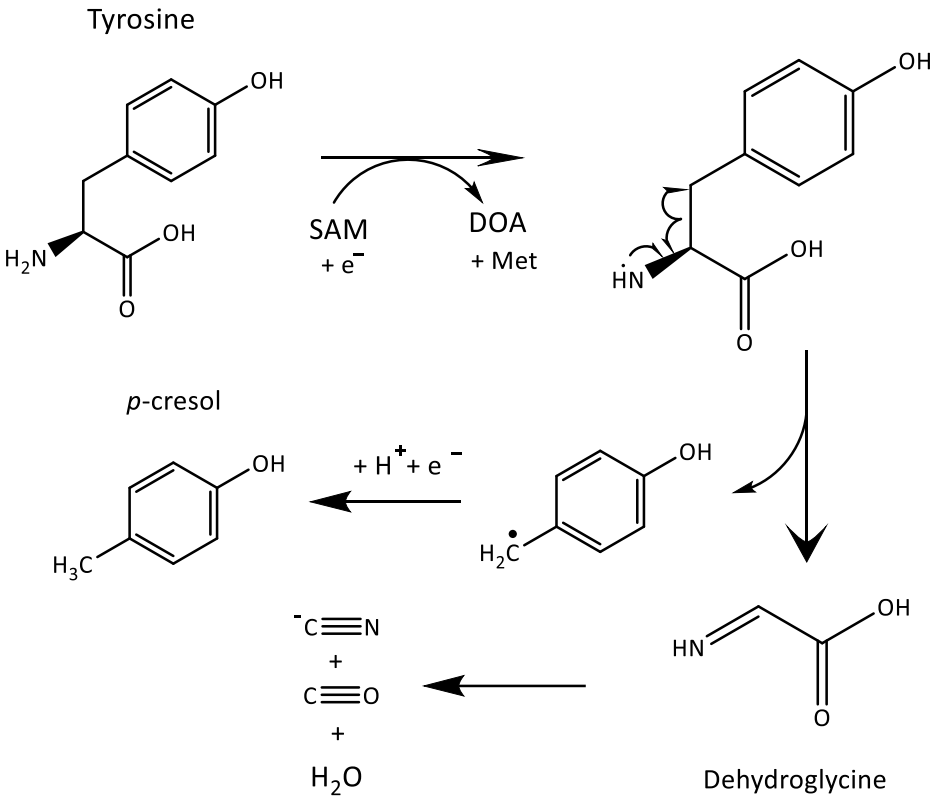

Figure 1.7 HydG abstraction of tyrosine, reproduced from [27].

The 5'DOA radical generated at the N-terminal [4Fe-4S] as a result of reductive cleavage of SAM abstracts a hydrogen atom from tyrosine resulting in Cα-Cβ bond cleavage leading to the production of *p*-cresol, cyanide, carbon monoxide and a water molecule (Figure 1.7) [27, 77]. Stopped flow Fourier transform infrared (SF-FTIR) and electron-nuclear double resonance (ENDOR) spectroscopies have been used to identify an organometallic $[Fe(CO)_2(CN)]$ synthon as the final product of HydG which is transferred to apoHydA to form the [2Fe] cluster [77]. This study was published prior to the availability of crystal structures for HydG and it was proposed tyrosine binding and synthon formation occurred at the C-terminal (auxiliary) cluster, supported by earlier EPR experiments [88]. Many RSAM enzymes have been found to contain auxiliary clusters with wide ranging functions, including sulfur donation, electron transfer, and as was proposed in this case, substrate binding [92]. This binding mechanism challenges studies of two highly similar radical SAM enzymes; a *Clostridium acetobutylicum* HydG mutant lacking the C-terminal cluster (whilst retaining the C-terminal domain) and ThiH (thiazole biosynthesis protein containing one N-terminal [4Fe-4S] cluster). Both the mutated HydG and ThiH enzymes can perform tyrosine

cleavage; as cyanide, *p*-cresol and dehydroglycine are detected products [20, 93, 94] . In the *C.butylicum* HydG mutant carbon monoxide synthesis does not occur without the C-terminal domain [94, 95].

1.3.2 Structure and function of HydG

A turning point in our understanding of HydG came with the characterisation of the X-ray structures of HydG from *Thermoanerobacter italicus* (*Ti*) (pdb.id 4WCX) [32] and *Carboxydothermus hydrogenoformans* (pdb.id 4RTB) [33].

The crystallographic characterisation of the *Ti* HydG structure SAM complex, with a complete approximately 24 Å (βα)8 TIM barrel fold and both N and C terminal [4Fe-4S] clusters, as well as an additional fifth labile Fe at the C-terminal cluster [32] provided a highly significant insight into canonical substrate binding which was previously absent. Arguably, the most significant discovery made whilst solving this structure was the fifth labile Fe (II) connected via a sulphide bridge to the C-terminal [4Fe-4S] cluster. The Fe was termed labile as it was only present in one of two monomers in the structure and it was noted to have potential for being the site of $[Fe(CO)_2(CN)]$ synthon assembly and subsequent transfer to HydA. The labile Fe has only one protein-derived ligand, His265 (this residue is widely conserved across HydG proteins) [32]. Another area of significant interest was the tyrosine binding site, which in this study was proposed to be proximal to the binding site of SAM in a binding pocket resembling that of tryptophan in NosL [96], while the labile Fe would then be well positioned to accept the dehydroglycine intermediate [32].

The X-ray crystallographic structure of *Carboxydothermus hydrogenoformans* HydG was described in an unbound state containing only the N-terminal [4Fe-4S] cluster [33]. It is suggested, based on cavity calculations, the enzyme contains two tunnels with distinct functions that are connected via the tyrosine binding pocket. The first tunnel is between the tyrosine binding pocket and the protein surface, while the second tunnel is between the tyrosine binding pocket and the expected position of the C-terminal [4Fe-4S] cluster [33]. The suggested binding site of tyrosine and subsequent dehydroglycine migration to the C-terminal cluster agrees with that proposed in the *Ti* HydG structure, and was again informed by NosL tryptophan binding [32, 96]. Based on the crystal structure attained being in a relaxed confirmation without bound tyrosine, it was proposed flexibility in the C-

terminal loop causes displacement of the three helix loop region. This movement causes burying of the C-terminal cluster (which is during this time reassembled) and stimulates tyrosine binding displacing Arg307, which in turn causes rearrangement of the N-terminal, closing the tunnel exposed to the protein surface. Tyrosine cleavage and subsequent movement of dehydroglycine to the C-terminal cluster (becoming Fe bound CN- and CO) permits the Arg307 to move back to its original position and open the tunnel at the protein surface allowing *p*-cresol to leave. A second cycle is required to form the complete [$Fe(CO)_2(CN)$] synthon, before the C-terminal pivots to expose the synthon bound cluster which transfers to HydE/ HydF for assembly and delivery of the [2Fe] cluster to HydA [33]. This mechanism is clearly lacking any reference to the labile Fe as this was not present in the crystal structure.

A summary of the current view of the role of HydG in [2Fe] maturation is shown above in Figure 1.6. Predominantly a combination of X-ray crystallography, EPR and FTIR spectroscopic techniques have been utilised to determine the intermediate structures involved in HydG maturation, in combination with mutagenesis studies, synthesis of synthetic products and analogous substrates. [97].

EPR and FTIR spectroscopy were used to investigate the formation of the cluster-bound synthon by alternatively comprised auxiliary clusters. The results suggest that L-cysteine and the labile Fe are both required to generate the [$Fe(CO)_2(CN)$] synthon and that [$(Cys)Fe(CO)_2(CN)$]- is an intermediate before transfer to HydF [98]. The [(Cys)Fe(CO)x(CN)y]- intermediate is yet to be freely observed [99]. However, ENDOR and hyperfine sublevel correlation (HYSCORE) spectroscopy were successfully applied to determine the presence of the specific complex bound to the auxiliary cluster as complex A (Figure 1.8, as described in [99]). Field-dependent HYSCORE spectra were also able to confirm the distance between the “dangler” (labile) Fe in complex A to the nearest Fe in the auxiliary cluster as approximately 4 Å. This proximity is fairly consistent with that reported in the *Ti* HydG crystal structure of 4.1 Å (however it should be noted this structure does not contain the cysteine bridge) [32, 99]. Recently a synthetic [$Fe^{II}(CO)_2CNCys]^-$ metallosynthon has been demonstrated to be an active substrate for HydE, further evidence confirming the product of HydG and its progression to HydE [80, 97].

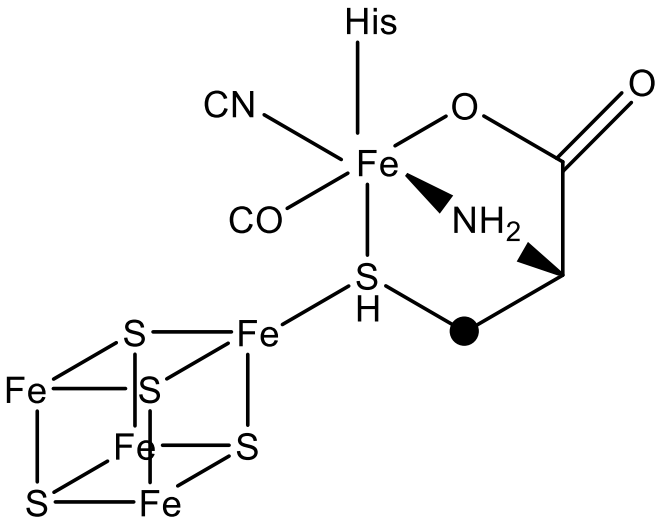

Figure 1.8 Complex A, reproduced from [99].

Although a significant number of intricacies relating to the HydG catalysis mechanism have been solved, the wider questions about how the maturase enzymes interact with one another is still in question. In relation to HydG in particular, the tyrosine binding site is yet to be observed and it is not clear how the $[(Cys)Fe(CO)_2(CN)]^-$ synthon is transported to HydE nor has it been observed free from native HydG. Other questions also surround the mechanism of how two tyrosine monomers are cleaved in order to generate the two cyanides present in the synthon.

1.4 Project Aims

RSAM enzymes are one of the largest enzyme families in nature and appear in countless biological pathways critical to life [100]. Despite the many thousands which have been identified by canonical sequence motifs denoting typical RSAM structural features very few have been experimentally characterised [14]. The key challenges in studying these enzymes stems from their highly reactive nature which can make "trapping" their intermediates and products in native environments problematic, further complicated by their oxygen sensitive catalytic active site, the [4Fe-4S] cluster. Spectroscopic techniques have so far proven to be the most fruitful in describing the RSAM enzyme HydG. In this study we aim to further characterise HydG, in the hope that not only will it be of direct benefit to HydG understanding but also the methods and techniques described could prove useful for studying other RSAM enzymes. This study aims to:

- Express, purify and chemically reconstitute HydG in an active state.
- Optimise the HydG activity assay with the objective to characterise the released metallosynthon.
- Co-crystallise HydG with the cysteine ligand bound to the labile iron of the auxiliary cluster.

Chapter 2 Expression and Purification of HydG

2.1 Plasmid design and Transformation

In earlier studies by Dr R Driesener [95], plasmids encoding HydG genes from *Thermoanaerobacter italicus* (*Ti*) and *Thermotoga lettingae* (*Tl*) were codon optimized [101] for expression in *E.coli* and subcloned into pFM024 plasmid (pBADHis derived vector[102]) between *NcoI* and *XhoI* restriction sites [95]. For the protein to be purified by Ni-NTA affinity purification, an *N*-terminal hexahistidine tag was inserted, in addition to *E.coli* ISC operon for co-expression of bacterial iron-sulfur cluster assembly proteins [95, 103-105].

Chemically competent (method 3) BL21 (DE3) and JM109 *E.coli* strains have been chemically transformed (method 4) with pBAD plasmids encoding the ISC machinery and His-tagged HydG genes from *Ti* (plasmid PRD003, Uniprot protein code D3T7F1) and *Tl* (plasmid PRD002, Uniprot protein code A8F818). A further pBAD vector containing only genes encoding the ISC machinery was transformed as a control to follow HydG expression. JM109 cells were transformed with the purpose of isolating the plasmid to be used for future transformations while BL21 (DE3) cells are used for protein expression. Transformation of the HydG plasmids into BL21 (DE3) proved difficult, presumably due to the large size of the plasmid (10+Kb).

To confirm cells had been successfully transformed with the desired plasmid an analytical digest (method 6) of isolated mini-prep plasmid (method 5) and colony PCR (method 8) were employed.

Colony transformation has been confirmed by analytical digest of isolated plasmid DNA, isolated DNA was digested by compatible restriction enzymes. Typically, restriction enzymes *XhoI* and *NcoI* were used as they provide the insert site of the HydG gene. After digestion fragments were visualised on 1% agarose gel (example Figure 2.1). The *Ti* HydG plasmid map is shown in Figure 2.2.

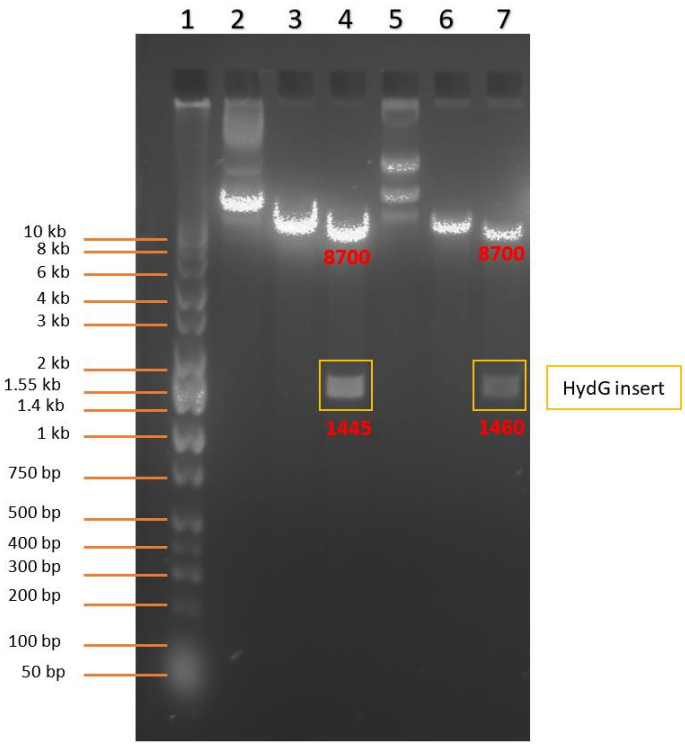

Figure 2.1 1 % Agarose gel of plasmid DNA Analytical digest

1: DNA ladder; **2**: Undigested PRD003 Mini-prep plasmid; **3**: XhoI digest of PRD003 Mini-prep; **4:** XhoI and NcoI digest of PRD003 Mini-prep; **5:** Undigested PRD002 Mini-prep; **6:** XhoI digest of PRD002 Mini-prep; **7:** XhoI and NcoI digest of PRD002 Mini-prep. All mini-preps shown have been isolated from BL21(DE3) cells.

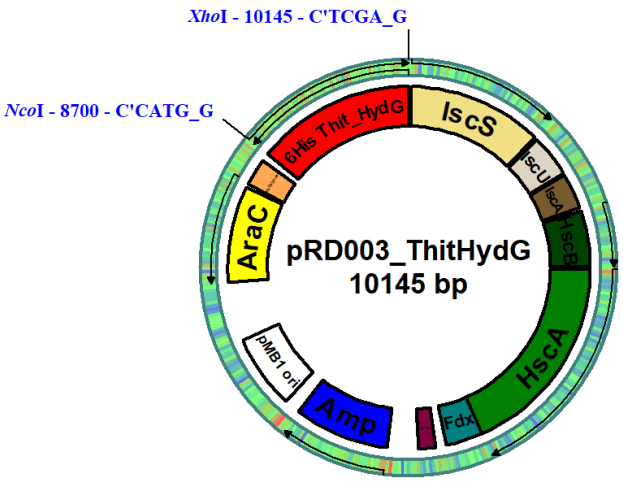

Figure 2.2 *Thermoanaerobacter italicus* (PRD003) plasmid map

2.2 HydG Expression and Purification

The method for *Ti* HydG expression, purification and reconstitution has been optimised previously by Dr P.Dinis and the same method has been used here (method 13) [106].

The expression efficiency for HydG has been assessed in small scale cultures (100 mL) (method 9) of BL21 (DE3) cells expressing *Ti* HydG (PRD003), *Tl* HydG (PRD002) and cells only expressing the ISC machinery as a control. Overnight cultures were used as a 1% inoculum into 100 mL of 2YT medium, cultured at 37°C, then induced by the addition of 20 % arabinose and temperature reduced to 27 °C for the remaining period of culture (a further 6 hours). Cell pellets were then collected by centrifugation, the cell pellets expressing HydG proteins were darker in colour, due to the presence of the iron-sulfur clusters (Figure 2.3). The purpose of the experiment was to assess the expression levels and not to purify or produce active protein, therefore for analysis of these small scale cultures, all experimental activities were outside of the glovebox. A summary of the mass of the cell pellets produced is shown below in Table 2.1.

Table 2.1 Mass of cell pellets produced from small scale expression

Plasmid	Cell pellet (mg)
ISC Machinery (Control)	951.6
PRD002 (*T. lettingae* HydG)	914.0
PRD003 (*T. italicus* HydG)	888.8

After lysis of the cell pellet the protein concentration of the cleared supernatant was determined by Bradford Assay (method 10) [107]. A calibration curve prepared from BSA standards of known concentrations (Figure 2.4) was used to calculate the unknown protein concentrations using their absorbance at 595 nm wavelength, shown in Table 2.2.

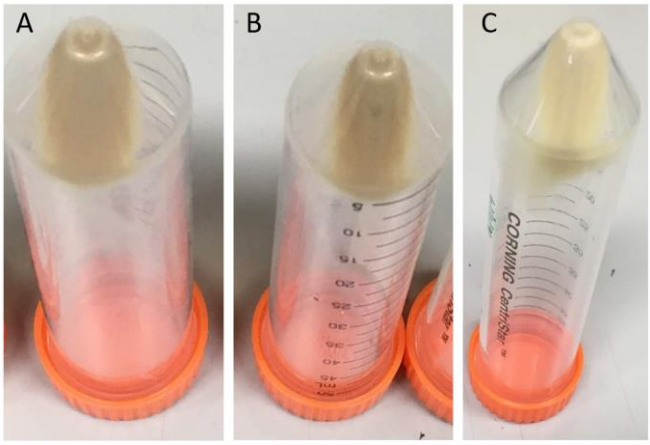

Figure 2.3 Cell pellets from small-scale protein expression

A: Cell pellet from BL21 (DE3) cells expressing *Tl* HydG (PRD002); **B**: Cell pellet from BL21 (DE3) cells expressing *Ti* HydG (PRD003); **C**: Cell pellet from BL21 (DE3) cells expressing ISC machinery proteins only.

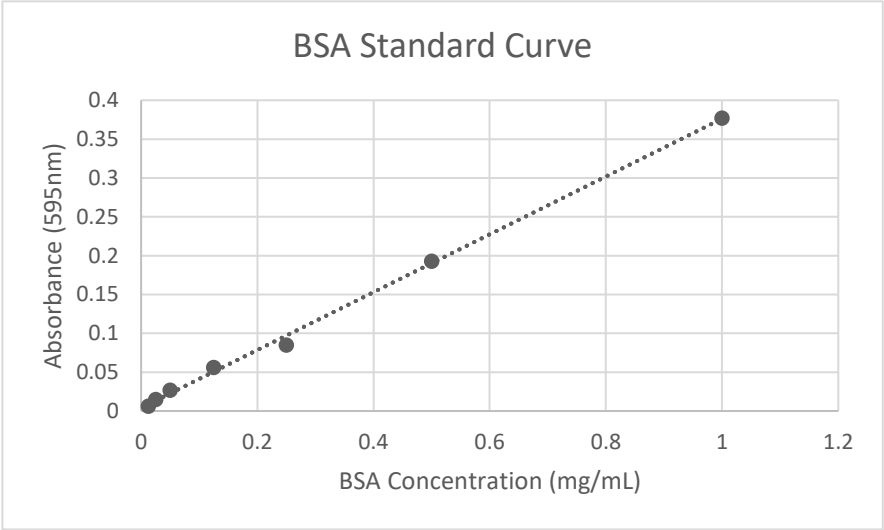

Figure 2.4 Example of BSA standard curve for Bradford Assay (Equation of line shown: *y=0.3722x + 0.0041*)

Table 2.2 Protein concentration of cleared cell lysate from small scale protein expression determined by method Bradford (method 10).

Protein concentrations are based on an average of four aliquots of the same cell pellet, which were lysed separately.

Protein expression	Protein concentration (mg/mL)
Only ISC Machinery	24.30 ±2.0
T.italicus HydG (PRD003)	17.75 ±1.9
T.lettingae HydG (PRD002)	20.37 ±7.4

SDS-PAGE (15 %) was used to further analyse the cell lysate, lysed pellet and cleared lysate in order to confirm the expected size of HydG and observe the relative amounts of soluble and insoluble protein (Figure 2.5). There is HydG protein present in the supernatant and the insoluble pellet of the lysed cells.

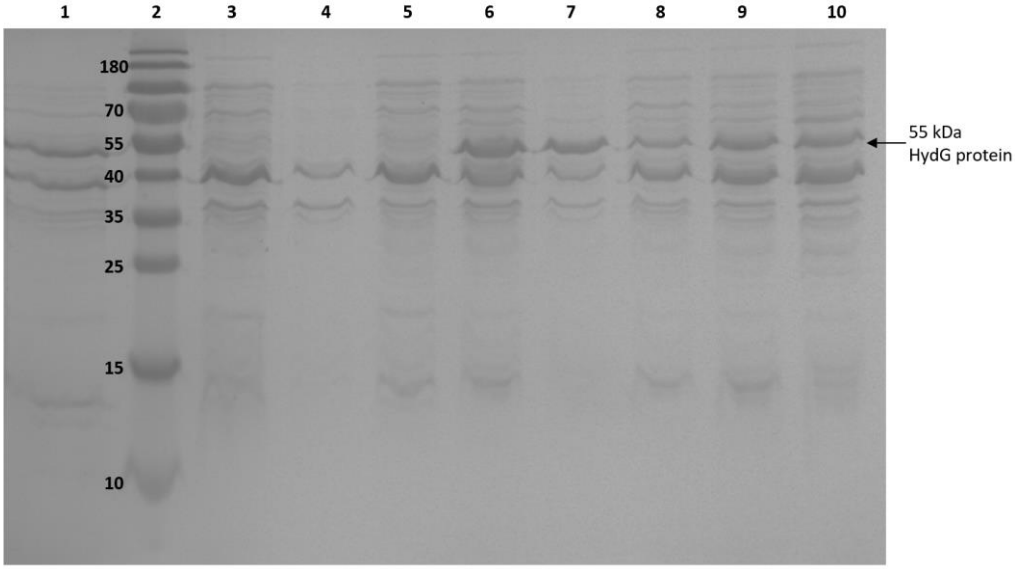

Figure 2.5 SDS-PAGE of small-scale expression of ISC Machinery, *Tl* HydG (PRD002) and *Ti* HydG (PRD003)

1: PRD003 cleared lysate; **2**: Molecular weight marker (kDa); **3**: ISC machinery cell lysate; **4:** ISC machinery lysed pellet; **5:** ISC machinery cleared lysate; **6:** PRD002 cell lysate; **7:** PRD002 lysed pellet; **8:** PRD002 cleared lysate; **9:** PRD003 cell lysate; **10:** PRD003 lysed pellet.

The slightly lower pellet yield for *Tl* HydG expression has been observed before and the resulting comparatively reduced protein yield is one of the reasons it has been studied less extensively than the *Ti* derived protein [106].

Large scale bacterial expression of *Ti* and *Tl* HydG was conducted in a BioFlo® 110 fermenter with a 7.5 L vessel (Eppendorf UK Ltd.). 2YT Media (5 L)was autoclaved in the vessel and allowed to equilibrate overnight at 37 °C before the appropriate antibiotic and overnight cell culture (transformed BL21 (DE3) cells) was added (method 12). When the OD_{600nm} reached between 0.6-0.7 the culture was induced with 20% (w/v) arabinose (50 mL/L of culture) and cells were left to incubate at 27 °C for approximately 6 hours of expression. Cells were harvested by centrifugation and the resulting cell paste was typically 30 g per 5 L of culture for *Ti* and approximately 20 g for *Tl* HydG. For *Tl* purification, two cell pellets were combined whereas for *Ti* purification only one cell pellet used.

Following expression of BL21 (DE3) cells on a 5 L scale in the fermenter unit the cell pellet was harvested by centrifugation and stored at -80 °C until purification. All future manipulations of the cell pellet and protein were conducted inside an anaerobic glovebox (Belle Technology, O_2 < 2 ppm, 18°C). The cell pellet was crushed and resuspended in purification buffer A (Table 7.12) containing an appropriate amount of lysozyme and protease inhibitor in a cooled water bath. Cells were then further lysed via sonication. Cell debris was then harvested by centrifugation and the resulting supernatant loaded onto a Ni-NTA affinity chromatography column. The amount of unbound protein eluted in the flow-through was monitored by a continual measurement of the absorbance at 280 nm. The top of the column developed a brown colour typical of binding an FeS cluster bearing enzyme (Figure 2.9A). When the absorbance of the eluate returned to baseline, a Buffer B gradient was started to elute the bound HydG protein and fractions collected. The typical protein concentrations of the collected Ni column fractions are shown below in Figure 2.6.

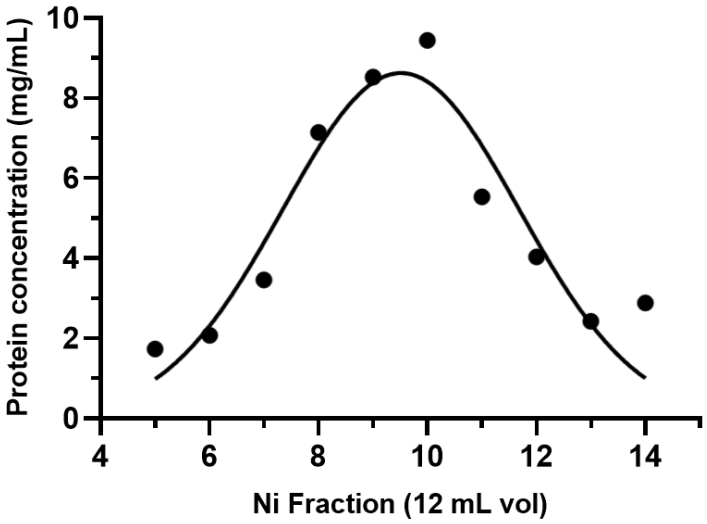

Figure 2.6 Protein concentration of collected Ni column fractions, fitted empirically to a Gaussian function (R^2 = 0.8841)

After concentrating the collected fractions containing the brown HydG protein. The protein was applied to the S-75 buffer exchange column equilibrated with Buffer C. The desalted brown fractions containing the HydG protein were then pooled and slowly reconstituted with ten molar equivalents of $FeCl_3$ and $Na_2S{\cdot}9H_2O$ and left stirring overnight [32, 108]. Where the protein concentration was low (typically during the first reconstitution), colour changes after the addition of the reconstituting compounds could be observed (Figure 2.7). During *Tl* purification during and after the reconstitution process protein precipitation was observed.

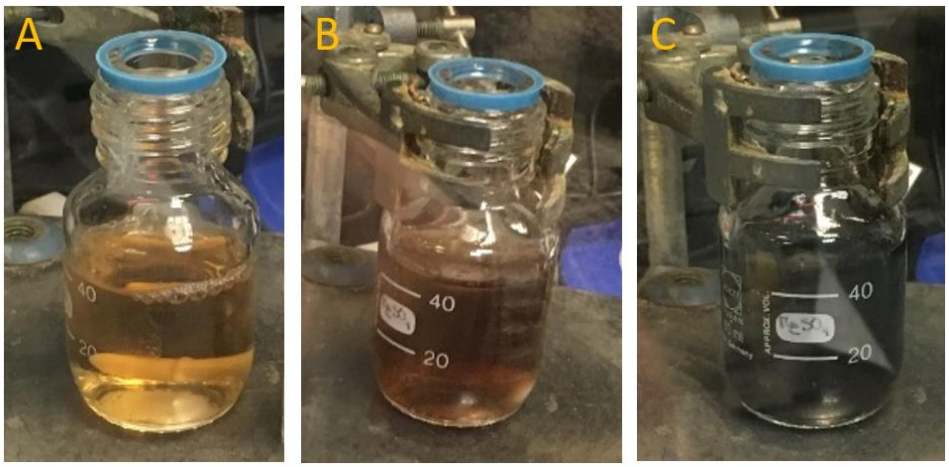

Figure 2.7 Fe-S Cluster Reconstitution of *Ti* HydG

A: Unreconstituted protein, **B:** protein after addition of 10 equivalents of $FeCl_3$ and **C:** protein after addition of 10 equivalents of $Na_2S{\cdot}9H_2O$.

The following day the reconstituted protein was centrifuged to remove some of the excess Fe-S colloid and any precipitated protein, before being concentrated and applied to a S200 gel filtration column (XK26, 300 mL) .This separated the reconstituted protein (brown in colour) from excess Fe-S colloid which eluted first as grey-coloured fractions. The protein fractions were then collected and pooled and further reconstituted with five molar equivalents of $FeCl_3$ and $Na_2S{\cdot}9H_2O$ before being concentrated to around 1 mM and frozen in small (100 µL) aliquots (method 13). The process is summarised in Figure 2.8 below.

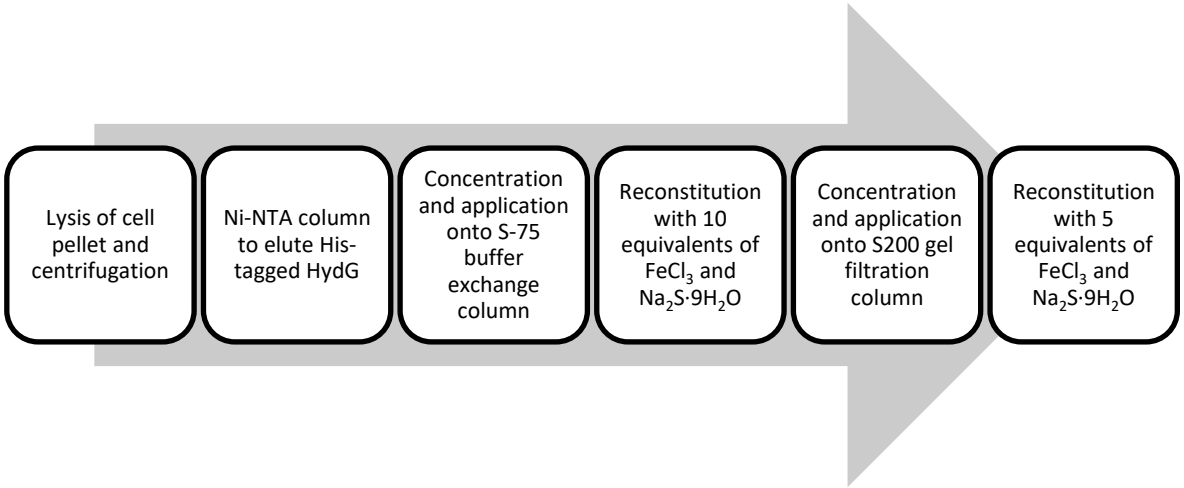

Figure 2.8 HydG Purification flow chart

Typical protein yield for *Ti* and *Tl* HydG expression are 120 and 25 mg from 30 g and 40 g cell pellets respectively.

Table 2.3 shows an example summary of the amount of protein present at each stage of the purification process for *Ti* HydGusing the Bradford assay.

Table 2.3 *Ti* HydG protein concentration during purification (one example purification).

Sample	**Protein concentration (mg/mL)**	**Total amount of protein (mg)**
Cell lysate	36.55	3430
Pooled Ni-NTA Fractions	46.22	1390
Pooled S-75 Fractions	8.63	315
Pooled S-200 Fractions (Final purified protein concentration)	42	109

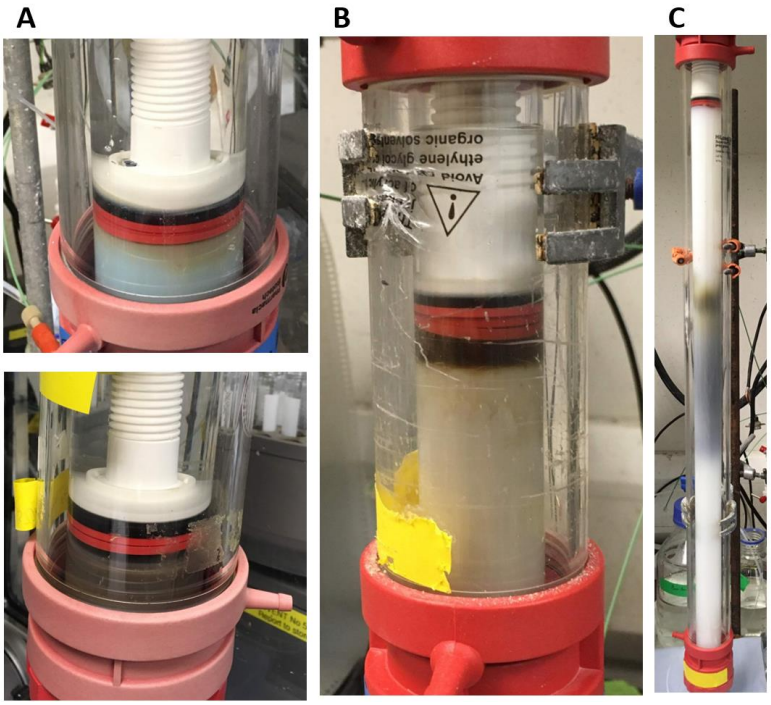

Figure 2.9 *Ti* HydG chromatography purification columns **A Top:** Initial stages of cell lysate being loaded on to Ni-NTA column; **A Lower:** Washing step of Ni-NTA purification, His tagged HydG bound to resin whilst unbound proteins elute; **B:** S-75 buffer exchange column; **C:** S-200 Size-exclusion column, Fe-s colloid elute first as grey/black band, golden brown HydG elutes later.

Throughout the purification process aliquots were collected for SDS-PAGE analysis (method 11) to monitor the purification (see Figure 2.10).

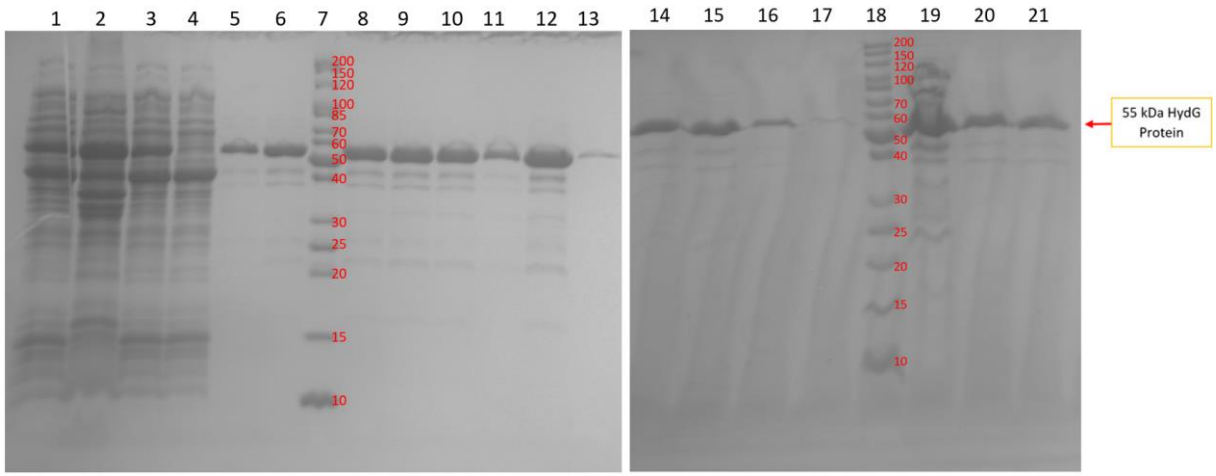

Figure 2.10 15% SDS-PAGE of *Ti* HydG Purification

1: Cell lysate; **2**: Lysed cell pellet; **3**: Lysed cell supernatant; **4:** Ni-NTA column flow-through; **5,6,8-11:** Ni column Fractions; **7:** Protein molecular weight ladder (kDa); **12:** Sample applied to S-75 column; **13:** Amicon waste (as a result of concentrating contents of lane 12); **14:** Pooled S-75 fractions; **15:** Protein solution after 1st reconstituion; **16,17:** Amicon waste (Concentration before spplication to S200 column); **18:** Protein molecular weight ladder (kDa); **19:** Solution applied to S200 column; **20:** Pooled S200 fractions; **21:** Protein solution after 2nd reconstituiton

SDS-PAGE analysis from *Ti* HydG purification (Figure 2.10) showed the final protein solution appears to have very few impurities (lane 21), the lower molecular weight bands present in the Ni-NTA column fractions are visibly less intense (mostly removed) after the S200 size-exclusion column (lanes 20-21). It is proposed that two of the bands in the Ni-NTA fractions (lanes 5-11) can be attributed to ISC machinery proteins which are co-expressed with *Ti* HydG (PRD003). The molecular weight of all ISC machinery proteins is shown below in Table 2.4. The bands at approximately 45 and 20 kDa are suggested to be IscS and HscB respectively. The other bands of the SDS-PAGE cannot be assigned to ISC protein and are likely to be *E.coli* cellular proteins.

Table 2.4 Molecular weight of ISC Machinery proteins [109, 110]

Protein	Molecular weight (kDa)
IscA	12
IscS	45
IscU	14
HscA	66
HscB	20
Fdx	12

It is possible to follow the reconstitution steps described above and in Figure 2.8 by UV-Visible spectroscopy [111], example traces are shown below in Figure 2.11.

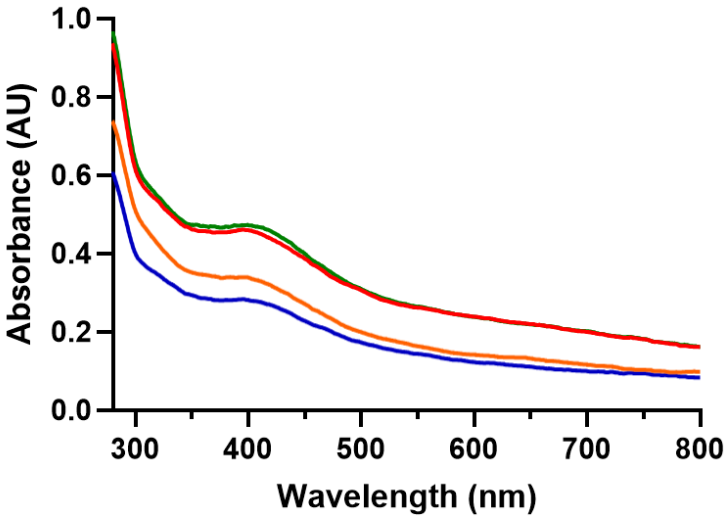

Figure 2.11 Representative UV-Vis spectra of HydG protein before and after reconstitution. Green trace; before first reconstitution, red trace; after first reconstitution, blue trace; before second reconstitution, orange trace; after second reconstitution.

There is a visible peak at approximately 410 nm for all traces in Figure 2.11 corresponding to the absorption of $[4Fe\text{-}4S]^{2+}$ clusters [111]. A smaller shoulder at 330 nm indicates the presence of $[2Fe\text{-}2S]^{2+}$ clusters [112]. After subtracting the background absorbance at 875 nm the extinction coefficient after the second reconstitution was calculated to be 32 mM^{-1} cm^{-1} (where the protein concentration has been calculated by Bradford assay). Assuming

an extinction coefficient of 16 mM^{-1} cm^{-1} for an $[4Fe\text{-}4S]^{2+}$ (4000 cm^{-1} M^{1} per iron atom) [111] this indicates the presence of two $[4Fe\text{-}4S]^{2+}$ clusters.

The reason there is no change after the first reconstitution is not known. The $[4Fe\text{-}4S]^{2+}$ peak at 410 nm suggests the protein had intact clusters before reconstitution, and co-expression with ISC machinery proteins should ensure partially reconstituted protein, however more likely the reconstitution step failed to incorporate further clusters, possibly Fe and S were added too quickly.

2.3 Summary

The expression and purification of the HydG RSAM enzymes from *Ti* and *Tl* using the pBAD vector system is already well established [32, 106]. Initially there were a few equipment issues caused by the apparatus being out of use for a period which had to be overcome. Specifically relating to the tricky nature of concentrating protein inside the glovebox (and powering the system). Once these issues were resolved the purification system worked reliably, which was key to the progress of this work.

This study replicated the previously established conditions for expression and purification producing comparable protein yields, approximately 24 mg of *Ti* HydG per litre of culture and 2.5 mg of *Tl* per litre of culture, with [Fe-S] cluster reconstitution confirmed via UV-vis. Due to the significantly lower yield of *Tl* HydG, future experimental work will be utilising *Ti* derived HydG.

Chapter 3 HydG Activity Assays

HydG catalyses the reductive cleavage of SAM to generate a 5'DOA radical which abstracts a hydrogen from tyrosine generating *p*-cresol, cyanide, carbon monoxide and water (Figure 1.7) [27, 77]. It is widely accepted that HydG generates an organometallic synthon containing an $Fe(CO)_2(CN)$ moiety which is incorporated into the H-cluster of HydA [77, 99]. This complex has been observed bound to HydG using EPR spectroscopy (Figure 3.1) [99], however, the metallosynthon has not been observed in an unbound form and therefore neither has the definitive [Cys][Fe(CO)x(CN)y] species released from HydG. The purpose of optimising HydG activity assays was to generate high concentrations of products to increase the likelihood of being able to observe the metallosynthon released from HydG using alternative techniques (for example HPLC, or XAFS). Previous work by Dr R. Driesener has established suitable buffer conditions for measuring the activity of HydG [95] and this method serves as the basis for the activity assays described herein (method 15).

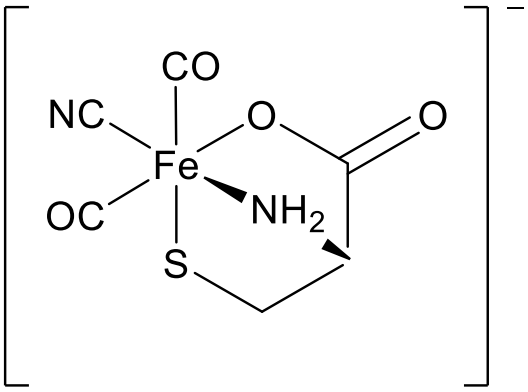

Figure 3.1 HydG metallosynthon $[Fe(CO)_2(CN)]$, reproduced from [99].

Initial experiments using synthetic standards of tyrosine, *p*-cresol, and 5'DOA established a suitable HPLC elution method, so that assay substrates and products could be reliably quantified. As SAM and tyrosine elute very quickly (within the first five minutes) it was necessary to reduce the flow from 1 mL/min to 0.8 mL/min and begin the organic buffer gradient at 0% to increase the retention times. A typical HPLC chromatogram from a one-hour end-point activity assay using the optimised elution method is shown below in Figure 3.2. The assay contained HydG (50 µM), tyrosine (1 mM), SAM (0.5 mM) and dithionite as a reductant, all components were prepared in assay buffer (50 mM HEPES, 500 mM KCl, pH7.4).

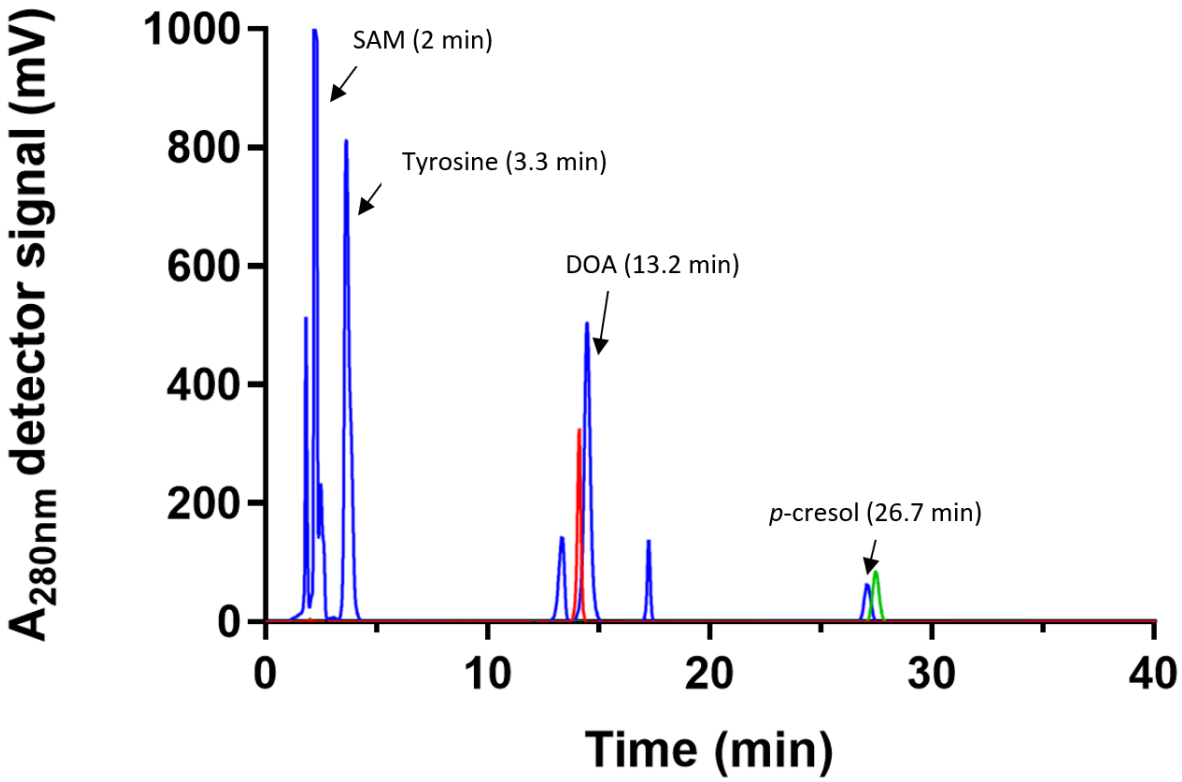

Figure 3.2 Chromatogram produced by end-point activity assay of HydG

Blue trace: Assay mixture after one hour incubation at 37 °C; Red trace: 100 µM DOA standard; Green trace: 75 µM *p*-cresol standard

The typical retention times for HydG assay substrates and products are as follows; SAM, 2 mins; adenine, 2.7 mins; tyrosine, 3.3 mins; DOA, 13.2 mins; MTA, 16.3 mins; and *p*-cresol, 26.7 mins.

Initial end-point HydG activity assays were prepared; HydG (50 µM) was incubated with SAM (0.5 mM), tyrosine (1 mM), dithionite (1 mM) and in the presence or absence of $MgCl_2$ (50 mM). Although $MgCl_2$ is not required for HydG to be active, it is a cofactor of the enzyme MTAN which we intended to use in future experiments. MTAN hydrolyses the N-ribosidic bond of adenine-based substrates, Figure 3.3 below shows the hydrolysis of DOA by MTAN [113-115]. The apparent activity of HydG was unaffected by the presence of $MgCl_2$ (data not shown).

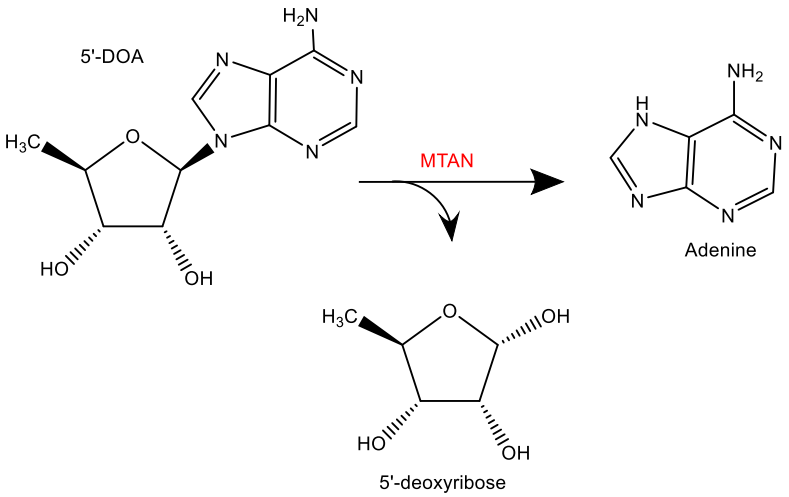

Figure 3.3 MTAN hydrolysis of DOA, reproduced from [113].

3.1 HydG Activity Time-course

Two time-course experiments were prepared where the activity of HydG was measured in the presence of commercially derived SAM and alternatively in the presence of enzymatically synthesized SAM.

Both assays also included incubation with an *E.coli* derived MTAN. This enzyme in addition to the SAM synthetase MAT enzyme were kindly provided by Lukas Karst and purified at the University of Freiburg.

The assay mix using synthetic SAM contained the following; tyrosine (4 mM), SAM (1 mM), dithionite (1 mM), HydG (40 µM), $MgCl_2$ (50 mM) MTAN (0.025 mg/mL).

The assay mix where SAM was enzymatically produced contained; tyrosine (4 mM), ATP (1 mM), Methionine (1 mM), dithionite (1 mM), $MgCl_2$ (50 mM), HydG (40 µM), MAT (methionine adenosyltransferase, 0.5 mg/mL) and MTAN (0.025 mg/mL). ATP and methionine are the substrates for the SAM synthetase enzyme MAT.

All substrates were prepared as stock solutions in degassed assay buffer (50 mM HEPES, 500 mM KCl, pH7.4) inside an anaerobic glovebox (80 µL final reaction volume). A stock mix of substrates and enzymes was prepared separately, and the enzyme mix added to the lid of the reaction tube. A negative sample was prepared without the enzyme mix and additional assay buffer added to the reaction. The reactions were initiated simultaneously

by inversion of the tubes immediately prior to incubation in a 37 °C water bath outside of the glovebox.

The reactions were stopped at the selected time-points by addition of 6 µL 20% perchloric acid; 0, 5, 10, 20, 25, 35, 65 and 125 mins. After addition of acid, the reaction tubes were gently mixed and stored at -20 °C until analysis by RP-HPLC (method 17).

The products of the assays were analysed by the HPLC separation method described in method 17; buffers contained 0.1 % acetic acid in water (inorganic) and acetonitrile (organic).

The accumulation of the reaction products *p*-cresol and adenine were measured to assess the activity of HydG. Figure 3.4 compares the accumulation of *p*-cresol from enzymatically produced SAM and commercial SAM. There is no discernable difference between the two assays when using the generation of *p*-cresol as a measure.

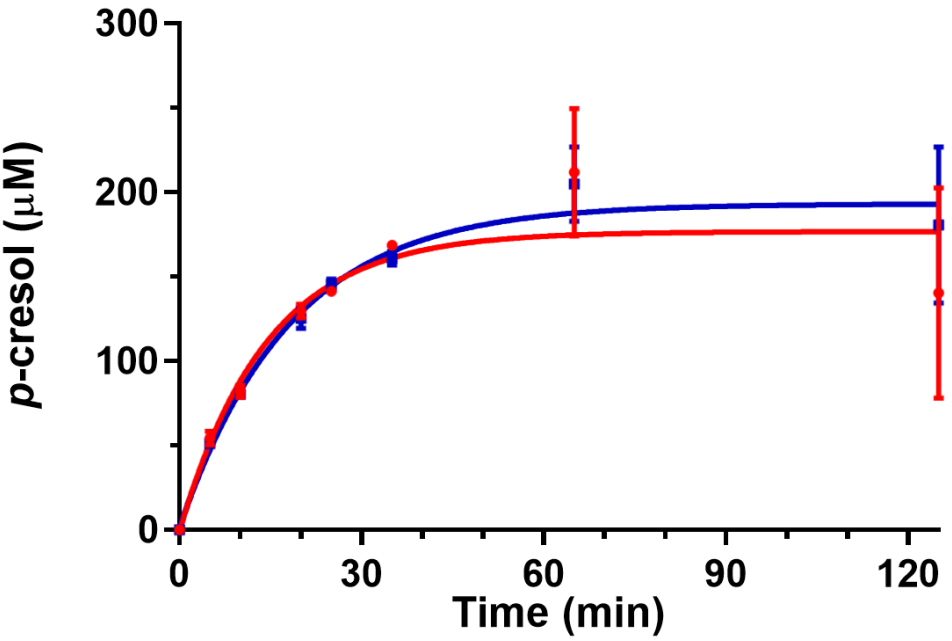

Figure 3.4 Accumulation of para-Cresol during HydG activity assay time-course, data fitted empirically to a one-phase association model (Y=Y0 + (Plateau-Y0)*(1-exp(-K*x))).

Blue trace: Enzymatically produced SAM assay; **Red trace**: Commercially produced SAM. HPLC separation method used for analysis here is 0.1% acetic acid in water/acetonitrile (method 17). Each time point is the mean and standard deviation of duplicates.

When analysing the accumulation of adenine (Figure 3.5) when commercially produced SAM is the substrate for radical generation there is overall a greater amount of adenine produced, indicating a higher turner over of HydG and MTAN. None of the time points measured had a quantifiable concentration of DOA present, indicating all that was produced was very quickly hydrolysed to adenine. This difference in adenine concentration is surprising as the amount of *p*-cresol produced is so similar for each assay.

For the enzymatically synthesised SAM the ratio of *p*-cresol to adenine is approximately 1:1 as you would expect, indicating no uncoupled SAM cleavage. However, in the commercially available SAM assay the ratio of adenine to *p*-cresol is approximately 1.4:1. As previously described, this could be due to the release of products being rate limiting after the initial turnover of SAM. This causes an increase in the chances of uncoupled SAM turnover [116]. Additionally, it has previously been reported that commercial SAM can contain 5'-methylthioadenosine which can also be hydrolysed by MAT to adenine which may account for the greater production of adenine [116, 117].

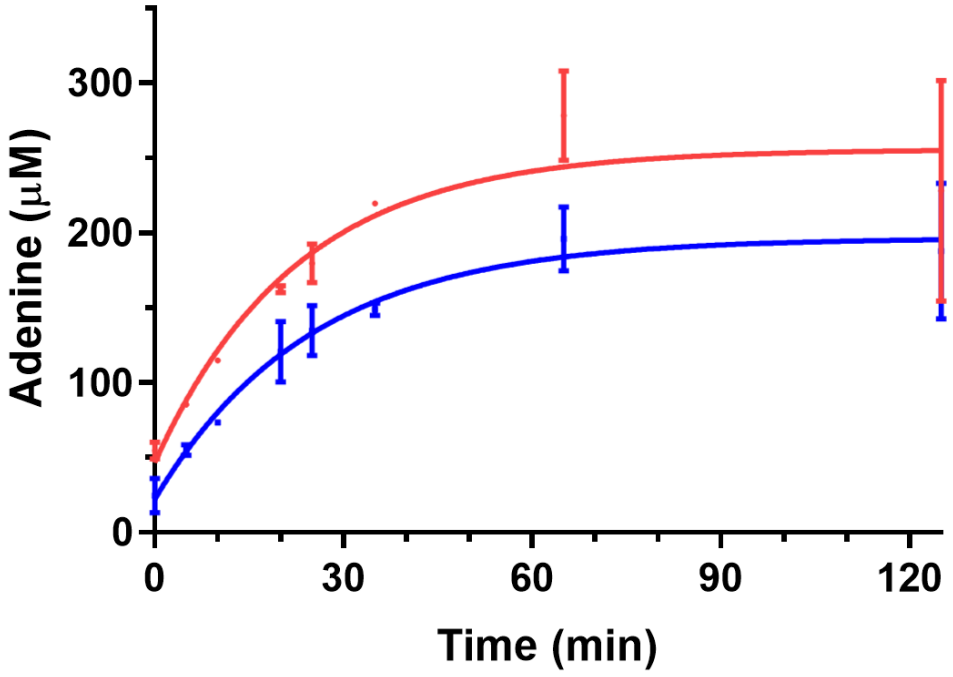

Figure 3.5 Accumulation of Adenine during HydG activity assay time-course, data fitted empirically to a one-phase association (Y=Y0 + (Plateau-Y0)*(1-exp(-K*x))).

Blue trace: Enzymatically produced SAM assay; **Red trace**: Commercially produced SAM. HPLC separation method used for analysis here is 0.1% acetic acid in water/acetonitrile (method 17). Each time point is the mean and standard deviation of duplicates.

The initial turnover number was calculated as previously described using the equation below [116]:

$$k_{cat}^{0} = \frac{k[\mathrm{p}]_{max}}{[\mathrm{E}]}$$

Where E is the HydG concentration.

A summary of the calculated kinetic data is shown in Table 3.1 below. The results summarised in Table 3.1 below are comparable to previously reported kinetic analysis of the radical SAM enzyme ThiH [116].

Table 3.1 Quantification of products produced during HydG assay time-course

SAM	Product	Final Concentration (µM)	Span (µM)	k (x10^{-4} s^{-1})	R^2	k_{cat}^{0} (x10^{-4} s^{-1})
Commercial	*p*-cresol	177 ±14.4	178 ±21.5	11.5 ±3.4	0.84	51.1 ±15.6
	Adenine	256 ±17.6	209 ±22.0	7.39 ±1.9	0.88	47.2 ±12.6
Enzyme synthesised	*p*-cresol	193 ±9.2	192 ±12.6	9.1 ±1.4	0.95	43.9 ±7.1
	Adenine	196 ±11.2	174 ±13.5	6.73 ±1.2	0.93	33.0 ±6.2

Kinetic analyses and the concentration of products in Table 3.1 indicate HydG activity is approximately equivalent in the presence of enzymatically produced and synthetic SAM, the final concentration of *p*-cresol and span (approximately plateau concentration minus t = 0) of adenine are very similar (overlapping standard deviations). For this reason all future activity assays described are tested in the presence of commercially derived SAM.

3.2 Optimising HydG Activity Assays

The aim of optimising the HydG activity assay is to maximise the concentration of released metallosynthon for it to be isolated and resolved.

It is proposed here that adding Fe (in the form of $Fe(II)SO_4$) and cysteine (Cys) to the activity assays will promote high concentrations of released metallosynthon as they may replace the labile Fe and Cys ligand lost from the [4Fe-4S] cluster upon release of the metallosynthon. Imidazole was also added as it could replace and stabilise the ring of the released metallosynthon [118]. Activity assays were run to assess if these additions would have any impact on the HydG activity, there was no notable difference with these additives present (data not shown). The concentration of Fe(II) and Cys was typically 0.5 mM, unless otherwise stated and imidazole 1 mM.

3.2.1 Alternative Reducing Agents

The [4Fe4S] cluster is only active in its 1+ reduced state, it is therefore necessary for the activity assay environment to contain a reducing agent. The reducing agent used in these experiments is dithionite [93, 108]. Alternative reducing agents have been used previously by Bridwell-Rabb *et al.* when investigating the catalytic activity of the Cbl-dependent radical SAM enzyme OxsB, in addition to sodium dithionite, reductants used in these experiments include NADPH/methyl viologen and titanium(III) citrate/methyl viologen amongst others [119].

We tested methyl and benzyl viologen as alternative reducing agents in *in vitro* HydG activity assays and found there was very little difference when compared to assays with sodium dithionite as the reductant. Increasing the concentration of the viologen also showed no notable improvement on activity (Figure 3.6 a,b). The concentration of dithionite used in the assay was titrated up to 20 mM and 3 mM was found to be a suitable concentration to achieve maximum activity (Figure 3.6 c) therefore this concentration was used for all future assays. To test whether the dithionite may be becoming less effective after prolonged incubation an alternative assay where aliquots of dithionite were added to the assay at intervals was set up (rather than only when the assay is initiated). There was no improvement in HydG activity observed (data not shown).

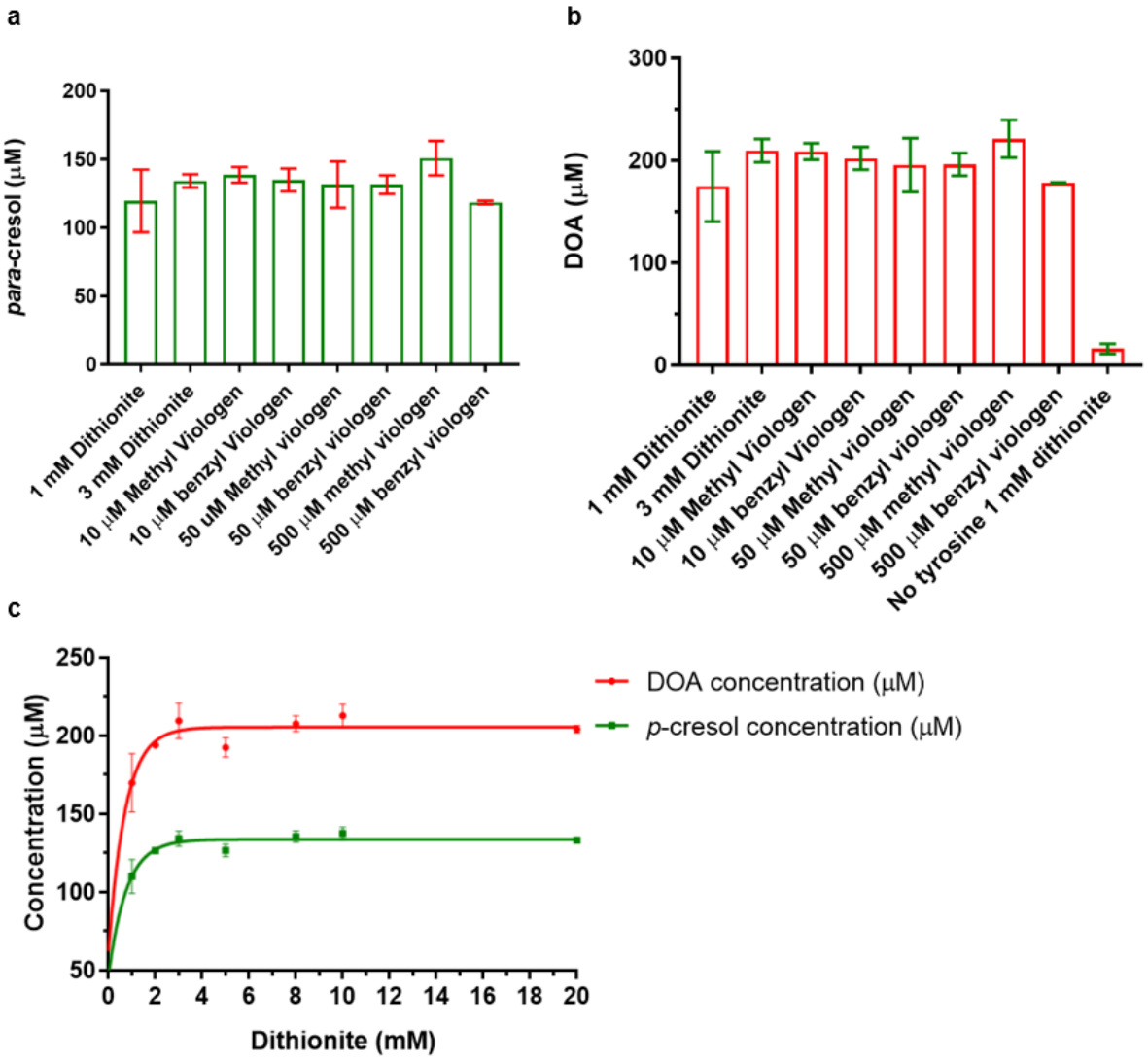

Figure 3.6 Reducing agent optimisation a,b, final concentration of DOA and *p*-cresol from HydG activity assay with dithionite, methyl, and benzyl viologen as reducing agents. c, final DOA and *p*-cresol concentration produced from dithionite titration HydG activity assays, data fitted to a one-phase association curve, R^2 0.73 and 0.65 for *p*-cresol and DOA respectively. Average and standard deviation for all assays are calculated from two replicates, assays incubated for 1 hour at 37°C.

3.2.2 DOA Inhibition and MTAN

DOA is known to be an inhibitor of various Radical SAM enzymes [115, 120, 121]. Specifically BioB, LipA and ThiH have all been shown to be inhibited by the products DOA and methionine [120]. All three enzymes were found to be inhibited by DOA weakly and only BioB and LipA were weakly inhibited by methionine [120]. As mentioned previously

MTAN hydrolyses the N-ribosidic bond of adenine based substrates, Figure 3.3 above shows the hydrolysis of DOA [113-115].

The addition of MTAN to an activity assay has been shown to increase the activity of radical SAM enzymes by removing the reaction products [120] for this reason, as part of the optimisation of the activity assay we investigated DOA inhibition of HydG and tested the addition of *E.coli* MTAN (kindly provided by Lukas Karst, University of Freiburg) to the assay.

DOA was found to inhibit HydG activity, and 1 mM DOA resulted in 60–70 % inhibition (Figure 3.7), the apparent IC_{50} is 48.5 ± 1.59 µM DOA. This is slightly greater than the inhibitory effect of 1 mM DOA observed for ThiH, LipA and BioB which was 50-60 % [120].

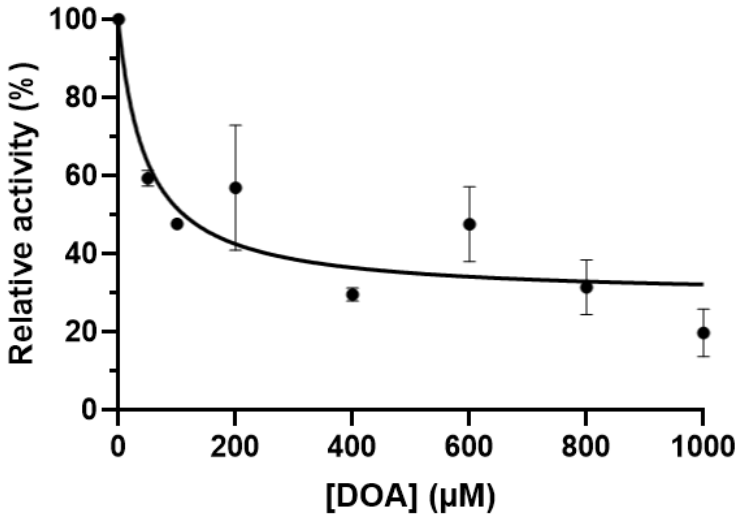

Figure 3.7 The effect of increasing concentrations of DOA on HydG activity. Data fitted to nonlinear regression, [inhibitor] vs. response (three parameters).

In assays prepared with MTAN, when measuring the formation of adenine relative to the amount of DOA produced in parallel reactions without MTAN there is no observable difference. There is a background level of adenine in all assays, 5'-methylthioadenosine (MTA) is known to be a contaminant of commercial SAM which can be hydrolysed by MTAN to produce adenine [116]. We have also found there is a background of adenine without enzyme present (observed on HPLC traces where only commercial SAM is present, data not shown) this could also be a contaminant or a product of degradation. For this reason, it is necessary to subtract the background adenine concentration observed in negative samples

to normalise the results. When this background, from an assay containing MTAN and no tyrosine (where only uncoupled turnover will occur) is subtracted the amount of DOA and adenine produced is comparable (when an assay is incubated at 37 °C for an hour). This is a surprising result and contrary to previous observations [120] although it may be due to the awkward nature of attempting to calculate the actual adenine concentration (Figure 3.8 **a**). However, when comparing the concentration of *p*-cresol in the presence/absence of MTAN there is a visible difference, with slightly more *p*-cresol produced in the presence of MTAN (Figure 3.8 **b**) supporting the conclusion from [120] that radical SAM enzymes have enhanced activity in the presence of MTAN. The calculated kinetics of these assays are shown below in Table 3.2.

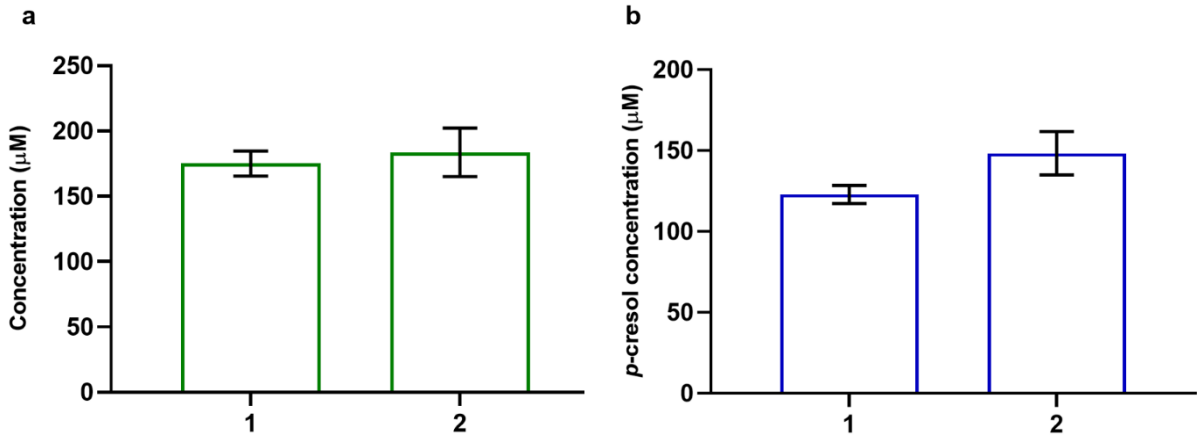

Figure 3.8 Effect of adding MTAN to HydG assay. **a,** Concentration 1 represents the concentration of DOA produced in a HydG assay in the absence of MTAN. Concentration 2 is the amount of adenine produced from a HydG assay containing 0.025 mg/mL MTAN. **b**, Concentration 1 represents the concentration of *p*-cresol produced in a HydG assay in the absence of MTAN. Concentration 2 is the amount of *p*-cresol produced from a HydG assay containing 0.025 mg/mL MTAN.

Both assays were set up in parallel, incubated at 37 °C for 1 hour, mean and standard deviation calculated from duplicates. In **a** the background concentration of uncoupled trunover (in the absence of tyrosine) for DOA and adenine has been subtracted from both data sets respectively, there is no background *p*-cresol peak to subtract.

Table 3.2 Kinetic characterisation of HydG assay in the presence and absence of MTAN.

Sample	Description	Product	Concentration (μM)	Apparent linear rate (nM s^{-1})	Apparent turnover number k_{cat}^{app} (x10^{-4} s^{-1})
1	HydG No MTAN	DOA	175 ± 6.8	48.7 ± 1.9	12.2 ± 0.5
		p-cresol	123 ± 3.9	34.1 ± 1.1	8.5 ± 0.3
2	HydG + MTAN	Adenine	184 ± 13.1	50.9 ± 3.6	12.7 ± 0.9
		p-cresol	148 ± 9.5	41.2 ± 2.6	10.3 ± 0.7

3.2.3 Temperature and Time

Previously HydG activity assays were incubated at 37 °C for up to 2 hours. We tested the activity for much longer at both lower and higher temperatures and made some interesting observations.

An activity assay was set up the same as previously described with and without MTAN and left to incubate overnight (approx. 16 hours) at 18 °C (the assay was incubated inside the glovebox. The glovebox is in a temperature controlled room). The amount of DOA/adenine and *p*-cresol produced by these assays is shown below in Figure 3.9.

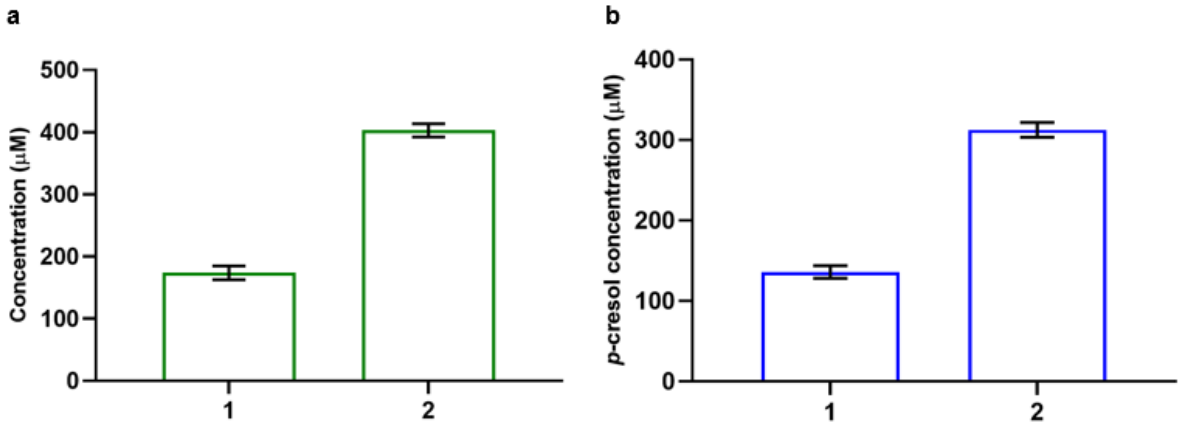

Figure 3.9 HydG assay incubated at 18 °C overnight in the presence and absence of MTAN. **a,** Concentration 1 represents the concentration of DOA produced in a HydG assay in the absence of MTAN. Concentration 2 is the amount of adenine produced from a HydG assay

containing 0.025 mg/mL MTAN. **b**, Concentration 1 represents the concentration of *p*-cresol produced in a HydG assay in the absence of MTAN. Concentration 2 is the amount of *p*-cresol produced from a HydG assay containing 0.025 mg/mL MTAN.

Both assays were set up in parallel, average and standard deviation calculated from duplicates. In **a** the background concentration of uncoupled turnover (in the absence of tyrosine) for DOA and adenine has been subtracted from both data sets respectively, there is no background *p*-cresol peak to subtract. The average unsubtracted DOA and adenine concentration are 193.7 ±7.9 µM and 585.7 ±7.5 µM respectively.

The data in Figure 3.9 and Table 3.3 clearly shows the addition of MTAN has improved the activity of HydG and that both HydG and MTAN remain active for much longer than previously tested. Comparing the data for both assays here with previously reported turnover numbers for wild-type HydG show we are making considerable improvements; apparent DOA and *p*-cresol turnover (k_{cat}^{app}) previously reported as 2.3 ± 0.3 and 1.8 ± 0.2 ($x10^{-3}s^{-1}$) respectively [93].

Table 3.3 Kinetic characterisation of overnight HydG assay in the presence and absence of MTAN.

Sample	Description	Product	Concentration (µM)	Apparent linear rate (nM s^{-1})	Apparent turnover number k_{cat}^{app} ($x10^{-4}s^{-1}$)
1	HydG No MTAN	DOA	174 ± 7.9	2.93 ± 0.13	43.5 ± 2.0
		p-cresol	135 ± 5.6	2.29 ± 0.09	34.0 ± 1.4
2	HydG + MTAN	Adenine	403 ± 7.5	6.79 ± 0.13	101 ± 1.9
		p-cresol	313 ± 6.5	5.26 ± 0.11	78.1 ± 1.6

The apparent linear rates described in Table 3.3 are significantly lower than for HydG assays incubated at 37 °C for 1 hour, this is understandable as the enzyme will be less active at lower temperatures and it is expected that the activity will decrease over time. In order to find some insight into how quickly the activity reduces a 120 hour time course was set up (with MTAN present), where the incubation temperature was 18 °C. After 24 hours HPLC

analysis had shown the concentration of SAM had been reduced to approximately 20 % of the starting concentration, therefore after stopping the 48 hour sample a further 1 mM SAM and 3 mM dithionite were added (so the final concentration in remaining time-points were 2 mM SAM and 6 mM dithionite). The accumulation of adenine and *p*-cresol is shown below in Figure 3.10.

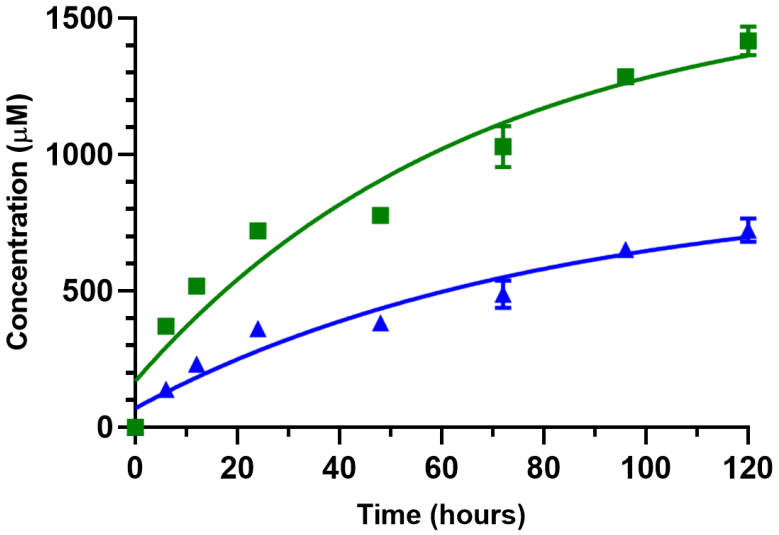

Figure 3.10 HydG 120 hour activity assay time-course incubated at 18 °C in the presence of MTAN. **Green squares** represent concentration of adenine, **blue triangles** represent concentration of *p*-cresol. Both data sets have fitted empirically to a one-phase association curve.

The initial turnover number was calculated as previously described using the equation below [116]:

$$k_{cat}^{0} = \frac{k[\mathrm{p}]_{max}}{[\mathrm{E}]}$$

Where E is the HydG concentration.

Table 3.4 Kinetic characterisation of HydG in the presence of MTAN 120-hour time-course.

Product	Final concentration (µM)	k (x10^{-6} s^{-1})	R^2	k_{cat}^0 (x10^{-4} s^{-1})
Adenine	1600 ±113	4.2 ±0.73	0.94	1.68 ±0.32
p-cresol	875 ±165	3.5 ±1.2	0.94	0.77 ±0.30

The adenine concentration should be treated with a high degree of caution as there was only one negative sample (incubation without tyrosine) taken at 120 hours. The adenine concentration of this sample was 641.9 ±30.8. Therefore background adenine from uncoupled turnover (which has been reported to be increased with the addition of MTAN [116]) and hydrolysis of MTA present in commercial SAM will be contributing to the overall adenine concentration. This second explanation for increased adenine may be particularly relevant for samples after 48 hours which contain additional SAM. The kinetic analysis for the first 48-hour samples only is shown below in Table 3.5.

Table 3.5 Kinetic characterisation of HydG in the presence of MTAN up to 48 hours of time-course.

Product	Final concentration (µM)	k (x10^{-6} s^{-1})	R^2	k_{cat}^0 (x10^{-4} s^{-1})
Adenine	786 ±8.9	27.0 ±1.4	0.996	5.32 ±0.27
p-cresol	403.6 ±4	21.4 ±0.93	0.991	2.16 ±0.10

The ratio of adenine to *p*-cresol is approximately 1.9:1 and surprisingly the ratio after the first 48 hours has a greater difference than 120 hours. It is difficult to compare the results of this activity assay with previously reported kinetics because of the unprecedented time the experiment has been allowed to run and the lower temperature [93, 116].

As HydG was shown to remain active at 18 °C much longer than previously investigated at 37 °C, activity assays were prepared in parallel (all containing MTAN, with 2 mM SAM)

and incubated at 18 °C, 37 °C and 60 °C for 1 hour and 24 hours. The amount of adenine and *p*-cresol produced are shown below in Figure 3.11.

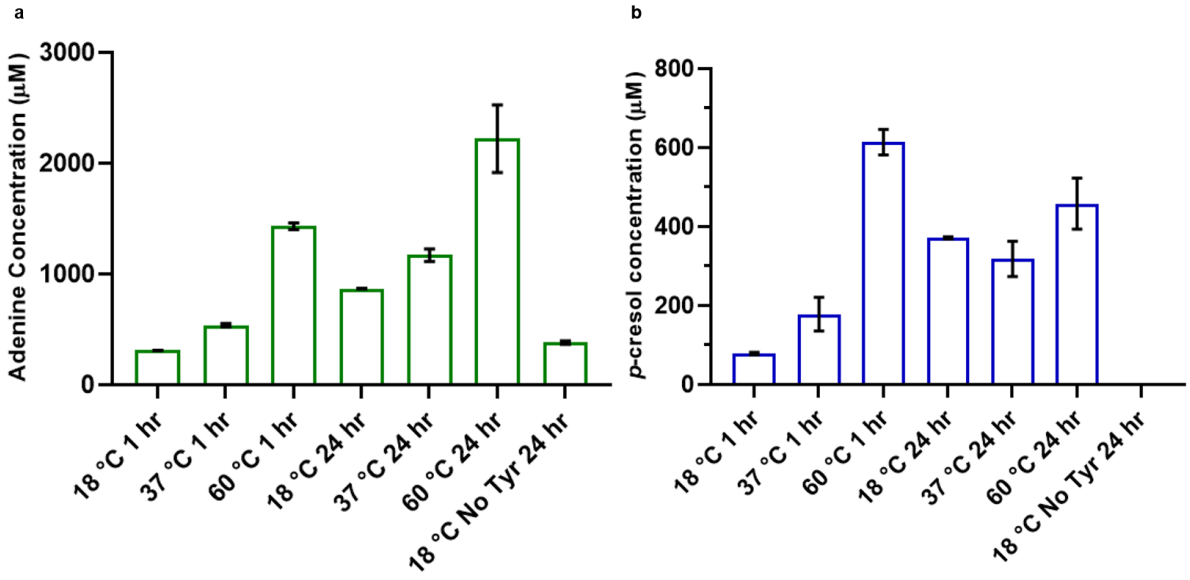

Figure 3.11 HydG Activity assay incubated at 18 °C, 37 °C and 60 °C in the presence of MTAN. **a,** shows the production of adenine, **b,** shows the production of *p*-cresol. All time and temperature samples are shown as an average of duplicates.

The adenine concentration in Figure 3.11**a** can be assumed to be an overestimation as the background concentration has not been subtracted. It is clear from the adenine concentration sample incubated at 18 °C for 24 hours in the absence of tyrosine (382.1 ±10.4 µM) that uncoupled turnover is occurring. To correct this concentration, it would be necessary to measure the background adenine concentration (produced in the absence of tyrosine) for all temperatures and incubation times. It is interesting to observe across the 1 hour samples, the assay incubated at 60 °C produced over three times the amount of *p*-cresol than the 37 °C sample produced, whereas over 24 hours the amount of *p*-cresol for all assays is almost within the standard deviation, and when comparing the amount of *p*-cresol in the 60 °C 1 hour and 24 hour sample there is a lower concentration after 24 hours. The reason for this is unknown, it is possible that the *p*-cresol has degraded over time. If this were the case it would be useful to investigate what the degradation product was and measure this. No assays contained a reliably quantifiable amount of DOA (<10 µM) indicating the MTAN remained active. SAM was always present in sufficient concentrations

at HPLC quantification that it is not predicted to have reduced HydG activity (approximately ≥ 100 µM). *Ti* is a thermophilic bacteria with an optimum growth temperature of 70 °C [122], it is therefore not surprising it's activity is greater at higher temperatures. The kinetic characterisation for the formation of *p*-cresol for 1 hour incubation samples (Figure 3.11) is shown below in Table 3.6.

Table 3.6 kinetic characterisation of 1 hour incubation of HydG activity assay in the presence of MTAN at 18 °C, 37 °C and 60 °C

Temperature (°C)	*p*-cresol concentration (µM)	Apparent linear rate (nM s^{-1})	Apparent turnover number k_{cat}^{app} (x$10^{-4}s^{-1}$)
18	78.5 ±2.2	21.8 ±0.62	5.5 ±0.15
37	178 ±30.1	49.5 ±8.4	12.4 ±2.1
60	614 ±22.7	170 ±6.3	42.6 ±1.6

As 60 °C is still lower than the optimum growth temperature it may not be the temperature where the *Ti* HydG is most active. To determine the optimum temperature a series of assays were set up and incubated at temperatures between 50 and 100 °C. The assays were incubated for 15 minutes as HydG should be in the linear phase of activity and the concentration of substrates will be saturating. A summary of the results for this experiment are shown below in Figure 3.12.

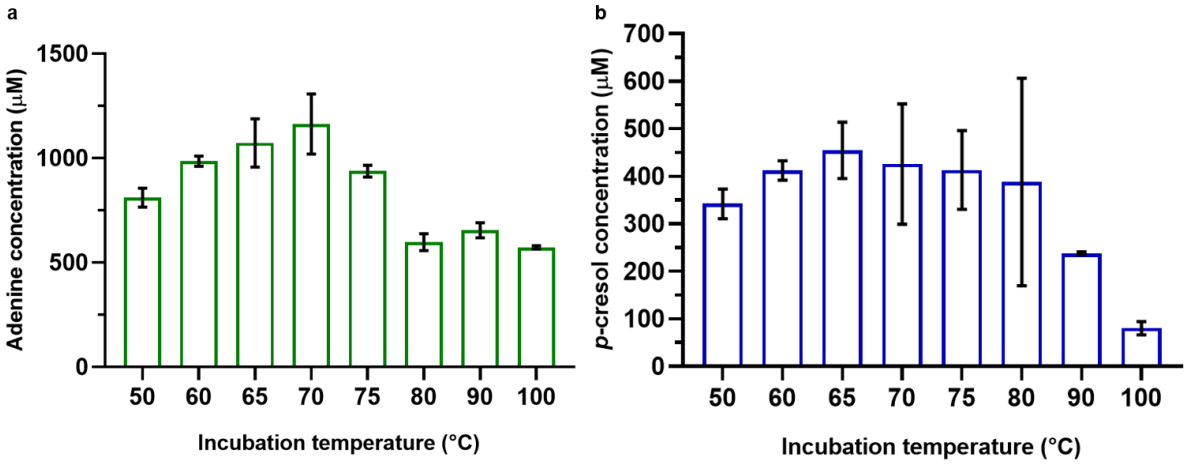

Figure 3.12 HydG activity assay in the presence of MTAN, 15 min temperature gradient incubation. **A,** shows the production of adenine, **b,** shows the concentration of *p*-cresol produced. All temperature samples are shown as an average of duplicates.

The reason for the large standard deviation between *p*-cresol replicates is not understood (Figure 3.12**b**) but could be attributed to the short incubation time highlighting any minor pipetting errors between replicates, which are less noticeable in adenine calculations due to the higher concentrations. For this reason, it is difficult to conclusively deduce the optimum temperature for the activity assay based on this experiment alone. However, we did think it was important to see how the amount of adenine produced quickly falls after 70-75 °C. We propose the reason for this is that the *E.coli* MTAN will become denatured at such high temperatures. The optimum growth temperature for *E.coli* is typically 27-39 °C [123] however particular strains (BJ5183 and DH5alpha) have been grown consistently up to 49 °C [124]. This explanation is supported by an increase in DOA produced at these temperatures (Figure 3.13**a** below). The kinetic analysis for the formation of *p*-cresol for the data in Figure 3.12**a** is shown below in Table 3.7.

Table 3.7 Kinetic analysis summary for HydG activity assay in the presence of MTAN, 15 min temperature gradient incubation.

Incubation Temperature (°C)	*p*-cresol concentration (μM)	Apparent linear rate (nM s^{-1})	Apparent turnover number k_{cat}^{app} ($x10^{-4}s^{-1}$)	Enzyme turnover [P]/[HydG]
50	342 ±22.0	380 ±24.5	95.0 ±6.12	8.55 ±0.550
60	412 ±14.4	458 ±16.0	115 ±4.01	10.3 ±0.361
65	454 ±41.8	505 ±46.4	126 ±11.6	11.4 ±1.04
70	426 ±89.5	473 ±99.5	118 ±24.9	10.6 ±2.24
75	413 ±58.6	459 ±65.1	115 ±16.3	10.3 ±1.46
80	388 ±154	431 ±172	108 ±42.9	9.69 ±3.86
90	237 ±2.14	264 ±2.38	65.9 ±0.595	5.93 ±0.0535
100	80.0 ±9.85	88.9 ±10.9	22.2 ±2.73	2.00 ±0.246

Another consideration when incubating the activity assays at high temperature is the stability of SAM under these conditions. To measure this, 2 mM SAM samples were prepared in assay buffer and incubated for 15 mins at the temperatures described above and the concentration of SAM remaining at the end of the incubation period calculated. The data is shown below in Figure 3.13**b**.

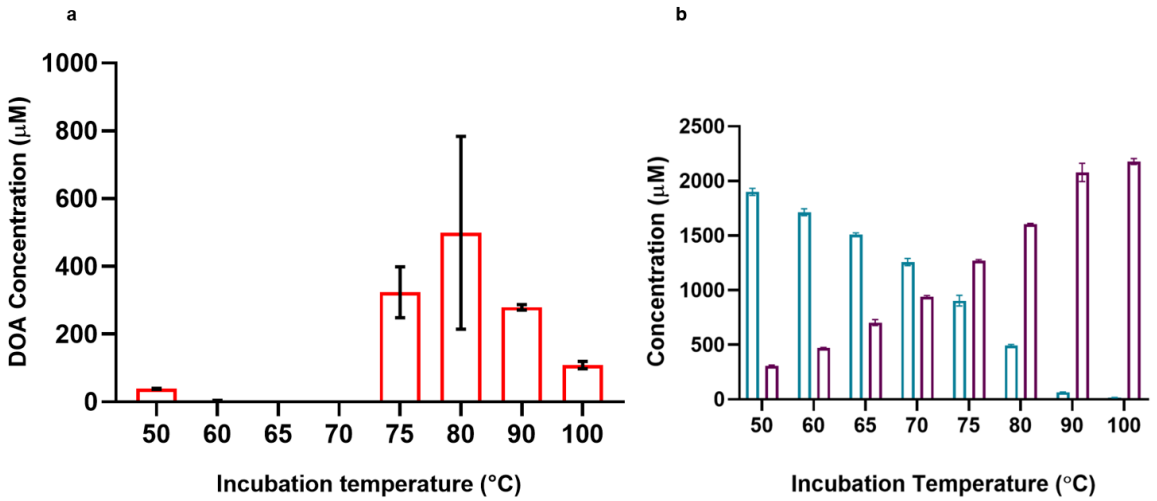

Figure 3.13**a** HydG activity assay in the presence of MTAN, 15 min temperature gradient incubation, red shows the concentration of DOA present at the end of the incubation time. 3.13**b,** Incubation of 2 mM SAM for 15 mins at assay temperatures, blue shows the concentration of SAM remaining at the end of the incubation and purple shows the concentration of MTA remaining at the end of the incubation time.

SAM degrades faster at higher temperatures, as demonstrated by the decrease in concentration of SAM as the incubation temperature increases in Figure 3.13**b**. SAM is capable of three degradation pathways. The SAM degradation is dependent on pH, at basic pH SAM degrades by nucleophilic addition by the α-carboxylate onto the γ-C of methionine forming MTA and homoserine lactone (HSL). In acidic pH SAM will become deprotonated at C-5' resulting in a cascade forming adenine and S-ribosylmethionine [125]. The assay buffer is basic (pH 7.4), Figure 3.14 shows the degradation of SAM forming MTA which is proposed to occur in the activity assay conditions.

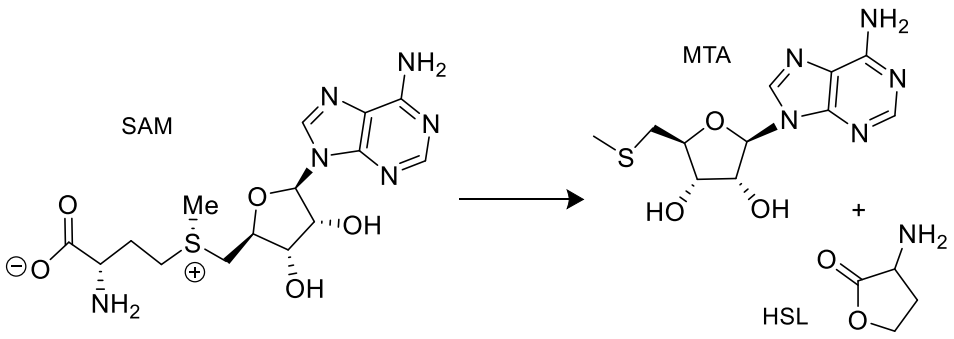

Figure 3.14 Degradation pathway of SAM resulting in MTA and homoserine lactone

3.3 Summary

In this chapter we probed several factors which could affect HydG activity; assay components including the reductant, substrate source, product inhibition and the time and temperature of the assay incubation. With the aim of improving the activity.

HydG activity appeared to be unaffected by the source of SAM and the reductant.

In agreement with previous work by Challand *et al.* on the RSAM enzymes BioB, LipA and ThiH [120], HydG showed inhibition in the presence of excess DOA (60–70 % reduction in activity in the presence of 1 mM DOA). The addition of MTAN alone resulted in only a small increase in the observed activity in assays incubated at 37°C for 1 hour, the apparent linear rate for *p*-cresol production increased from 34.1-41.2 nM s^{-1}.

However, upon incubating HydG activity assays for longer periods of time and at higher temperature the presence of MTAN significantly increased the concentration of product produced compared to assays without MTAN (Table 3.3 and Table 3.6). The *E.coli* MTAN appears to remain active at temperatures ≤70 °C, Figure 3.13a shows a DOA peak at 75 °C but not at 70 °C, indicating the temperature where the enzyme becomes deactivated/denatured is between 70-75 °C. Another consideration of incubating the assay at high temperature was the affect this would have on the stability of SAM. SAM is in excess in the activity assays and the concentration after incubation at 80 °C 15 minutes remained high (approximately 500 µM) suggesting this had not become a limiting factor in HydG activity.

Chapter 4 MTAN

HydG activity assay results suggest that incubation above 70 °C causes the *E.coli* MTAN protein lose activity/denature. This chapter describes attempts to express and purify an alternative hyperthermophilic MTAN species.

4.1 *T.maritima* Expression and Purification

The *T.maritima* nucleotide sequence encoding the MTAN gene was codon optimised for expression in *E.coli* and synthesised and sub cloned between *NcoI* and *XhoI* restriction sites of an empty pET-16b vector by Invitrogen GeneArt™ ThermoFisher Scientific. An N-terminal 6xHistidine tag was inserted to allow Ni-NTA purification and an *NdeI* restriction site inserted between the His tag and coding sequence (to allow the his tag to be removed).

JM109 and BL21 (DE3) competent cells were chemically transformed with the *T.maritima* MTAN plasmid (method 4). JM109 *E.coli* cells were used to prepare plasmid stocks and BL21 (DE3) strain used for protein expression. Successful transformation was confirmed by analytical digest of isolated plasmid DNA, see Figure 4.1 (method 6).

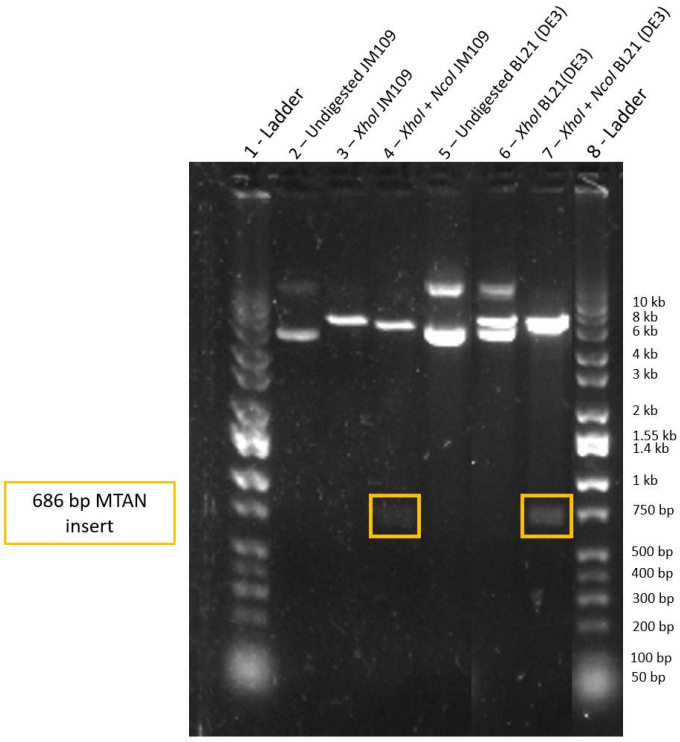

Figure 4.1 Analytical digest of *E.coli* strains transformed with *T.maritima* MTAN plasmid.

A small scale expression study (method 9) was used to identify the optimum conditions to express the *T.maritima* MTAN protein.

Table 4.1 below describes the conditions tested, all cell cultures were induced with IPTG at approximately 0.6 OD_{600nm}.

Table 4.1 *T.maritima* MTAN small-scale expression conditions

Condition	[IPTG] mM	Expression (hours)	Expression (°C)	Pellet mass (g)
1	1	4	27	1.01
2	1	4	16	0.87
3	1	6	27	1.17
4	1	6	37	1.05
5	1	16	27	1.55
6	1	16	37	1.39
7	1	16	16	1.27
8	1	16	4	0.58
9	0.4	4	16	0.88
10	0.4	4	4	0.67
11	0.4	4	27	1.05
12	0.4	4	37	0.89
13	0.4	16	16	1.15
14	0.4	16	4	0.72

The cell lysate, insoluble protein in the pellet and soluble protein in the supernatant were analysed by SDS-PAGE, Figure 4.2. BL21 (DE3) cells expressing an empty pET16b plasmid were included in the expression study to identify the MTAN protein band on the gel.

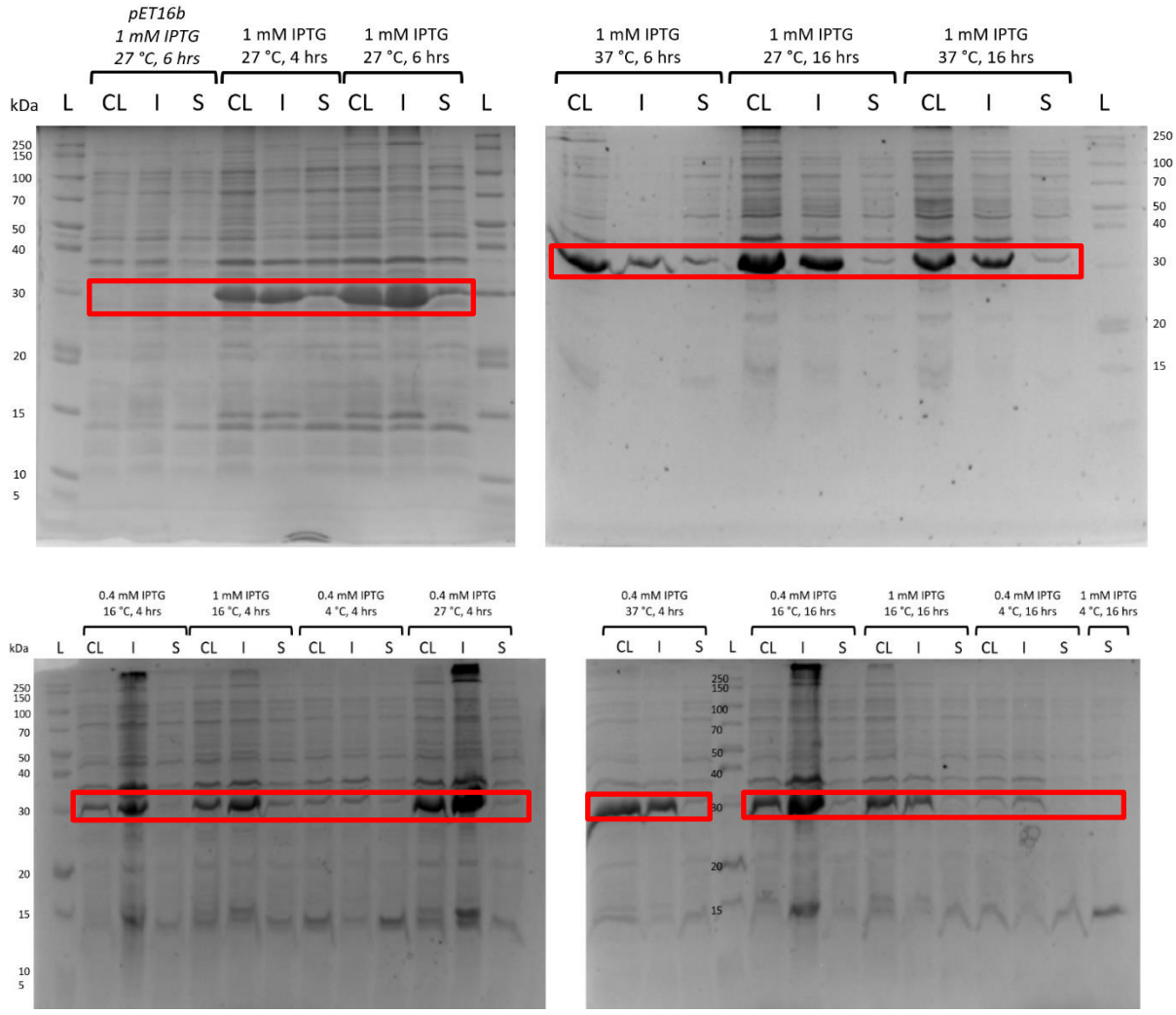

Figure 4.2 SDS-PAGE analysis of *T.maritima* MTAN small scale expression. L = protein molecular weight ladder, CL = whole cell lysate, I = insoluble protein pellet, S = soluble protein. Red boxes indicate MTAN protein band.

The expected molecular weight of His-tagged *T.maritima* MTAN is 25 kDa however when analysed using SDS-PAGE the protein appears at approximately 30 kDa. As this is larger than expected, it may be due to incomplete unfolding, or the amino acid composition of the protein.

All conditions produced highly insoluble protein, only a very small proportion of the protein is found in the lysate supernatant, as indicated by the faint band on the supernatant/soluble lanes of the gel. With the exception of incubation at 4 °C (which produced very little insoluble and soluble protein) all conditions were comparable, the condition taken forward for large scale expression was condition 5 (1 mM IPTG, 27 °C, 16 hours) as it resulted in the largest cell pellet.

Large scale expression (5 L) of BL21 (DE3) *E.coli* cells expressing *T.maritima* MTAN (using condition 5 Table 4.1) produced a 35.8 g cell pellet. Initially, purification of the MTAN was attempted using the same buffers as for HydG (Table 7.12). Similar to HydG purification (method 13) (in an aerobic atmosphere) after lysis, the soluble fraction was purified via Ni-NTA chromatography. A buffer B gradient of length 150 mL to 70 % was used to elute bound protein (UV trace shown in Figure 4.3).

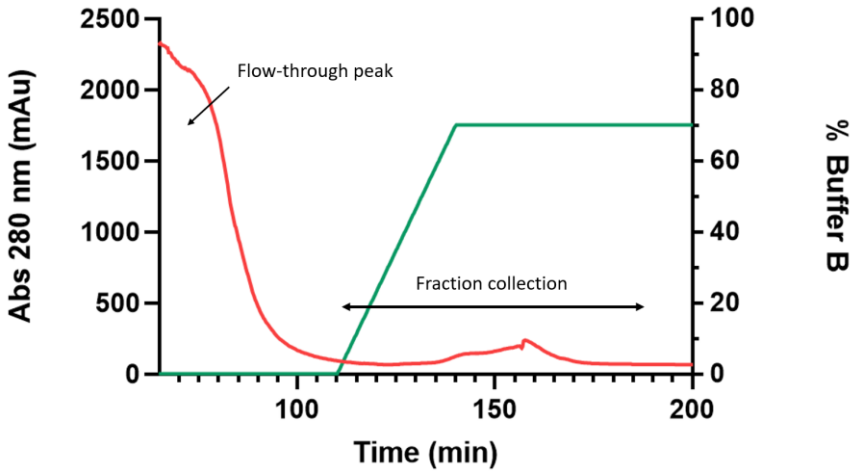

Figure 4.3 UV trace of Ni-NTA chromatography of *T.maritima* MTAN

8 mL fractions were collected as indicated in Figure 4.3, aliquots of each fraction were taken and the remaining volume frozen at -80°C. Fraction aliquots were analysed by Bradford and 15% SDS-PAGE to determine their concentration and purity (Figure 4.4).

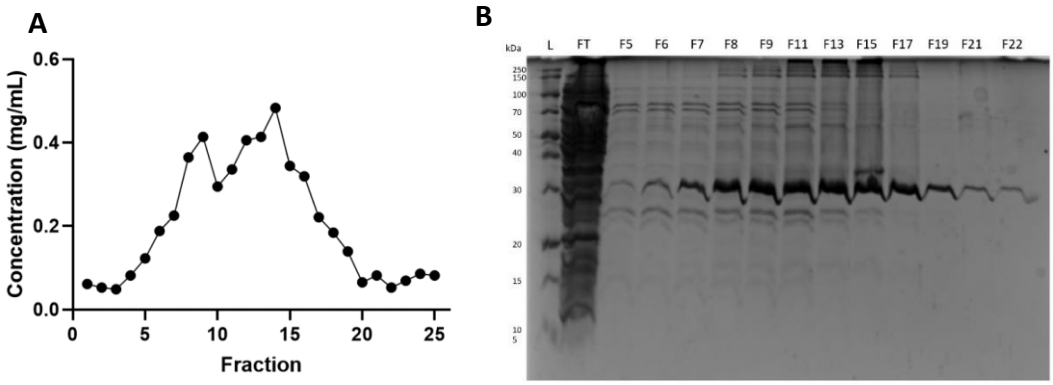

Figure 4.4 A Bradford and B 15% SDS-PAGE analysis of Ni-NTA chromatography fractions of *T.maritima* MTAN. L = protein molecular weight ladder, FT = column flow-through, F = fraction.

Fractions 7 – 19 were defrosted, pooled, and dialysed into buffer C (Table 7.12)**.** The protein solution was dialysed using a 12.4 kDa molecular weight cut-off cellulose tubing in 1 L of buffer C (4 °C), after 1 hour the buffer was replaced with fresh buffer and left to dialyse for a further hour. After dialysis the protein solution was transferred to a 350 mL Amicon and concentrated to approximately 30 mL using a 10 kDa molecular weight cut-off PES filtration membrane. This caused the protein to precipitate. Precipitated protein was collected via centrifugation and the remaining protein solution concentrated to approximately 8 mL using 20 mL Sartorius 10 kDa MWCO ultrafiltration centrifugal concentrator at 10,000 g for 40 mins, this resulted in further precipitation. The resulting protein solution and precipitated protein were stored at -80 °C.

To identify buffer conditions that would prevent the precipitation observed during protein concentration, the protein pellet collected was thawed and solubility screened in several buffers (Table 4.2 below).

Table 4.2 Buffer Screen for *T.maritima* MTAN purification, all buffers were adjusted to pH 7.5

Buffer	HEPES (mM)	NaCl (mM)	Glycerol (%)	DTT (mM)	Additive
1	25	500	10	5	0.1 % Tween 20
2	25	500	10	5	250 mM KCl
3	25	500	10	5	250 mM Ammonium chloride
4	25	-	10	5	-
5	25	500	10	5	100 mM Potassium phosphate
6	25	500	10	5	50 mM Arginine 50 mM Glutamic acid
7	25	-	-	-	-

Buffer condition 4 (No NaCl, Table 4.2) appeared to be effective at resolubilising the protein. Large scale expression of *T.maritima* was reattempted using buffers not containing NaCl (Table 4.3 below).

Table 4.3 *T.maritima* MTAN protein purification buffers

	Buffer A		Buffer B		Buffer C	
	Concentration	Amount	Concentration	Amount	Concentration	Amount
HEPES	25 mM	4.77 g	25 mM	4.77 g	25 mM	4.77 g
Glycerol	10 %	100 g	10 %	100 g	10 %	100 g
Imidazole	20 mM	1.36 g	500 mM	34.05 g	-	-
Dithiothreitol	-	-	-	-	5 mM	0.77 g
DI water adjusted to 1L						
pH adjusted to 7.5						

In an attempt to improve the purity and concentration during protein elution a steeper buffer B gradient was applied (length 75 mL to 100 % B). The UV trace is shown below in Figure 4.5 and SDS-PAGE and Bradford analysis in Figure 4.6.

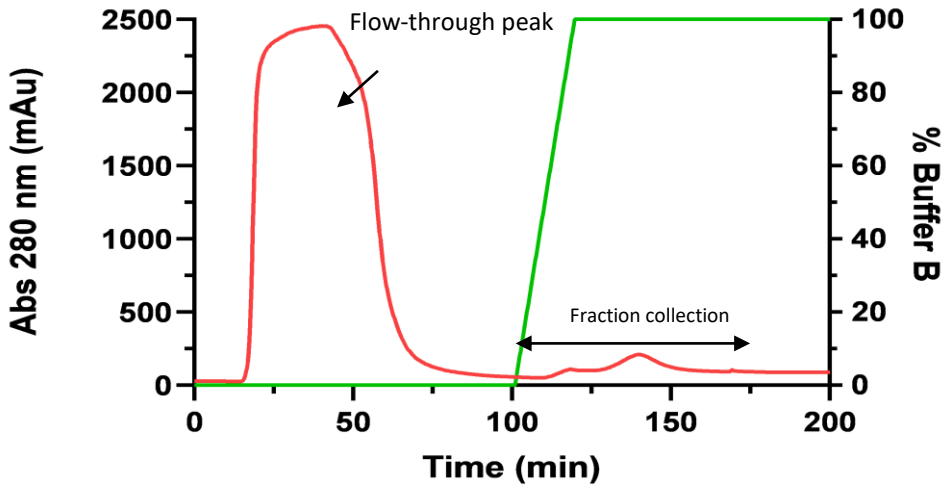

Figure 4.5 UV trace of Ni-NTA chromatography of second *T.maritima* MTAN purification

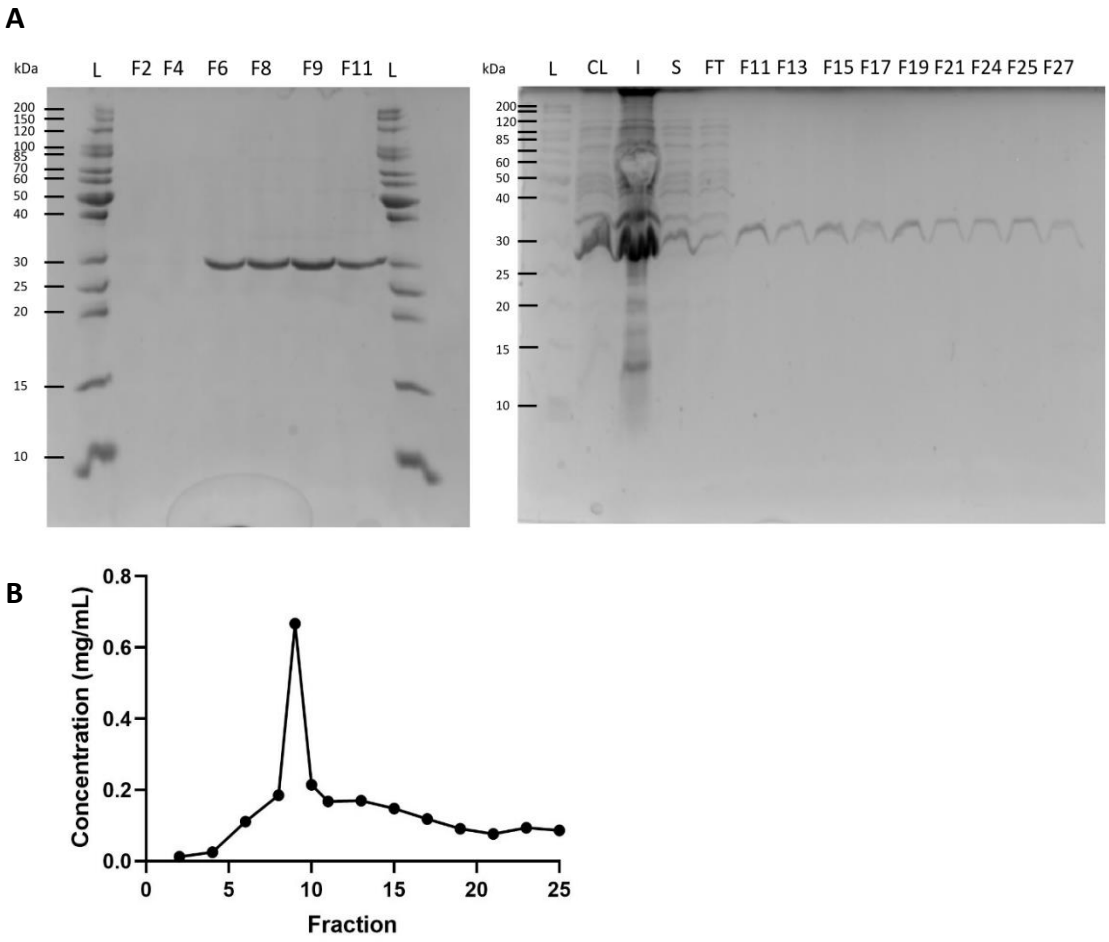

Figure 4.6 **A** 15% SDS-PAGE analysis of Ni-NTA chromatography fractions of second *T.maritima* MTAN purification L = protein molecular weight ladder, FT = column flow-through, F = fraction; CL = cell lysate; I = Insoluble protein; S = soluble protein. **B** Bradford assay of collected fractions.

As is shown in Figure 4.6B there does not appear to be a significant increase in protein recovered (see Figure 4.4A for first purification); total protein recovered from pooled Ni-NTA fractions during the first purification experiment was approximately 30 mg and the second purification pooled fractions were split and had approximately 28 mg total. However comparing the SDS-PAGE gels (Figure 4.4B and Figure 4.6A) the steeper buffer B gradient and/or removing NaCl from the purification buffers appears to have improved the purity of the eluted protein, shown by a single band on the gel.

Pooled fractions (F6, 8, 9, 11, 13, 15 and 17, total volume 56 mL) were dialysed as described previously and concentrated in an amicon at 4 °C with a 10 kDa molecular weight cut-off cellulose membrane to approximately 17.5 mL. Precipitated protein was observed at this

point and removed by centrifugation, the protein was concentrated to a final volume of 2 mL (approximately 1.5 mg/mL). Despite the change in buffer constituents the protein still appeared to be highly insoluble during the purification, prior to purification the expressed protein is also mostly present as insoluble in the cell pellet (Figure 4.2).

T.maritima MTAN was initially chosen as an alternative MTAN due to being hyper thermophilic and as *T.maritima* HydG has previously been purified although producing comparatively low yields (compared to *T.lettingae* and *T.itallicus*) [106]. Further work would be needed to improve the expression and purification of *T.maritima* MTAN such as further buffer and pH screening or addition of charged amino acids [126, 127].

4.2 Activity Assays of *T.maritima* MTAN

The activity of the purified *T.maritima* MTAN was measured in assay buffer (50 mM HEPES, 500 mM KCl, 50 mM $MgCl_2$) at a concentration of 0.025 mg/mL (1 nM) in the presence of 1 mM DOA (total volume 100 µL). Reactions were incubated at 37 °C for 1 hour and stopped by addition of 10 µL 20 % perchloric acid. After removal of precipitated protein assays were analysed using the previously described HPLC method for HydG assays (method 17). Results indicated the enzyme was not active as there was no adenine peak and the concentration of DOA present was equivalent to the concentration in a control sample containing no enzyme.

The activity assay was repeated at higher temperature (70 °C) and with a greater concentration of MTAN (0.25 mg/mL 10 nM) alongside an assay containing *E.coli* MTAN (0.125 mg/mL, 5.2 nM). *E.coli* MTAN showed almost 100 % conversion of DOA to adenine however *T.maritima* MTAN again appeared inactive.

As MTAN is known to have multiple substrates [113, 114, 128] a further activity assay was tested utilising MTA rather than DOA. MTA is hydrolysed by MTAN to produce 5-methylthioribose (MTR) and adenine (Figure 4.7)

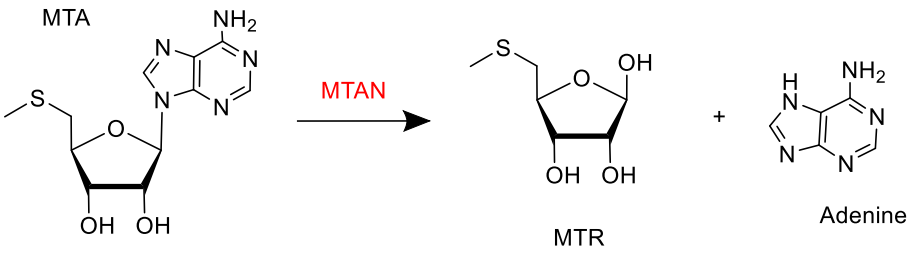

Figure 4.7 MTAN hydrolysis of MTA (reproduced from [113])

Duplicate assays containing either 0.25 mg/mL *T.maritima* MTAN or 0.125 mg/mL *E.coli* MTAN in assay buffer (as previously described) were incubated for 1 hour at 37 °C in the presence of 1mM MTA (total volume 100 µL). Reactions were stopped by the addition of 10 µL 20% perchloric acid and centrifuged prior to HPLC analysis. A negative control containing no MTAN and 1 mM MTA was also incubated alongside. The resulting adenine and MTA concentrations for this experiment are shown below in Table 4.4.

Table 4.4 MTA and adenine concentrations produced by 0.25 mg/mL *T.maritima* and 0.125 mg/mL *E.coli* MTAN incubated at 37 °C for 1 hour. Concentrations are shown as means of two replicated ± standard deviation.

Sample	Adenine concentration (µM)	MTA concentration (µM)
T.maritima MTAN + MTA	31.6 ± 1.70	613 ± 6.32
E.coli MTAN + MTA	466 ± 2.40	6.19 ± 8.76
No MTAN + MTA	0	616 ± 5.73

When comparing adenine concentrations it would appear from Table 4.4 that the *T.maritima* MTAN enzyme is partially active (hydrolysing approximately 5% MTA, compared to approximately 75% hydrolysis by *E.coli* MTAN). However there is no significant corresponding decrease in MTA concentration when comparing to the no MTAN control. An alternative explanation is not proposed as there is no adenine peak in the no MTAN control, which would suggest degradation or contamination of the MTA stock.

MTA and DOA (1 mM) substrate assays were repeated at 37 and 70 °C with a higher concentration of *T.maritima* MTAN (1 mg/mL, 40 µM) and 0.125 mg/mL, 5 µM *E.coli* MTAN. A summary of the results is shown below in Table 4.5. The method is the same as previously described above.

Table 4.5 *T.maritima* and *E.coli* MTAN activity assays with 1 mM DOA or MTA incubated for 1 hour at 37 or 70 °C.

Results for MTAN containing samples are shown as an average of duplicates ± standard deviation. There was one replicate of samples incubated without MTAN. To avoid over estimation, enzyme turnover has been calculated by subtracting the concentration of adenine present in the relevant negative controls from the MTAN samples. Where negative concentrations were calculated 0 has been recorded in the table.

Sample	Temperature (°C)	Adenine (μM)	MTA (μM)	DOA (μM)	Enzyme turnover [Adenine]/[MTAN]
T.maritima MTAN + DOA	37	146 ± 3.63	-	601 ± 37.5	1.88 ± 0.0907
T.maritima MTAN + DOA	70	68.0 ± 9.21	-	631 ± 32.4	0.0787 ± 0.230
T.maritima MTAN + MTA	37	82.7 ± 45.9	499 ± 104	-	2.04 ± 1.15
T.maritima MTAN + MTA	70	289 ± 6.43	259 ± 21.0	-	5.96 ± 0.161
E.coli MTAN + DOA	37	636 ± 16.1	-	0	113 ± 3.21
E.coli MTAN + DOA	70	63.9 ± 0.442	-	614 ± 14.0	0
E.coli MTAN + MTA	37	468 ± 27.7	6.26 ± 8.86	-	93.4 ± 5.53
E.coli MTAN + MTA	70	449 ± 26.0	0	-	79.7 ± 5.20
No MTAN + DOA	37	70.5	-	617	-
No MTAN + DOA	70	64.8	-	418	-
No MTAN + MTA	37	1.04	602	-	-
No MTAN + MTA	70	50.2	568	-	-

The results in Table 4.5 appear to confirm *T.maritima* MTAN is active, the greatest turnover is observed in samples incubated at 70 °C with MTA (approximately 55%). Conversely when incubated with DOA *T.maritima* MTAN appears to be more active at 37 °C. At 37 °C approximately 25 % of DOA has been converted to adenine and at 70 °C approximately 20 % has.

Based on the calculated enzyme turnover in Table 4.5 the *E.coli* MTAN is clearly more active at 37 °C compared to 70 °C and to *T.maritima* MTAN at 37 and 70 °C. The reason for this is not fully understood although solubility is thought to be a factor, a stored aliquot of

T.maritima was centrifuged and protein pellet visible. Further work is required to find conditions to improve the solubility.

Due to the solubility issues observed here and seen previously during HydG *T.maritima* purification [106] utilising an alternative thermophilic MTAN was investigated.

4.3 Sequence Analysis to Identify an Alternative Thermophilic MTAN

Crystallography experiments by Lee *et al.* revealed a number of key residues in the *E.coli* MTAN enzyme active site with potential involvement in adenine and ribose binding [129]. A BLAST search of the *E.coli* MTAN protein sequence (NCBI protein reference NP_308190.1) was used to identify thermophilic species with highly similar MTAN protein sequences. Several species were identified and aligned to view possible mismatches of key residues (Figure 4.8).

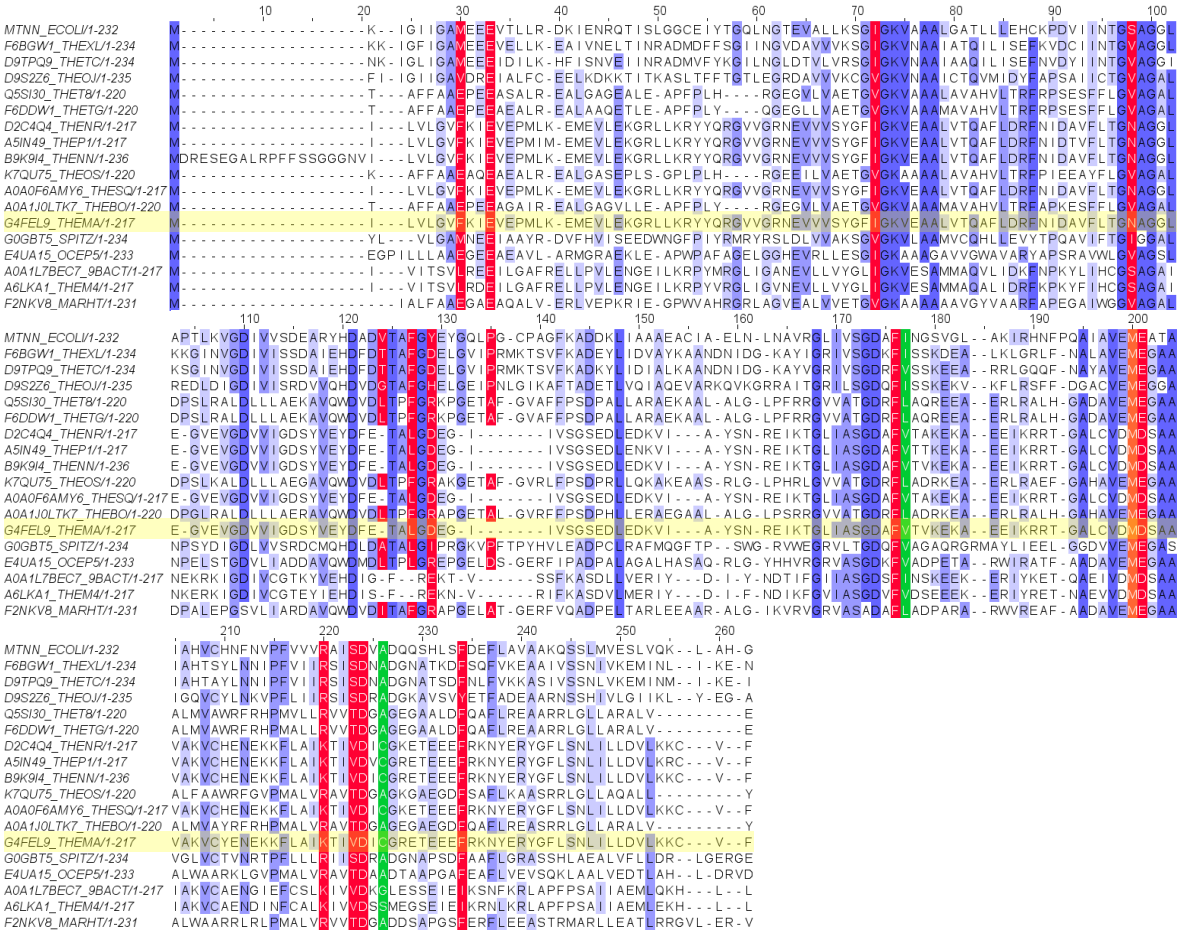

Figure 4.8 Sequence alignment of MTAN proteins. In order, species aligned; *Escherichia coli*, *Thermoanaerobacterium xylanolyticum*, *Thermoanaerobacterium thermosaccharolyticum*, *Thermosediminibacter oceani*, *Thermus thermophilus* strain ATCC 27634, *Thermus*

thermophilus strain SG0.5JP17-16, *Thermotoga naphthophila*, *Thermotoga petrophila*, *Thermotoga neapolitana*, *Thermus oshimai*, *Thermotoga sp.* strain RQ2, *Thermus brockianus*, *Thermotoga maritima* (highlighted yellow), *Spirochaeta thermophila*, *Oceanithermus profundus*, *Thermosipho sp.* strain 1063, *Thermosipho melanesiensis* and *Marinithermus hydrothermalis*.

T.xylanolyticum (*Txy*) was identified as having the most similar protein sequence to the *E.coli* sequence, having only 3 key residue mismatches. Alignments are shown above in Figure 4.8, pairwise alignment coloured by percentage identity (purple), residues involved in substrate binding and catalysis are shown in red and green respectively, Met^{200} shown in orange is involved in both substate binding and catalysis (Fig.9 [129]). The *T.maritima* protein sequence is highlighted yellow and has 10 mismatches with the *E.coli* sequence. *Txy* is a thermophile with an optimum growth temperature of 60 °C with a range of 45-70 °C [130]. It is hoped the similarity between *Txy* and *E.coli* sequences will translate to similarities in *in vitro* activity, at increased temperatures.

4.4 *T.xylanolyticum* MTAN

4.4.1 Plasmid Design

The *Txy* nucleotide MTAN sequence was codon optimised for expression in *E.coli* by GeneArt™ and synthesised into a pET151/D-TOPO vector by Invitrogen GeneArt™ ThermoFisher Scientific (Figure 4.9, A.1.5). The protein has an N-terminal 6xHis tag for Ni-NTA purification, and unique *NdeI* and *XhoI* restriction sites for analytical plasmid digest.

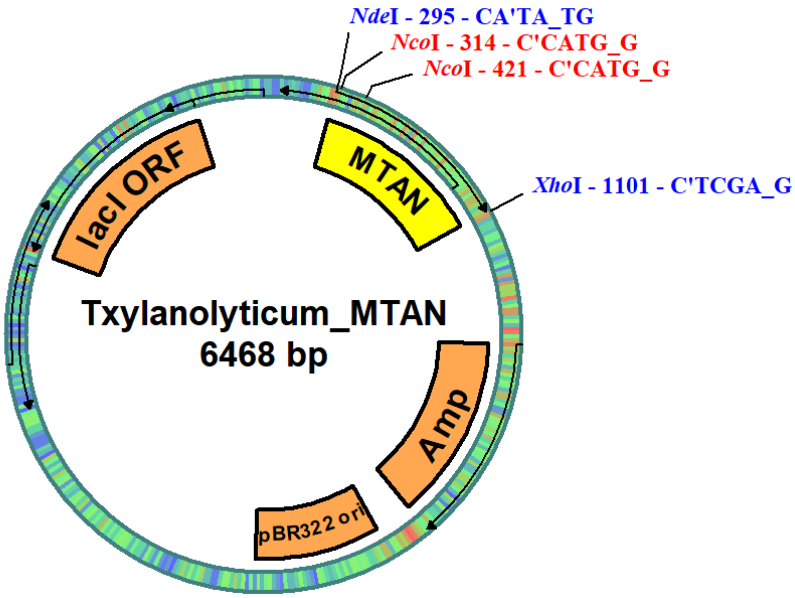

Figure 4.9 *T.xylanolyticum* MTAN expression plasmid map

4.4.2 Small Scale Expression

Competent JM109 and BL21 (DE3) *E.coli* cells were chemically transformed (method 4) with the *Txy* MTAN plasmid and successful transformation confirmed by analytical digest (Figure 4.10).

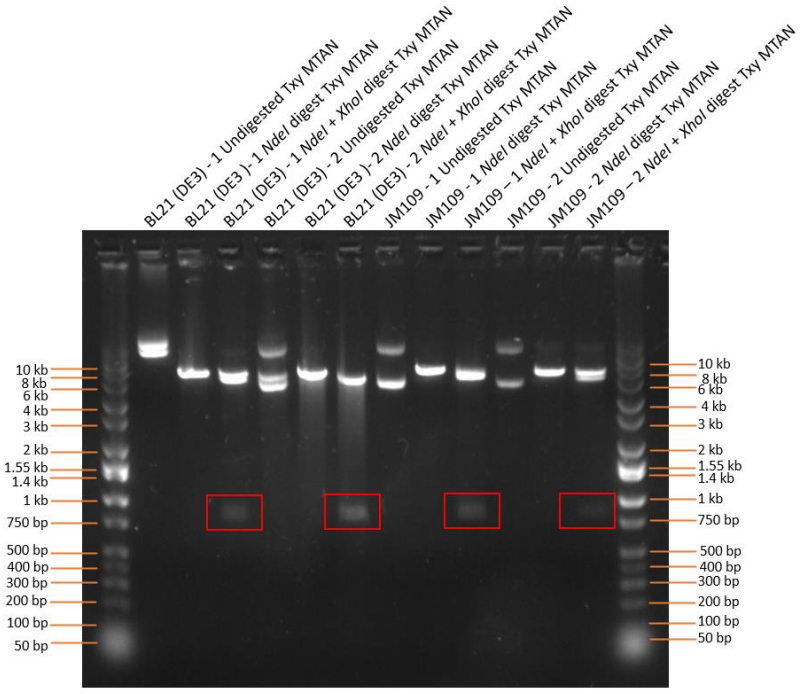

Figure 4.10 1% agarose gel *T.xylanolyticum* MTAN analytical plasmid digest. Red box indicates 806 bp MTAN insert.

A small scale expression study of transformed BL21 (DE3) *E.coli* cells (method 9) established optimum conditions for *Txy* MTAN expression, the conditions tested and results are shown below in Table 4.6. An uninduced culture was tested alongside as a control.

Table 4.6 Small Scale expression of Txy MTAN

Condition	[IPTG] mM	Expression (hrs)	Expression (°C)	Pellet mass (g)
1	0	4	37	0.97
2	1	4	37	0.80
3	1	4	27	0.96
4	1	6	37	0.89
5	1	6	27	1.11
6	1	17	37	1.10
7	1	17	27	1.51

Cell pellets were lysed and the resulting supernatant containing the soluble fraction of protein and cell pellet (containing the insoluble protein) analysed by 15% SDS-PAGE (method 11, Figure 4.11).

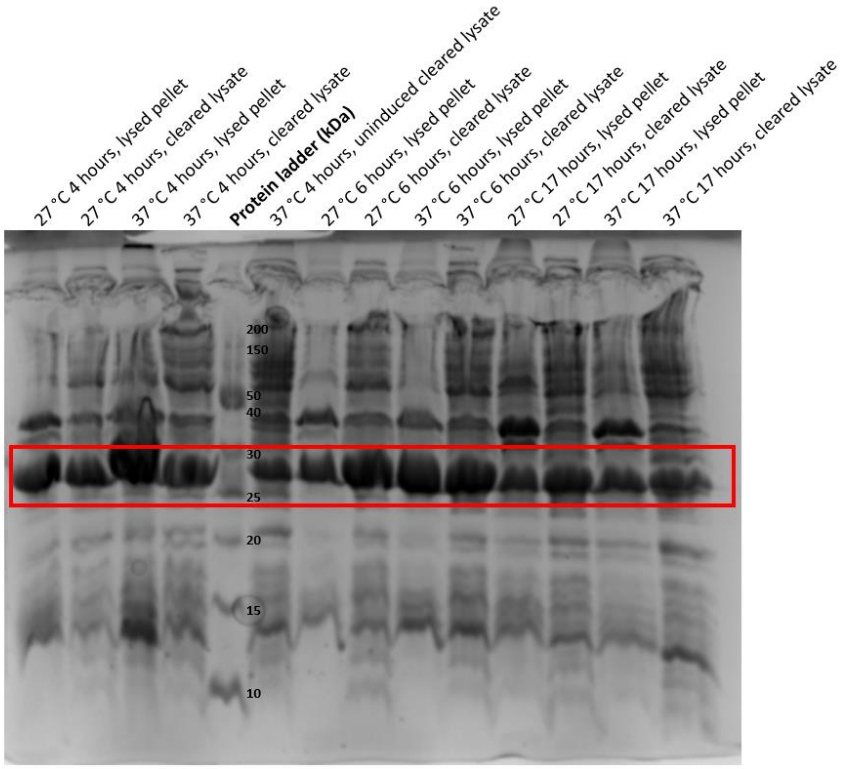

Figure 4.11 SDS-PAGE of *Txy* MTAN small-scale expression. Red box indicates 29 kDa *Txy* MTAN band.

For most conditions Figure 4.11 shows a similar portion of protein present in the insoluble and soluble fractions (lysed pellet and cleared lysate respectively). This is in contrast to SDS-PAGE analysis of the small scale expression of *T.maritima* MTAN where the protein was predominantly present in the insoluble portion (Figure 4.2). Based on the cell pellet mass and SDS-PAGE the recommended expression conditions for *Txy* MTAN would be for cell cultures to be induced with 1 mM IPTG for 17 hours at 27 °C.

4.5 Summary

Attempts to express and purify *T.mar* MTAN have so far been unsuccessful, producing highly insoluble protein with very low levels of activity. The low activity could be explained by protein precipitating in the assay, resulting in a lower than calculated/expected concentration being present.

T.xy MTAN has been identified as an alternative candidate for use in the high temperature HydG activity assay due to its high sequence similarity with *E.coli* MTAN. A small-scale expression study has shown promise for the solubility of the protein (Figure 4.11).

Chapter 5 Crystallography

Crystallisation of biological macromolecules can be divided into three phases: nucleation, growth and cessation of growth [131, 132]. Nucleation and growth are both directed by supersaturation: a nonequilibrium state determined by pH, temperature, and the presence of precipitating agents such as polymers and salts [133, 134]. The structural state of the macromolecule and therefore crystallisation process is strongly affected by the presence of cofactors, substrates, and inhibitors (amongst other small molecules) [134]. Molecules of this type can stabilise the protein and where enzymes are co crystallised with substrates/ligands/inhibitors can provide insight to their reaction mechanisms [32, 129]. There are several well-established methods for crystallising biological macromolecules: liquid-liquid diffusion, batch, dialysis and the most popular, vapour diffusion[134].

The vapour diffusion method of growing protein crystals allows the protein-precipitant solution to equilibrate in a sealed environment to reach optimal precipitant concentration for crystallisation. A large reservoir containing a higher precipitant concentration results in net transfer of water from the sub-wells or protein drops [135]. The diffusion process stimulates self-screening of the crystallisation experiment as the precipitant and protein concentrate (a phase transition [136]) until the precipitant concentration almost equalises and is then maintained [135, 137]. A crystallisation phase diagram is shown below in Figure 5.1a, alongside schematics of the hanging and sitting drop vapour diffusion methods, Figure 5.1b and c respectively.

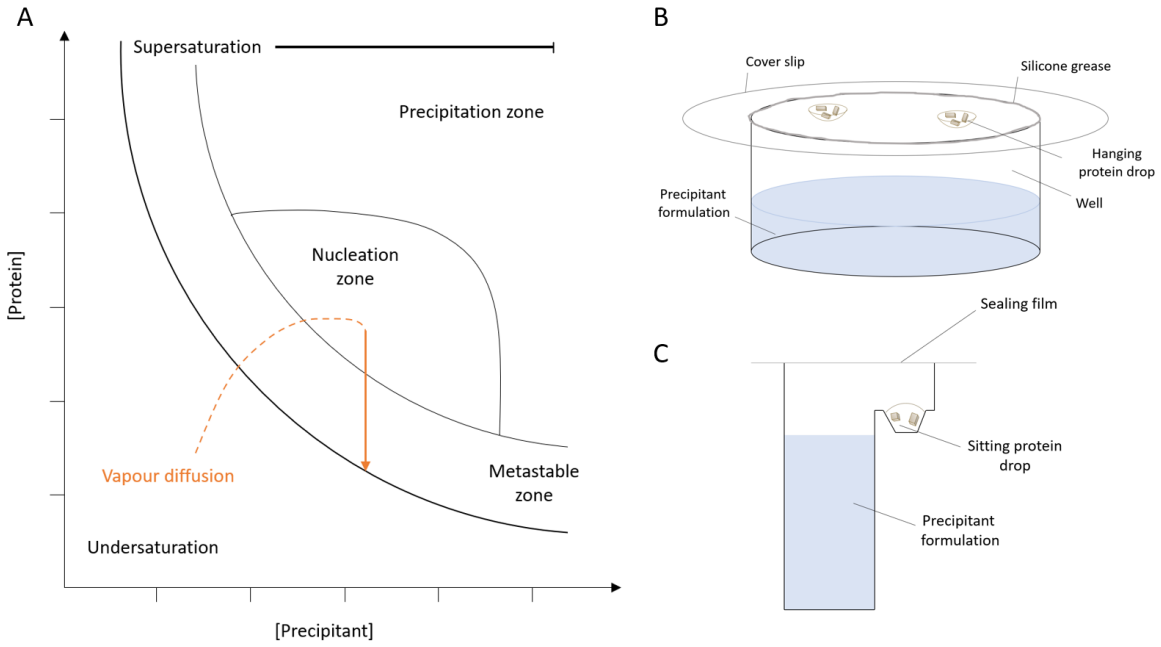

Figure 5.1 **A**: Schematic of a crystallisation phase diagram. For a protein to crystallise it must first become supersaturted in order to form nuceli (dashed line), once nuclei have formed the protein conentration of the solution decreases and the drop transitions to the metastable zone where nucleation should end and crystal growth should occur, until the saturation zone is reached, diagram adapted from [137]. **B & C**: Experimental set up for hanging and sitting drop vapour diffusion techniques.

5.1 Co crystallising Experiments with Fe and Cysteine

The crystal structure of HydG from *C.hydrogenoformans* and *Ti* HydG complexed with SAM have been characterised by Nicolet *et al.* and Dinis *et al.* respectively (Protein Data Bank IDs 4RTB and 4WCX) [32, 33]. The structure of *C.hydrogenoformans* HydG is incomplete (missing the C-terminal cluster) however based on the structural characteristics of the tryptophan lyase NosL suggestions can be made on tyrosine binding and migration of DHG [33, 96]. The *Ti* HydG crystal structure contained two HydG monomers per asymmetric units with distinctly different auxiliary Fe-S clusters. One monomer contained a [4Fe-5S] cluster and the second a [4Fe-4S] cluster bridged via a μ_2-sulfide to a mononuclear Fe(II) (referred to as the labile/dangler Fe) [32].

Clearly significant findings have so far come from crystal structures of HydG species and confirmations of indirectly determined hypotheses relating to the Fe-S clusters [32]. The aim of the crystallography experiments in this work were to further these findings and co-

crystallise *Ti* HydG with the exogenous cysteine which is suggested to coordinate the dangler Fe [98, 99, 138]. These experiments were unsuccessful in producing high quality crystals but after a summary of the work completed suggestions for the next steps are made in 6.2.

In this work sitting drop and hanging drop vapour diffusion experiments were trialled. Sitting drop reservoir wells contained 102 µL of the screening solution from which 0.5 or 0.6 µL was pipetted to the three sub-wells. The corresponding volume of protein solution was added forming a 1:1 mixture of protein and precipitant.

Initial crystal screens were formulated that included conditions which had successfully produced isomorphous crystals previously [32, 106].

Conditions screened are shown below in Table 5.1, sitting drop (96 well, three-subwell plates) and hanging drop (24 well plates) vapour-diffusion experiments were prepared inside an anaerobic glovebox, and drops visualised regularly under microscope. Protein solutions all contained HydG (approx. 750 µM), SAM (10 mM) and either Cys (0.5 mM) or Cys and Fe_2SO_4 (0.5 mM or 1 mM) method 18.

Example sitting drop wells are shown below in Figure 5.2 and Figure 5.3 after 24 hours and 6 days respectively. In general, the sitting drops appear to contain amorphous precipitate and oils. Typically where HydG crystals have been observed previously they are much darker than the starting solution and the solution around them clears [106] most likely due to the concentration of [Fe-S] clusters in the crystals. This has not occurred in drops which look like they may contain crystals in these experiments. Drops were observed for approximately 4 weeks and little change occurred in the wells post 6 day observations, *Ti* HydG crystals have previously been reported after 5 days in sitting drop wells in the presence of formulation 1, described in Table 5.1 [32] .

Table 5.1 Initial *Ti* HydG crystal screen

Formulation	[Buffer] (M)			Buffer pH	[Precipitant] (%)			[Salt] (M)
	Bistris propane	Bistris	MES		PEG 3350	PEG 400	PEG 5000 MeE	NaF
1*	0.1	0	0	6.5	20	0	0	0.2
2	0.1	0	0	6.5	0	22	0	0.2
3	0.1	0	0	6.5	0	0	20	0.2
4	0	0.1	0	6.5	20	0	0	0.2
5	0	0.1	0	6.5	0	22	0	0.2
6	0	0.1	0	6.5	0	0	20	0.2
7	0	0	0.1	6	20	0	0	0.2
8*	0	0	0.1	6	0	22	0	0.2
9	0	0	0.1	6	0	0	20	0.2
10	0.1	0	0	6.5	20	0	0	0
11	0.1	0	0	6.5	0	22	0	0
12	0.1	0	0	6.5	0	0	20	0
13	0	0.1	0	6.5	20	0	0	0
14	0	0.1	0	6.5	0	22	0	0
15*	0	0.1	0	6.5	0	0	20	0
16	0	0	0.1	6	20	0	0	0
17	0	0	0.1	6	0	22	0	0
18	0	0	0.1	6	0	0	20	0

*Conditions previously successful for *Ti* HydG crystal growth [32, 106].

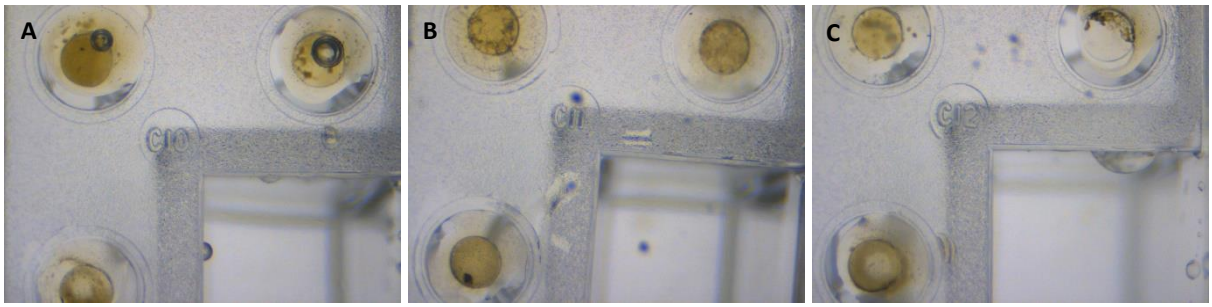

Figure 5.2 Examples of 96-well sitting drop *Ti* HydG crystallisation wells, imaged after 24 hours, wells clockwise from bottom: HydG + SAM; HydG + SAM + 0.5 mM Cys and Fe_2SO_4; HydG + SAM + 1 mM Cys and Fe_2SO_4. **A**: Formulation 16, **B**: Formulation 17, **C**: Formulation 18 (Table 5.1).

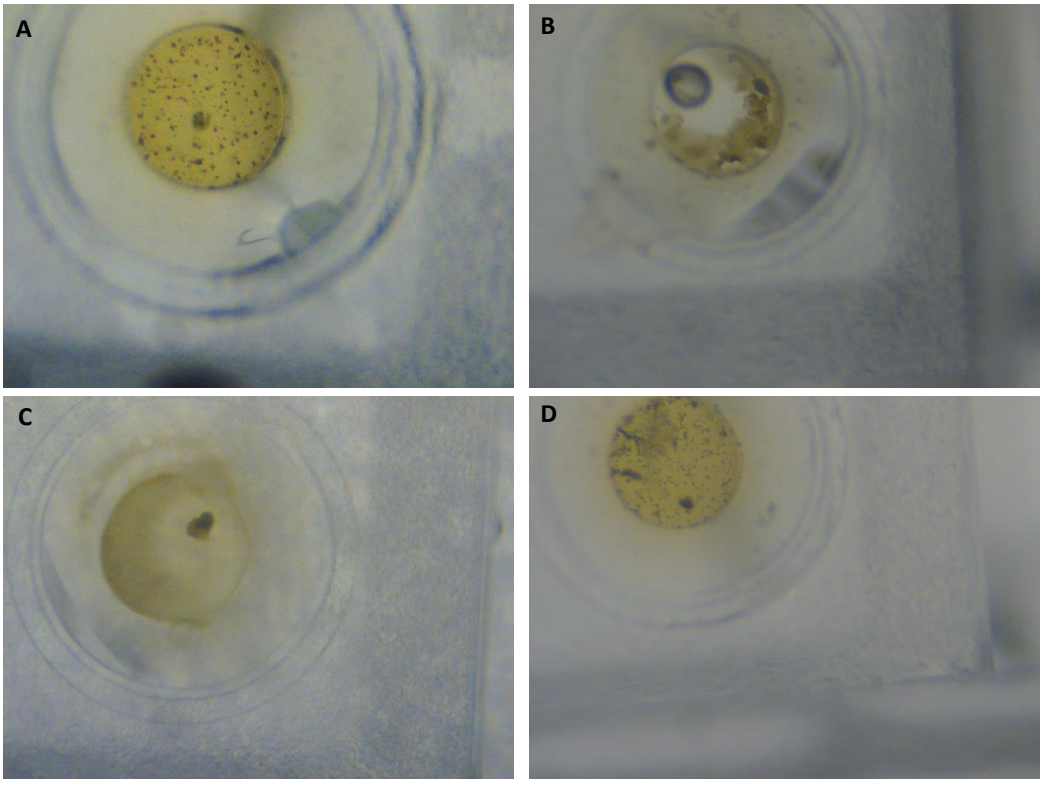

Figure 5.3 Examples of 96-well sitting drop *Ti* HydG crystallisation wells, imaged after 6 days. **A**: Formulation 2 HydG + SAM; **B**: Formulation 3 HydG + SAM + 1 mM Cys and Fe_2SO_4; **C**: Formulation 13 HydG + SAM + 0.5 mM Cys and Fe_2SO_4; **D**: Formulation 2 HydG + SAM. Formulations can be found below in Table 5.1.

Hanging drop vapour-diffusion crystallisation experiments with the conditions described in Table 5.1 (above) were also prepared. Protein solutions tested all contained HydG (approx.

750 µM) in the presence of 10 mM SAM with either no further additive, 0.5 mM Cys, 0.5 mM Cys and Fe_2SO_4, or 1 mM Cys and Fe_2SO_4 in 24-well Linbro-style plates. 505 µL of the crystallisation screen was pipetted into the reservoir, and 2 x 2 µL drops containing protein solution mixed in a 1:1 ratio with the screening formulation were pipetted on to a 22 mm cover slip, sealing the well with grease (as shown in Figure 5.1**B**).

Examples of wells after 24 hours and 5 days are shown below in Figure 5.4 and Figure 5.5 respectively.

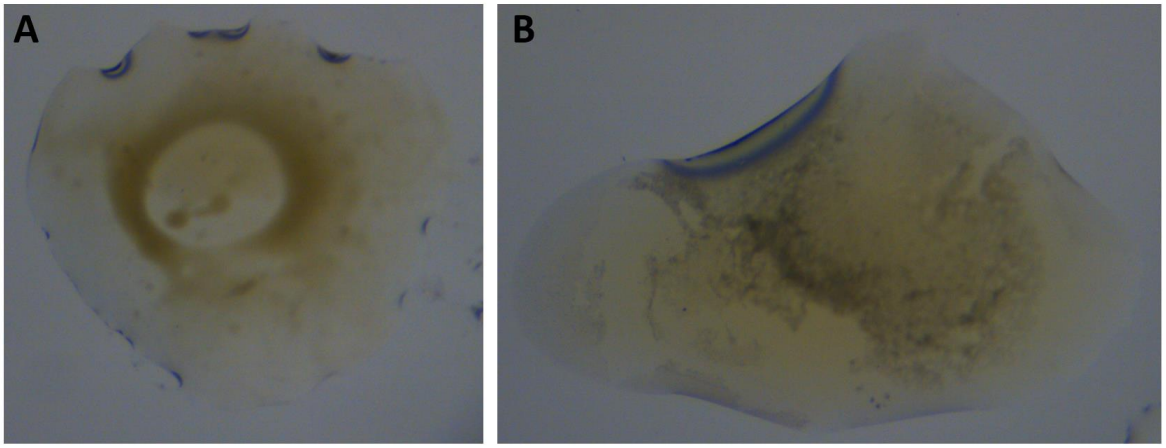

Figure 5.4 Hanging drops observed after 24 hours. **A**: Condition 6, HydG + SAM + 1 mM Cys and Fe_2SO_4; **B**: Condition 14, HydG + SAM + 1 mM Cys and Fe_2SO_4

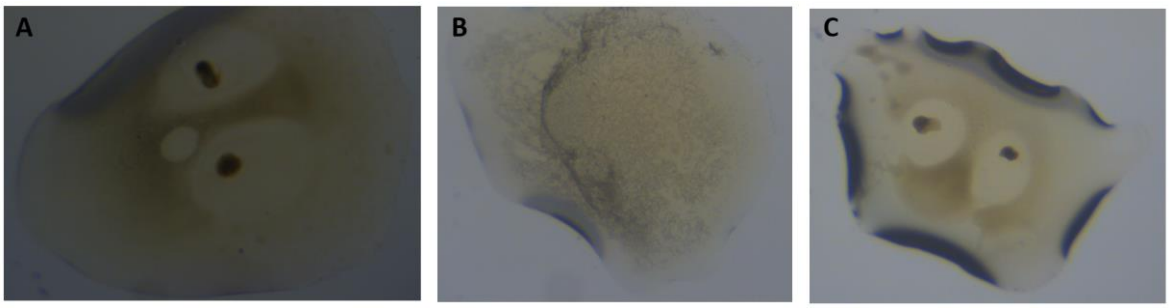

Figure 5.5 Hanging drops observed after 5 days. **A**: Condition 1, HydG + SAM + 0.5 mM Cys **B**: Condition 14, HydG + SAM; **C**: Condition 13, HydG + SAM + 1 mM Cys and Fe_2SO_4.

Similar to the sitting drop results, wells appear to have either formed amorphous precipitation or oils. Both observations are indications of supersaturation, however when no crystal forms suggest protein or precipitant concentration may be too high to promote crystallisation. Undersaturated drops would appear clear [139].

5.2 Summary

Attempts to crystallise *Ti* HydG have in this work have been unsuccessful. Experimental conditions which had previously produced crystals using commercial screens [32] were repeated with solutions prepared in-house in the presence of HydG and SAM as well as trials of new conditions in the presence of Cys and Fe_2SO_4.

The reason these trials have been unsuccessful is not known however could be a result of many factors as protein crystallisation is a highly sensitive process [133]. The most likely reasons are thought to be small variations in screening solutions and differences in protein concentration or purity. Signs which would indicate poor experimental setup, such as drops drying or losing their characteristic [Fe-S] cluster brown colour due to unsealed plates or exposure to oxygen were not observed.

Chapter 6 Conclusions and Future Work

6.1 HydG Activity

The overall aim of optimising the HydG activity assay is to accumulate the released metallosynthon product of HydG in order for it to be better characterised. There is compelling FTIR and EPR evidence for the characterisation of the HydG bound metallosynthon [97, 98]. In addition to X-ray and EPR studies on HydE utilising a synthetic [Fe^{II}(Cys)$(CO)_2$(CN)], proposed to be the product of HydG as its substrate [80, 81].

Significant progress was made in optimising the assay by increasing the incubation temperature and successfully averting production inhibition by introduced MTAN to the assay mix. The immediate future steps of this work would be to express and purify the *Txy* thermophilic MTAN protein and find the optimum temperature for incubation. By measuring the activity of HydG at varying temperatures, using the Arrhenius equation, the activation energy and rate constants can be determined [140, 141].

Once optimised, FTIR and low temperature EXAFS spectroscopy are suggested as tools to characterise the released and HydG bound synthon, using a combination of HydG end-point and time-course activity samples and synthetic Fe-CO-CN model compounds. To confirm the coordination geometry of the bound synthon and characterise the released synthon in solution.

6.2 Crystallography

Since the initial publications by Dinis and Nicolet *et al.* on HydG crystal structures in 2015 there have be no more described [32, 33]. This in itself may highlight the difficulty of the process, however as at the time it proved so key in improving our understanding of the enzyme clearly it is an area of research which should be pursued despite the difficulty.

The crystal screening described in this work was unsuccessful in yielding crystals. The first suggested step in reattempting these experiments is to revert back to commercial screening solutions to broadly attempt to generate *de novo* crystals. In addition to co-crystallising with Fe and cys, as the ligands are relatively small another approach would be to soak native crystals [131, 142].

Chapter 7 Materials and Methods

7.1 Materials and Reagents

A summary of materials used in this study a shown below in Table 7.1. All reagent grade chemicals and laboratory consumables were purchased from Sigma Aldrich or Fisher Scientific UK Ltd unless otherwise stated.

Table 7.1 Summary of materials

Material	**Source**
Bacto-tryptone Yeast extract	Oxoid
DTT IPTG Antibiotics	Melford Laboratories Ltd.
Antifoam 240	Merck Life Science UK Ltd.
EDTA-free protease inhibitor tablets	Roche
Plasmid synthesis and subcloning pET151/D-TOPO Expression vector synthesis	Invitrogen GeneArt™ ThermoFisher Scientific
Restriction Enzymes	New England Biolabs (UK)
Wizard® Plus SV Minipreps DNA Purification System kit	Promega
GeneRuler 1kb DNA ladder EZ-Run protein ladder	Fisher Scientific
S-75 and S-200 Superdex resin	GE Healthcare
Consumable	**Source**

PES Ultrafiltration Discs (10kDa and 30 kDa) NMW 0.22 and 0.45 µm syringe filters	Millipore UK Ltd
Pipette tips Microcentrifuge tubes	Starlab (UK) Ltd
96-well crystallisation plates 24-well XRL crystallisation plates CrystalClene Slips (plastic) Coverslides	Molecular Dimensions Ltd

7.2 Equipment

Microbiology

Bacterial growth media and deionised water was sterilised in an Astell AMA260BT autoclave at 121°C for 15 min. Arabinose, IPTG and antibiotic solutions were filter sterilized through 0.22-0.45 µm syringe filters. To ensure sterility, agar plates were poured inside a BioMAT Class 1 microbiological cabinet.

Bacterial cultures and plates were incubated, and cultures shaken in an Innova 4230 incubator shaker (≤ 200 mL, New Brunswick Scientific), Stuart orbital incubator SI 600 (<200 mL) or Innova 4400 Incubator Shaker (5 L, New Brunswick Scientific).

Fermenter expression was carried out in a BioFlo® 115 (New Brunswick, Eppendorf Uk Ltd.) fermentor equipped with a 7.5 L vessel.

Bacterial optical density and Bradford readings were recorded on a Thermo Scientific Biomate 3 spectrophotometer.

Centrifugation of volumes ≤ 50 mL were carried out using a Stratos Heraus centrifuge and volumes ≤1.5 mL in a bench top 5415D Eppendorf micro centrifuge. Solutions were mixed using a Fisherbrand ZX3 vortex mixer.

PCR and incubation of small volumes ≤200 µL (e.g. activity assays and analytical digest samples) was carried out using a BioRad T100™ Thermal Cycler. BioRad electrophoresis

apparatus was used to run agarose and SDS-PAGE gels. Gels were imaged using a Gel Doc™ EZ Imager (BioRad). DNA concentrations were quantified using a NanoDrop® ND-1000 Spectrophotometer.

pH Determination

pH determination was carried out using a HI 2210 pH meter (HANNA Instruments) and HI-1131B pH electrode calibrated at pH 4.0, pH 7.0, pH 10.0 when required.

Anaerobic protein purification

All HydG protein manipulations were carried out inside an anaerobic glovebox (Belle Technology, O_2 < 2 ppm, 19 °C). All HydG associated buffers were deoxygenated inside the glovebox overnight (stirring).

Cells were lysed in a cool water bath using a VC 130 Sonicator (Sonics and Materials) and centrifuged in a Sorval Lynx 6000 (F21-8x50y rotor). Supernatant was purified with Pharmacia XK columns equilibrated with deoxygenated buffer (located outside the glovebox) connected to a ÄKTAPrime plus system, GE Healthcare (inside the glovebox). Protein solutions were concentrated using an Amicon ultrafiltration pressure-cell (10 or 50mL chamber size).

Aerobic protein purification

Cells were sonicated on ice using a MSE Soniprep 150. All purification chromatography was carried out on an ÄKTAPrime plus system (GE Healthcare) using Pharmacia XK columns and data analysed using Primeview software (GE Healthcare). Centrifugation and protein concentration was carried out as described for anaerobic purification.

Spectroscopy

UV-Vis absorbance measurements were taken in either 1 cm or 1 mm UV quartz cuvettes with a USB2000 spectrophotometer using a Mini D2-GS light source and QP400-2-SR-BX fibres (Ocean optics software, Netherlands), located inside an anaerobic glovebox.

HPLC Analysis

All HPLC data was generated on a Gilson System WorkCentre including 321 pumps, H1 heads and a 234 Gilson Autoinjector connected to a Gilson UV/Vis-155 detector. Data analysed was analysed using Unipoint software (Gilson v5.11).

Crystallography

Crystallography plates were observed using a Mejii EMZ-13TR microscope connected to an infinity 1 camera situated inside glovebox. Images were taken using Infinity Capture software.

7.3 Methods

7.3.1 Media

Table 7.2 Composition of liquid media (1 L)

Component	2YT
Bacto-tryptone	16 g
Bacto-yeast extract	10 g
NaCl	5 g
Deionised water	Final volume 1 L

Table 7.3 Composition of media for plates (500 mL)

Component	2YT
Bacto-tryptone	8 g
Bacto-yeast extract	5 g
NaCl	2.5 g
Agar	7.5g
Deionised H_2O	Final volume 500mL

Liquid media was autoclave sterilised at 121°C for 15 minutes, plates poured and left to dry in microbiological safety cabinet before storage at 4°C.

Relevant antibiotic stock is sterile filtered and added to media after autoclaving (cooled to 50°C) at the appropriate concentration (Table 7.4 below).

Table 7.4 Antibiotic stock solutions

Antibiotic	Stock concentration (mg/mL)	Concentration in media (µg/mL)
Ampicillin (in H_2O)	100	100

7.3.2 Microbiology Methods

Method 1 Overnight cell growth

Isolated single colonies grown on agar plates or glycerol stock samples were transferred using a sterile loop to 10 mL 2YT media containing relevant antibiotic (in 50 mL sterile falcon tubes). A fresh sterile loop was used in a negative control falcon tube. All solutions including the negative control were incubated overnight at 37 °C, 180 rpm in an incubator shaker.

Method 2 Glycerol stock preparation

Following overnight growth 0.5 mL of 10 mL cell culture was added to 0.5 mL 75% (v/v) sterile glycerol solution in a sterile 1.5 mL Eppendorf, mixed by pipetting and stored at -80 °C.

Method 3 $CaCl_2$ Preparation of chemically competent cells

A 500 mL conical flask containing 100 mL 2YT media was inoculated with 1% (1 mL) overnight cell culture and incubated at 37 °C, 180 rpm until an OD_{600nm} of between 0.4-0.6 was reached. The cell culture was then split into two sterile 50 mL flacon tubes and stored on ice for 10 min. Cells were harvested by centrifugation at 4000 rpm, 4°C for 10 min. Supernatant was discarded and pellet re-suspended in 20 mL $CaCl_2$ buffer (Table 7.5) and stored on ice for 30 min. Cells harvested by centrifugation 4000 rpm, 4°C for 10 min. Supernatant was discarded and pellet re-suspended in 5mL $CaCl_2$ buffer and 1 mL 75% sterile glycerol, mixed well by pipetting. The resulting cell suspension was aliquoted into 50 or 150 µL, flash frozen in liquid nitrogen and stored at -80°C. *E.coli* strains were used

throughout experimentation, JM109 strain was used for plasmid preparation and BL21 (DE3) for protein expression.

Table 7.5 Preparation of $CaCl_2$ Buffer

Component	Amount
Tris-base	121.44 (mg)
$CaCl_2$	554.9 (mg)
Deionised H_2O	Final volume 100 mL

pH adjusted to 7.4 using 10 % HCl and filter sterilised

Method 4 Chemical transformation of competent cells

Competent cells were defrosted on ice for 10 min. 50 µL cell aliquot was mixed with 1 µL Mini-prep plasmid and incubated on ice for 30 min. A negative control was always prepared with 1 µL sterile water in the absence of plasmid. Cells heat shocked in a water bath at 42 °C for 40 sec then immediately returned to ice for 3 min. Cell/plasmid mix was transferred to a 1.5mL Eppendorf containing 250 µL SOC media (Table 7.6). Incubated at 37 °C, 180 rpm for 1-3 hr (BL21 (DE3) cells were typically incubated for longer than JM109). 50 µL of culture is then transferred to 2YT agar plate containing the appropriate antibiotic and spread. Incubated overnight at 37°C. Provided negative plates were free from growth transformed colonies can then be used for Mini-prep or protein expression.

Table 7.6 SOC Media

Component	Amount
Bacto-tryptone	20 g
Bacto-yeast extract	5 g
NaCl	0.5 g
Glucose (1M)	20 mL
$MgCl_2$ (2M)	5 mL
Deionised H_2O	Final volume 1 L

Method 5 Plasmid Isolation

10 mL overnight culture of transformed cells was harvested by centrifugation at 6000 rpm, 4 °C, 5 min. Supernatant was discarded, and plasmid DNA isolated as per manufacturer's instructions for the Wizard Plus SV Miniprep plasmid DNA purification system (Promega). Plasmid DNA eluted in 100 µL deionised nuclease free water. The concentration of DNA in the eluate was measured at 260 nm using a Nano drop. Plasmid solution stored at -20°C.

Method 6 Analytical Digest

Analytical digest reaction mix (Table 7.7) was prepared in a PCR tube and briefly centrifuged to ensure contents were collected at the bottom of the tube. The preparation was incubated at 37 °C for 2 hrs. 2 µL of 6x gel loading dye was added and 10 µL analysed on 1% agarose gel containing Nancy-520 dye, visualised immediately under UV light.

Table 7.7 DNA digest reaction mixture

Component	Analytical digest amount
Mini-prep plasmid	5 µL
Sterile water	3 µL
Cut Smart buffer*	1 µL
Restriction enzyme 1	0.5 µL
Restriction enzyme 2	0.5 µL

*Buffer suitable for both restriction enzymes was used (NEB). Where one/no restriction enzyme was used the volume of sterile water was adjusted accordingly.

Method 7 1% Agarose gel electrophoresis

Gel was prepared by dissolving 0.4 g agarose in 40 mL 1xTris-Acetate-EDTA (TAE) buffer (Table 7.8) in the microwave. When gel preparation had cooled to approximately 50 °C 2 µL (approx. 2 µL/50 mL) of Nancy-520 dye was added and mixed by swirling. Gel was then poured into a suitable mould and comb inserted. Gels were left to set at RT for approximately 15 min. Once set the gel was transferred to an electrophoresis reservoir, filled with 1xTAE buffer and comb removed. Where necessary 2µL 6x gel loading dye was

added to digest samples (mixed by pipetting). 5 µL of suitable DNA ladder was added to the first and final well on the gel and 10 µL DNA sample to appropriate wells. Gels were run at constant 90V for approximately 30 min (or until the dye has migrated three fourths the length of the gel). Gel was visualised immediately under UV light.

Table 7.8 50 x TAE buffer

Component	Amount
Tris-base	242 g
Acetic acid (Glacial)	57.1 mL
EDTA, pH 8 (0.5M)	100 mL
Deionised H_2O	1 L

Method 8 Colony PCR

Colony PCR was used to quickly confirm whether a colony has been successfully transformed with a specific plasmid. A sterile tip was used to transfer a small amount of a colony from an agar plate to the bottom of a PCR tube (the tip was streaked on a fresh plate to culture the colony). 25 µL PCR reaction mix was prepared according to Table 7.10 below (batch reaction mixes were prepared according to number of reactions being performed and 25 µL added to each template). A negative control was prepared containing no DNA template, positive control prepared containing 0.5 µL plasmid DNA Mini-prep (sterile water volume was adjusted accordingly). PCR thermal profile was run according to Table 7.11.

Table 7.9 Colony PCR primers to detect the plasmid backbone, confirming the presence of HydG insert sequence

Primer	Sequence	Product length (bases)
Forward	CGGATCCTACCTGACGCTTT	1619
Reverse	TCATTTTCTCGGCAACACGC	

Table 7.10 Colony PCR reaction mix

Component	Amount for 1 x 25 µL reaction
5x Green GoTaq Reaction buffer	5 µL
10 mM dNTPs	0.5 µL
10 µM Forward primer	0.5 µL
10 µM Reverse primer	0.5 µL
GoTaq G2 DNA polymerase	0.125 µL
25 mM $MgCl_2$	1 µL
DNA template	Small colony smear
Sterile nuclease free water	17.375 µL

Table 7.11 Colony PCR thermal profile

Step	Time	Temperature	Cycles
Cell lysis/Enzyme activation	5 min	95 °C	1
Denaturation	30 sec	95 °C	35
Annealing	30 sec	55 °C	
Extension	2 min*	72 °C	
Final extension	10 min	72 °C	1
Incubation	Hold	10 °C	1

*Approximately 1 min for each 1k bases to be amplified.

Post PCR samples were analysed by 1 % agarose gel (method 7).

7.3.3 Protein Expression

Method 9 Small scale expression

100 mL sterilised 2YT media containing the appropriate antibiotic was inoculated with 1% (1 mL) overnight growth culture. Culture incubated at 37 °C, 180 rpm until the OD_{600nm} measures between 0.6-0.8 (approximately 3 hours). For pBAD vectors protein expression was induced by addition of 5 mL (50 mL/L culture) 20% (w/v) arabinose. pET vecotrs induced with 0.4 – 1 mM IPTG. Incubation temperature was reduced to 27°C and cells left to incubate for 4-16 hours. After this time cells were harvested by centrifugation, 6000 rpm, 10 mins, 4°C. The supernatant was discarded, and mass of cell pellet recorded before storage at -80°C until further use.

For analysis of the cell pellet, cell paste was thawed and re-suspended in cold lysis buffer (3 mL/g of pellet) (buffer A, Table 7.11). Lysozyme was added (1mg/g of pellet) and Roche protease inhibitor tablets (according to manufacturer's instructions – 1 tablet per 50mL culture) and incubated on ice for 30 minutes. In order to ensure cell walls were sufficiently lysed cells were sonicated for 1 minute (1 sec on/1 sec off). 50µL of cell lysate was taken for SDS-PAGE. Remaining lysate was centrifuged 13,200/8,000 rpm, 10 min, RT/4 °C. Samples of the resulting supernatant and pellet were taken for SDS-PAGE analysis and the soluble protein concentration of the supernatant determined using Bradford Assay (method 10).

Table 7.12 Protein purification buffers

	Buffer A		Buffer B		Buffer C	
	Concentration	Amount	Concentration	Amount	Concentration	Amount
HEPES	25 mM	4.77 g	25 mM	4.77 g	25 mM	4.77 g
NaCl	500 mM	29.22 g	500 mM	29.22 g	500 mM	29.22 g
Glycerol	10 %	100 g	10 %	100 g	10 %	100 g
Imidazole	20 mM	1.36 g	500 mM	34.05 g	-	-
Dithiothreitol	-	-	-	-	5 mM	0.77 g
DI water adjusted to 1L						
pH adjusted to 7.4 for HydG expression and 7.5 for MTAN expression						

Method 10 Bradford Assay

A stock solution of 5mg/mL BSA was prepared in sterile water and used to make up the standard solutions in Table 7.13 below. To measure protein concentration, 20µL of BSA standard or protein sample (diluted in water) were added to 1mL Bradford Reagent in a 1mL cuvette and allowed to react for approximately 5 mins. The absorbance was then measured at 595 nm and standard curve used to calculate the unknown protein concentrations [107].

Table 7.13 BSA Standards

Final concentration (mg/mL)	Stock BSA (µL)	Sterile water (µL)
1	200	800
0.5	100	900
0.25	50	950
0.125	25	975
0.05	10	990
0.025	5	995
0.0125	2.5	997.5

Method 11 15% SDS-PAGE

Typically 4 gels were prepared at once and gels not immediately required stored at 4°C until future use. Resolving gel mix was prepared (Table 7.14) and 5 mL pipetted into each gel mould, 1 mL of isopropanol added to remove bubbles. Left to set at RT for 30-45 mins. Stacking gel prepared (Table 7.14), isopropanol removed and 1 mL of stacking gel pipetted on top of resolving gel. Comb inserted and gel left to set for 30-45 mins. Mould was then removed from holder and comb removed, wells were then rinsed with DI water and stored until required.

Table 7.14 15% SDS-PAGE gel composition for 5x gels

Component	Resolving gel (mL)	Stacking gel
H_2O	5.7	3.4
30% Acrylamide mix	12.5	0.83
1.5 M Tris (pH 8.8)	6.3	0.63
10% SDS	0.25	0.05
10% Ammonium persulfate	0.25	0.05
TEMED	0.01	0.005

Samples for SDS-PAGE analysis were first diluted to approximately 1-2 mg/mL. 20 µL protein sample was mixed with 20 µL 2x SDS-PAGE loading buffer (Table 7.15) and incubated at 95 °C for 5 mins in a thermal cycler. 10 µL of sample was loaded onto the gel (one well should contain a suitable protein ladder) and run for 45 min continuous 200V in 1x SDS-PAGE running buffer (Table 7.15)

Table 7.15 SDS buffer Composition

2x SDS-PAGE Loading Buffer		
Component	Concentration	Amount
400mM Tris-HCl pH 6.8	100 mM	25 mL
Bromophenol Blue	0.2 % (w/v)	0.2 g
SDS	4 % (w/v)	4 g
Glycerol	20 % (w/v)	20 g
DTT*	200 mM	-
DI water final volume 100 mL		
*Add 31 mg DTT to 1 mL buffer before use		
1x SDS-PAGE Running Buffer		
Component	Concentration	Amount
TrisBase	125 mM	15.1 g
Glycine	1.25 M	94 g
10% (w/v) SDS	3.5 mM	5 g
DI water final volume 5L		

Gels were stained using Coomassie Brilliant Blue R250 stain (Tab;e 7.16) in the microwave for approximately 30 secs and left to cool on a rocker for 5 mins. Staining solution was then replaced with de-staining solution (table 7.16) and gel left to de-stain on the rocker overnight before imaging.

Table 7.16 SDS-PAGE Staining solutions

SDS-PAGE staining solution		
Component	Concentration	Amount
Acetic acid	10 % (v/v)	100 mL
Methanol	10 % (v/v)	100 mL
Coomassie Brilliant Blue R250	0.25 % (w/v)	2.5 g
DI water final volume 1 L		
SDS-PAGE destaining solution		
Component	Concentration	Amount
Acetic acid	7.5 % (v/v)	375 mL
Methanol	5 % (v/v)	250 mL
DI water final volume 1 L		

Method 12 Large scale expression in fermenter

5 L of sterilised 2YT media (Table 7.2) was equilibrated in the fermenter unit overnight at 37 °C. The following day the media was supplemented with 500 µL antifoam, the appropriate antibiotic (Table 7.4) and a 1 % inoculum of an overnight culture of BL21 (DE3) cells containing *T.itallicus* or *T.lettingae* 6His-HydG plasmids. Cells were grown at 37 °C with optimal oxygen set to 40 °C (agitation ranged from 50-250 rpm) until the OD_{600nm} reached between 0.6-0.8. The culture was then induced with 20 % (w/v) L (+) arabinose (50 mL/L). The temperature of the media was then reduced to 27 °C and cells left to incubate for 6 hours. Cells were harvested by centrifugation, 8000rpm, 30 min, 4°C and cell pellet stored at -80°C until further use.

Method 13 Anaerobic Protein Purification

Inside an anaerobic glovebox the cell pellet was thawed and re-suspended in buffer A (Table 7.12) (to X g frozen pellet 3X mL Buffer A, 0.1 mg/mL lysozyme and 1 protease

inhibitor tablet per 50 mL of buffer). The cell pellet was left to stir in a cool water bath for 30-45 mins, to ensure complete resuspension. The cells were then sonicated for 4x 10 min at 20W (1 sec on/ 1 sec off). Lysed cells were then harvested by centrifugation for 30 mins, 8000 rpm, 4 °C. Supernatant was then loaded onto a Ni-NTA column (XK50, 50 mL, Ni Sepharose Fast Flow resin) and washed with buffer A until all unbound protein had flowed through (indicated by a return to baseline absorbance at 280 nm). A buffer gradient to 65 % buffer B (Table 7.12) over 75 mL eluted bound protein. The eluted protein was collected in fractions and pooled before concentrating to 30 mL using an Amicon system (30kDa Ultracel® regenerated cellulose membrane). The concentrated protein was then applied to a S-75 buffer exchange column (XK26, 50 mL, pre-equilibrated with buffer C, Table 7.12). The resulting brown fractions were then pooled, 5 mM DTT added and allowed to equilibrate with gentle stirring for 30 mins before the protein concentration was estimated using the Bradford method [107]. The protein was then slowly reconstituted with 10 molar equivalents of $FeCl_3$ (prepared in buffer C), followed by slow addition of 10 molar equivalents of $Na_2S{\cdot}9H_2O$ (prepared in buffer C). The resulting reconstituted protein was then left to incubate overnight with gentle stirring. Iron-sulfide collide was removed by centrifugation, 8000 rpm, 15 mins, 4 °C. The protein was then concentrated to 3-5 mL and applied to the S200 gel filtration column (XK26, 300 mL, equilibrated with buffer C). The golden-brown fractions which elute after the black iron-sulfur aggregates are collected and pooled. The resulting protein solution is equilibrated for 30 mins with 5 mM DTT before the protein concentration is measured by the Bradford method [107]. The protein was then slowly reconstituted with 5 molar equivalents of $FeCl_3$, followed by slow addition of 5 molar equivalents of $Na_2S{\cdot}9H_2O$. The resulting reconstituted protein was then left to incubate for 2 hours or overnight. Iron-sulfide collide was removed by centrifugation, 8000 rpm, 15 mins, 4°C. The final protein solution was concentrated to around 1 mM using an Amicon protein concentrator, 100 µL aliquots prepared and frozen in liquid nitrogen before storage at -80°C for future use.

Method 14 UV-Vis Spectroscopy

UV-Vis spectra of HydG enzymes were recorded inside an anaerobic glovebox using a USB2000 spectrophotometer with a Mini D2-GS light source (Ocean optics software, Netherlands) in a 1 mm or 10 mm quartz cuvette.

7.3.4 Enzyme Activity Assays

Method 15 HydG Activity Assays

Assay mixtures containing variations of HydG 40-50 µM, SAM 1 mM, *ATP 1mM, methionine 1mM, MAT 0.5mg/mL (SAM synthetase)*, tyrosine 4 mM, MTAN 0.025 mg/mL (nucleosidase), $MgCl_2$ 50 mM (as a cofactor for the MTAN enzyme), $Fe(II)SO_4$ 0.5-1 mM, cysteine 0.5-1 mM, imidazole 1 mM and dithionite 1 – 3 mM (for reaction initiation) were prepared in reaction buffer (50mM HEPES, 500mM KCl, pH 7.4).

Due to the high insolubility of tyrosine a 20 mM stock solution was prepared as follows; a 25.71 mM tyrosine solution was prepared in 200 mM HCl. 700 µL of this 25.71 mM stock was added to a 1.5 mL Eppendorf containing 40 µL assay buffer and 160 µL 1 M NaOH, resulting in a 20 mM stock [143].

Except for SAM, all components were weighed out and left to degas in the glovebox overnight, before being resuspended in degassed assay buffer immediately prior to the experiment. SAM was weighed out just before it was required (outside the glovebox), resuspended inside the glovebox in degassed buffer and immediately transferred to a new tube which had been in the glovebox for ≥ 24 hours to reduce the possibility of introducing oxygen to the assay. Frozen aliquots of reconstituted HydG enzyme were defrosted inside the glovebox immediately prior to use.

Two assay stock mixes were prepared (for duplicate assays) and the enzyme mix pipetted into the lid of the reaction tube (80 or 100 µL total reaction volume). The tubes for all time points (200 µL PCR tubes) were simultaneously inverted to mix the enzyme and substrates immediately prior to incubation. Reaction mixes were all incubated outside of the glovebox. When incubated at 37 °C the assays were incubated in a water bath and where the incubation temperature was greater than 37 °C assays were incubated in a PCR thermal cycler. Negative controls were prepared in the absence of enzyme with additional reaction buffer. The reaction was stopped at each time point by the addition of 20 % perchloric acid (6 µL), tubes were briefly shaken and stored at -20°C (a white precipitate formed after addition of acid) prior to RP-HPLC analysis.

Method 16 MTAN Activity Assays

Frozen MTAN enzyme aliquots were defrosted at room temperature before use.

Assay substrates DOA and MTA were weighed out and suspended in assay buffer (50 mM HEPES, 500 mM KCl, 50 mM $MgCl_2$). The assay concentration of *E.coli* MTAN was 0.125 mg/mL throughout and *T.maritima* MTAN concentration varied between 0.125 and 1 mg/mL. The concentration of substrate was 1 mM.

Reactions were prepared in duplicate in 200 µL PCR tubes and enzyme mixes pipetted into the lid of the tube, each experiment also contained duplicate negative samples incubated in the absence enzyme. The reaction volume was 100 µL and reactions were initiated by simultaneous inversion of all tubes (to mix the enzyme).

Reactions were incubated at 37 °C in a water bath and >37 °C in a thermal cycler. Assays were stopped by the addition of 10 µL 20% perchloric acid, gently shaken (until a white precipitate was visible) and stored at -20 °C prior to HPLC analysis.

Method 17 HPLC Analysis

To quantify the products resulting from the enzyme activity assays, RP-HPLC analysis was used. After addition of 20 % perchloric acid to stop the reaction, assays were centrifuged at 13,200 rpm (RT) for 10 mins to remove precipitated protein. Assays that were not to be analysed immediately were stored at -20 °C and defrosted prior to centrifugation. 40 µL of the supernatant was injected into Gemini C18 reverse phase column (110Å, 5µm, 150 x 4.6 mm). DOA, adenine and *p*-cresol production was measured by monitoring changes in $Abs_{280\ nm}$. The following method was used to elute the assay products (0.8 mL/min) :

0 % B	5 min	Isocratic
50 % B	32 min	Buffer gradient
100 % B	1 min	Prepare for wash
100 % B	5 min	Wash
0 % B	1 min	Prepare for re equilibration
0 % B	5 min	Re equilibration

Where buffer A was 0.1 % (v/v) acetic acid in deionised water and buffer B was 0.1 % (v/v) acetic acid in acetonitrile.

To quantify the amount of product produced standards of known concentrations for DOA, adenine, SAM, *p*-cresol, adenine and MTA were prepared and used to calculate a standard curve (examples shown in Figure 7.1).

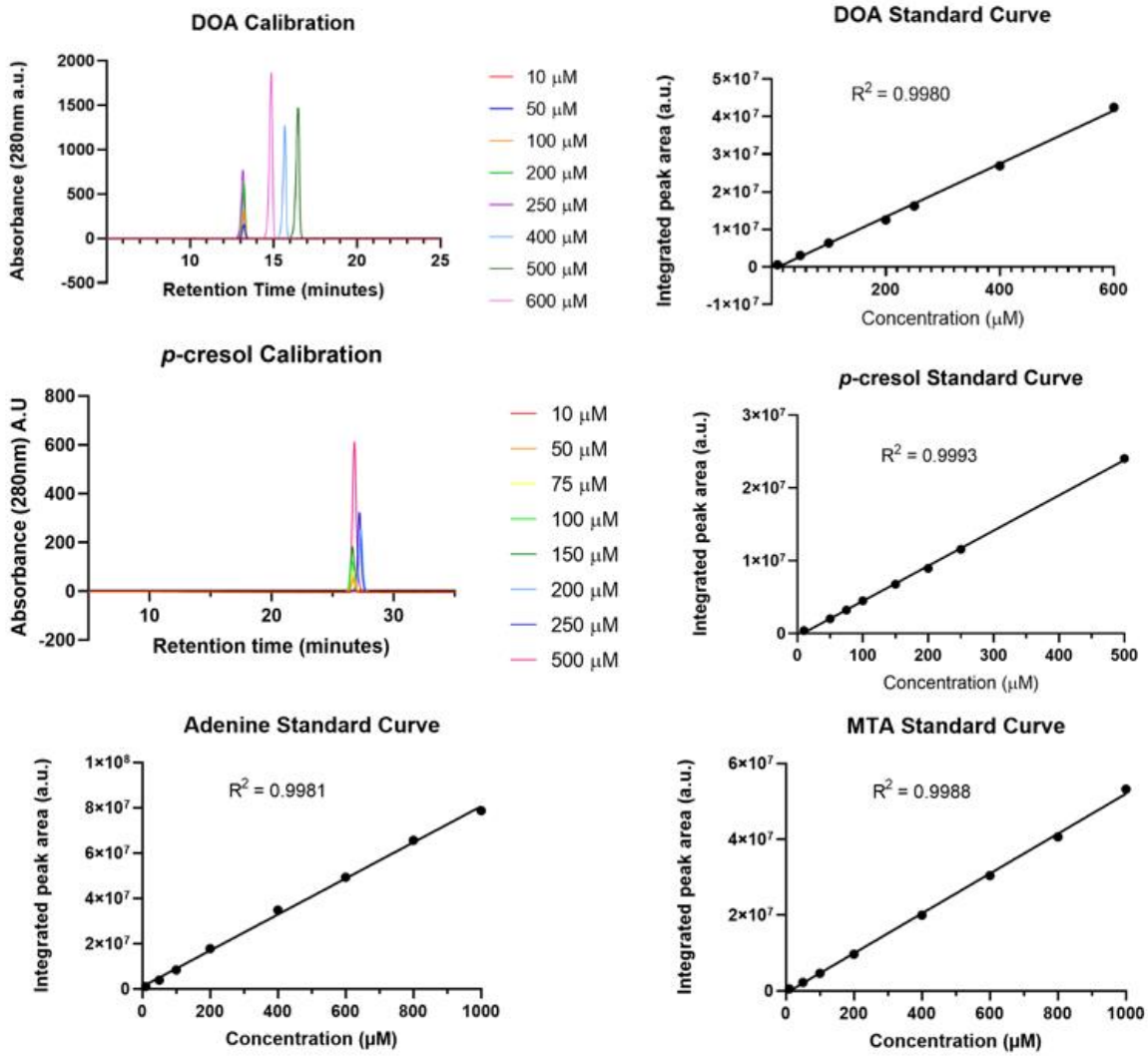

Figure 7.1 HPLC Calibration Standards. DOA, *p*-cresol, adenine, and MTA standards for 0.1 % (v/v) acetic acid HPLC separation method (method 17).

7.3.5 Crystallography

Method 18 Preparation of crystallisation plates

Purified HydG protein aliquots prepared in purification buffer C (25 mM HEPES, 500 mM NaCl, 10 % (w/v) glycerol, 5 mM DTT) concentrated to approximately 850 µM were used for crystallisation experiments. Aliquots were defrosted and centrifuged for 10 mins at 13,200 rpm to pellet any Fe-S colloid prior to transfer to the glovebox. Stock solutions of SAM (80 mM), Fe_2SO_4 (20 mM) and Cys (30 mM) were prepared anaerobically in degassed DI water.

96 and 24-well sitting and hanging drop plates (pre greased) were stored inside the glovebox along with their respective seals for ≥48 hours to degas prior to use. Crystallisation screens were prepared aerobically (5 mL in 15 mL falcon tubes, constituents can be found in Table 5.1) and left to degas inside the glovebox for 72 hours (with the lids removed), and stored in the glovebox with the lids on thereafter. Very little evaporation was observed after 72 hours with the lids removed.

Protein and additive (SAM, Fe, and/or Cys) mixture stocks were prepared inside the glovebox, where the volume was ≥25 µL. For sitting drop 96-well experiments, 102 µL of crystallisation solution was pipetted into the reservoir, 0.5 – 0.6 µL protein pipetted into the three reservoir sub-wells and immediately an equal volume of reservoir solution added to the drop (1:1 mixture). Plates were sealed with transparent film. For 24-well plates, 505 µL of crystallisation solution was pipetted into the well and two 1 µL drops of protein solution pipetted on to a cover slip. 1 µL of reservoir solution was added to each drop (1:1 mixture) and slips were carefully placed over the well and firm pressure applied to ensure a seal. All plates were incubated inside the glovebox at approximately 19 °C.

Plates were viewed under microscope inside the glovebox approximately daily for one week and weekly thereafter.

Appendix A

A.1 Plasmid Maps

Plasmid maps, nucleotide and protein insert sequences

A.1.1 pBAD containing *T.italicus* HydG

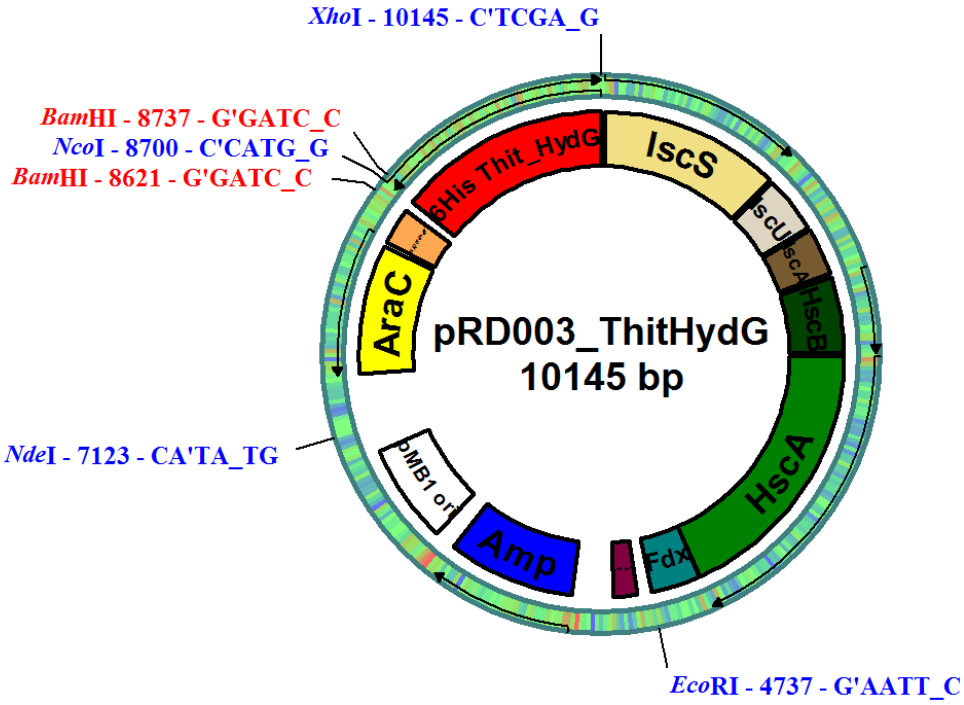

His-tagged *Ti*HydG nucleotide sequence

CATCACCATCATCACCACAGCCAGGATCCGATGGTTAAAGAAAAAGCCGATTTCATCAACGACGAAAAAATTC
GTCAGGATCTGGAAAAAGCCAAAAAAGCAACCAGCAAAGATGCCCTGGAAATTATCGAGAAAGCGAAAAATCT
GAAAGGCATCACACCGGAAGAAGCAGCAGTTCTGCTGAATGTTGAAGATGAAGATCTGCTGAACGAGATGTTT
AAAGTTGCCCGTTATATCAAAGAAGAGATCTACGGTAATCGCATCGTTATTTTTGCACCGCTGTATGTGAGCA
ATTATTGCGTGAATAATTGCCGCTATTGCGGTTATCGTCATAGCAATGAACAGCAGCGTAAAAAACTGACAAT
GGAAGAAGTTCGTCGCGAAGTTGAAATTCTGGAAGAAATGGGTCATAAACGTCTGGCAGTTGAAGCCGGTGAA
GATCCGGTTAATTGTCCGATTGATTATATCGTGGATGTGATCAAAACCATCTACGATACCAAACTGAAAAATG
GTAGCATTCGTCGCGTGAATGTTAATATTGCAGCAACCACCGTGGAAAACTACAAAAAACTGAAAAAAGTGGG
CATCGGCACCTATGTTCTGTTTCAAGAAACCTATCATCGTCCGACCTATGAATATATGCATCCGCAGGGTCCG
AAACACGATTATGATTATCATCTGACCGCAATGGATCGTGCAATGGAAGCAGGTATTGATGATGTTGGTCTGG
GTGTTCTGTATGGTCTGTATGATTACAAATATGAAACCGTGGCCATGCTGTATCATGCAAATCATCTGGAAGA
GAAATTTGGTGTTGGTCCGCATACCATTAGCGTTCCGCGTCTGCGTCCGGCACTGAATATTAGCATTGATAAA
TTTCCGTACATCGTGAGCGATAAAGATTTCAAAAAACTGGTTGCCGTTATTCGTATGGCAGTTCCGTATACCG

GCATGATTCTGAGCACCCGTGAAAAACCTAAATTTCGCGAAGAAGTGATTAGCATCGGTATTAGCCAGATTAG
CGCAGGTAGCTGTACCGGTGTTGGTGGTTATCATGAAGAAATTAGCAAAAAAGGTGGTAGCAAACCGCAGTTT
GAAGTGGAAGATAAACGTAGCCCGAACGAAATTCTGCGTACCCTGTGTGAACAGGGTTATCTGCCGAGCTATT
GTACCGCATGTTATCGTATGGGTCGTACCGGTGATCGTTTTATGAGCTTTGCAAAAAGTGGCCAGATCCATAA
CTTTTGTCTGCCGAATGCAATCCTGACCTTCAAAGAATTTCTGATCGATTATGGTGATGAGAAAACCAAAAAA
ATCGGCGAAAAAGCGATTGCCGTTAACCTGGAAAAAATCCCGAGCCGTACCGTTCGTGAAGAAACCAAACGTC
GTCTGACCCGTATTGAAAATGGTGAACGTGATCTGTACTTTTAA

His-tagged *Tl*HydG protein sequence

HHHHHHSQDPMVKEKADFINDEKIRQDLEKAKKATSKDALEIIEKAKNLKGITPEEAAVLLNVEDEDLLNEMF
KVARYIKEEIYGNRIVIFAPLYVSNYCVNNCRYCGYRHSNEQQRKKLTMEEVRREVEILEEMGHKRLAVEAGE
DPVNCPIDYIVDVIKTIYDTKLKNGSIRRVNVNIAATTVENYKKLKKVGIGTYVLFQETYHRPTYEYMHPQGP
KHDYDYHLTAMDRAMEAGIDDVGLGVLYGLYDYKYETVAMLYHANHLEEKFGVGPHTISVPRLRPALNISIDK
FPYIVSDKDFKKLVAVIRMAVPYTGMILSTREKPKFREEVISIGISQISAGSCTGVGGYHEEISKKGGSKPQF
EVEDKRSPNEILRTLCEQGYLPSYCTACYRMGRTGDRFMSFAKSGQIHNFCLPNAILTFKEFLIDYGDEKTKK
IGEKAIAVNLEKIPSRTVREETKRRLTRIENGERDLYF – STOP

A.1.2 pBAD containing *T.lettingae* HydG

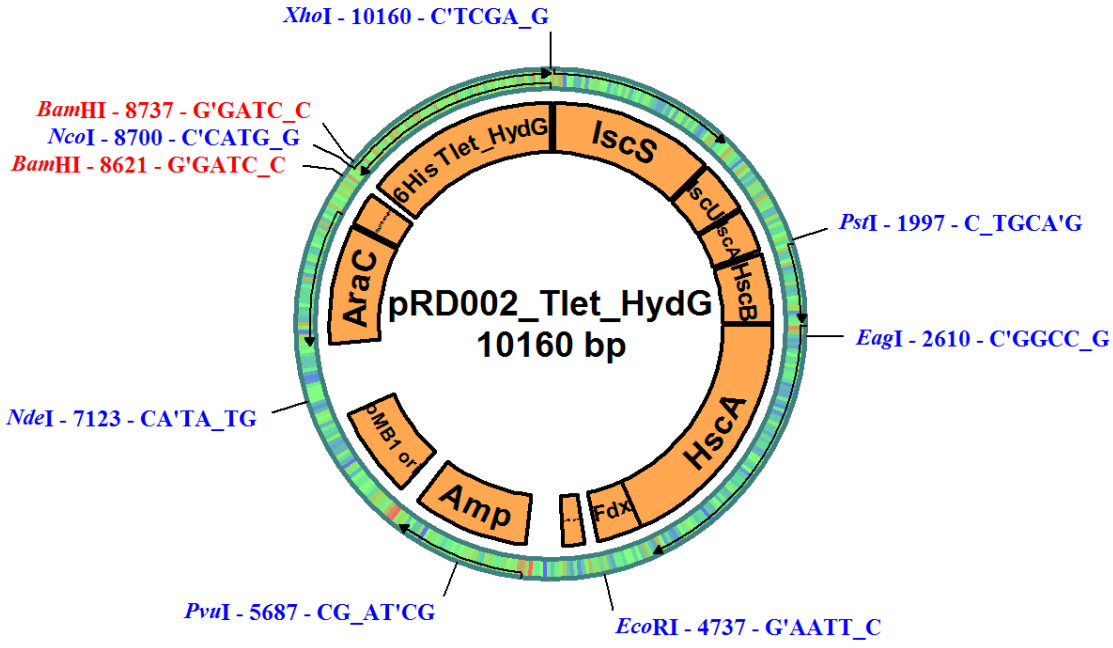

His-tagged *Tl*HydG nucleotide sequence

CATCACCATCATCACCACAGCCAGGATCCGATGTATACCTTTGTGAAAAAAATCCTGGATAGCGAAAGCTTTA
TCCCGCATGAAGAAATTAATCGTCTGCTGAGCCTGACCAAAAACCCGGACAAAAAATACATTGAAGAGATCCT
GGAAAAAAGCCTGAATAAAGAACGTCTGGATCTGAGCGAAACCGCAGCACTGCTGAATGCAGAAAATCCGGAA
CTGGTTGAAATGATTTTTACCGCAGCAAAATCCCTGAAAGAGAAAATTTACGGTAATCGCATTGTTCTGTTTG
CACCGCTGTATATTGGTAACGAATGCATTAACAATTGCAGCTATTGTGGTTTTCGCAGCGAGAATAAACAGGT
GATTCGTAAAACCCTGACCGATGAAGAACTGACCAATGAACTGTTTGCCCTGACCAGCAAAGGTCATAAACGT

CTGATTGTTGTGTTTGGTGAACATCCGGTTTATAGCCCTGAATATATTGCCAAAACCATCGAAAAAATCTATA
GCTATCGCAATGGCAATGGTGAAATTCGTCGTGTTAATGTTAATGCCGCACCGCAGACCGTTGAAGGTTATAA
AACCATTCGTAATGCAGGCATTGGCACCTTTCAGATTTTTCAAGAAACCTATCATCTGCCGACCTACAAAAAA
TACCATAAAGCAGGTCCGAAAAGCAGCTATACCTATCGTCTGTTTGGTCTGGATCGTGCAATGATTGCAGGTA
TTGATGATGTTGGTATTGGTGCACTGTTTGGCCTGTATGATTGGAAATTTGAAGTTATGGGTCTGATGTGTCA
TACCCGTCATCTGGAAGAACGTTTTGGTGTTGGTCCGCATACCATTAGCTTTCCGCGTATTGAACCGGCAGTT
GGTACACCGCTGACAGAAAAACCGCCTTATGCAGTTAGCGATTATGATTTTAAACGCCTGGTTGCCATTATTC
GTCTGAGCGTTCCGTATACCGGTCTGATTCTGACCGCACGTGAAAAAGTTCAGCTGCGTGATGAAGTTATTAA
ACTGGGTGTTAGCCAGATTGATGCAGGTAGCAGCATTGGTGTGGGTAGCTATGCACAGAAAGATCAAGAAATT
GTTCGCAAAAGCCAGTTTATTCTGGGTGATACCCGTACCCTGGATGAAGTGATCAAAGAACTGGCAATGGAAG
GCTATATTCCGAGCTTTTGTACCGCATGTTATCGTGCAGGTCGTACCGGTCAGCATTTTATGGAATTTGCAAT
TCCGGGTTTCGTGAAAGAATTTTGTACCCCGAATGCCCTGCTGACCTTTAAAGAATATCTGATTGATTACGCC
ACCAACGAAACCAAACTGATTGGTGAAAAACTGATCGAAAAAGAACTGCTGAAAATTCCGGATAGCCGTCGTG
AAACCGTGCGCAAAATGCTGGTTAATATTGAAAAAGGTGAACGTGATGTGCGCCTGTAA

His-tagged *Tl*HydG protein sequence

HHHHHHSQDPMYTFVKKILDSESFIPHEEINRLLSLTKNPDKKYIEEILEKSLNKERLDLSETAALLNAENPE
LVEMIFTAAKSLKEKIYGNRIVLFAPLYIGNECINNCSYCGFRSENKQVIRKTLTDEELTNELFALTSKGHKR
LIVVFGEHPVYSPEYIAKTIEKIYSYRNGNGEIRRVNVNAAPQTVEGYKTIRNAGIGTFQIFQETYHLPTYKK
YHKAGPKSSYTYRLFGLDRAMIAGIDDVGIGALFGLYDWKFEVMGLMCHTRHLEERFGVGPHTISFPRIEPAV
GTPLTEKPPYAVSDYDFKRLVAIIRLSVPYTGLILTAREKVQLRDEVIKLGVSQIDAGSSIGVGSYAQKDQEI
VRKSQFILGDTRTLDEVIKELAMEGYIPSFCTACYRAGRTGQHFMEFAIPGFVKEFCTPNALLTFKEYLIDYA
TNETKLIGEKLIEKELLKIPDSRRETVRKMLVNIEKGERDVRL – STOP

A.1.3 pET28a(+) containing *E.coli* MTAN

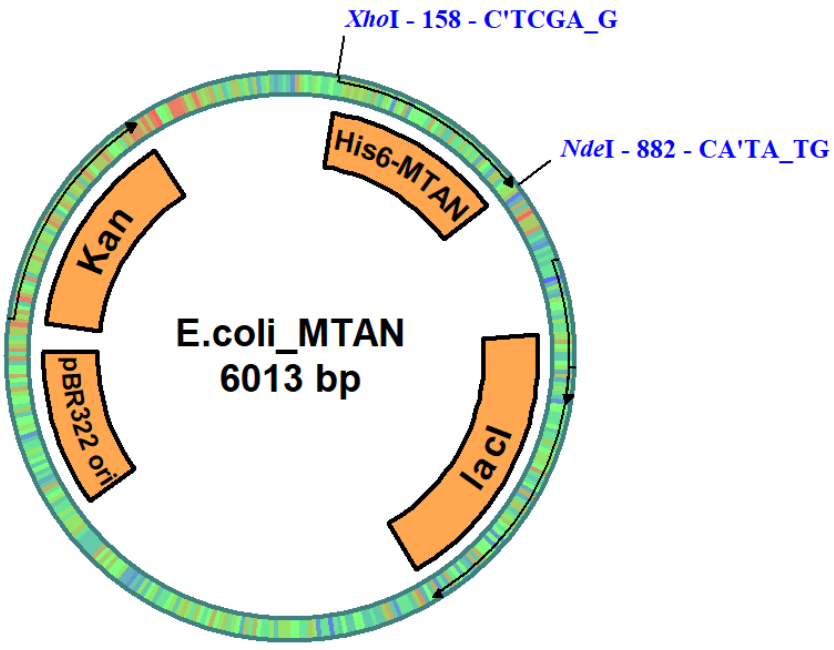

His-tagged *E.coli* MTAN nucleotide sequence

ATGCATCATCACCATCACCATAAAATCGGCATCATTGGTGCAATGGAAGAAGAAGTTACGCTGCTGCGTGACA
AAATCGAAAACCGTCAAACTATCAGTCTCGGCGGTTGCGAAATCTATACCGGCCAACTGAATGGAACCGAGGT
TGCGCTTCTGAAATCGGGCATCGGTAAAGTCGCTGCGGCGCTGGGTGCCACTTTGCTGTTGGAACACTGCAAG
CCAGATGTGATTATTAACACCGGTTCTGCCGGTGGCCTGGCACCAACGTTGAAAGTGGGCGATATCGTTGTCT
CGGACGAAGCACGTTATCACGACGCGGATGTCACGGCATTTGGTTATGAATACGGTCAGTTACCAGGCTGTCC
GGCAGGCTTTAAAGCTGACGATAAACTGATCGCTGCCGCTGAGGCCTGCATTGCCGAACTGAATCTTAACGCT
GTACGTGGCCTGATTGTTAGCGGCGACGCTTTCATCAACGGTTCTGTTGGTCTGGCGAAAATCCGCCACAACT
TCCCACAGGCCATTGCTGTAGAGATGGAAGCGACGGCAATCGCCCATGTCTGCCACAATTTCAACGTCCCGTT
TGTTGTCGTACGCGCCATCTCCGACGTGGCCGATCAACAGTCTCATCTTAGCTTCGATGAGTTCCTGGCTGTT
GCCGCTAAACAGTCCAGCCTGATGGTTGAGTCACTGGTGCAGAAACTTGCACATGGCTAA

His-tagged *E.coli* MTAN protein sequence

MHHHHHHKIGIIGAMEEEVTLLRDKIENRQTISLGGCEIYTGQLNGTEVALLKSGIGKVAAALGATLLLEHCK
PDVIINTGSAGGLAPTLKVGDIVVSDEARYHDADVTAFGYEYGQLPGCPAGFKADDKLIAAAEACIAELNLNA
VRGLIVSGDAFINGSVGLAKIRHNFPQAIAVEMEATAIAHVCHNFNVPFVVVRAISDVADQQSHLSFDEFLAV
AAKQSSLMVESLVQKLAHG - STOP

A.1.4 pET-16b containing *T.maritima* MTAN

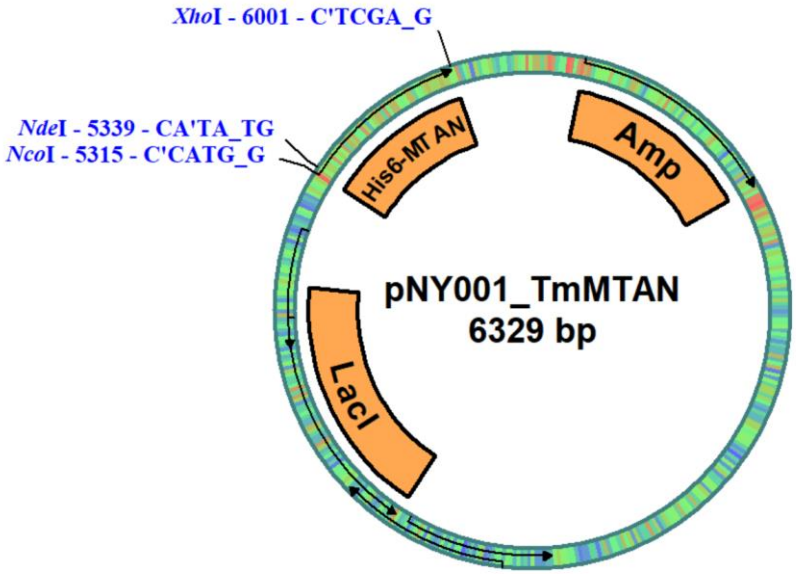

His-tagged *Tmar*MTAN nucleotide sequence

ATGGCCCATCACCATCATCATCATATGAGCGCAATTCTGGTTCTGGGTGTGTTTAAAATCGAAGTTGAACCGA
TGCTGAAAGAAATGGAAGTTCTGGAAAAAGGTCGTCTGCTGAAACGTTATTATCAGCGTGGTGTTGTTGGTCG
TAATGAAGTTGTTGTTAGCTATGGCTTTATCGGTAAAGTTGAAGCAGCACTGGTTACCCAGGCATTTCTGGAT
CGTTTTAACATTGATGCAGTTTTTCTGACCGGTAATGCCGGTGGTCTGGAAGGTGTTGAAGTTGGTGATGTTG

TTATTGGTGATAGCTATGTGGAATACGATTTTGAAACCGCACTGGGTGATGAAGGTATTATTGTTAGCGGTAG
CGAAGATCTGGAAGATAAAGTTATTGCCTATAGCAACCGCGAAATCAAAACCGGTCTGATTGCAAGCGGTGAT
GCATTTGTTACCGTTAAAGAAAAAGCCGAAGAAATCAAACGTCGTACCGGTGCACTGTGTGTTGATATGGATA
GCGCAGCAGTTGCAAAAGTGTGCTATGAAAACGAGAAAAAATTCCTGGCCATCAAAACCATTGTGGATATTTG
TGGTCGTGAAACCGAAGAAGAATTCCGCAAAAACTATGAACGCTATGGTTTTCTGAGCAACCTGATTCTGCTG
GATGTTCTGAAAAAATGCGTGTTTTAA

His-tagged *Tmar*MTAN Protein sequence

MAHHHHHHMSAILVLGVFKIEVEPMLKEMEVLEKGRLLKRYYQRGVVGRNEVVVSYGFIGKVEAALVTQAFLD
RFNIDAVFLTGNAGGLEGVEVGDVVIGDSYVEYDFETALGDEGIIVSGSEDLEDKVIAYSNREIKTGLIASGD
AFVTVKEKAEEIKRRTGALCVDMDSAAVAKVCYENEKKFLAIKTIVDICGRETEEEFRKNYERYGFLSNLILL
DVLKKCVF- STOP

A.1.5 pET151/D-TOPO containing *T.xylanolyticum* MTAN

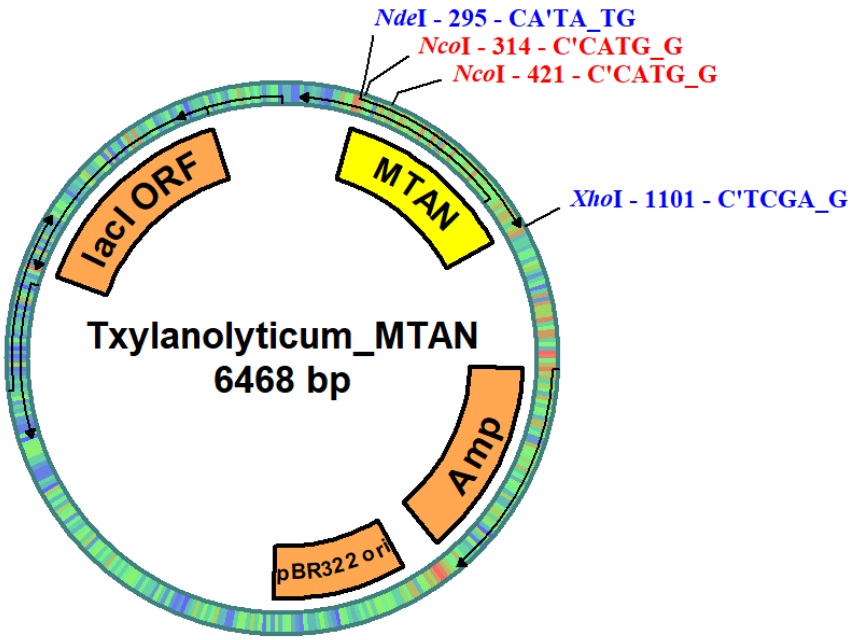

His-tagged *Txy*MTAN nucleotide sequence

ATGCATCATCACCATCACCATGGTAAGCCTATCCCTAACCCTCTCCTCGGTCTCGATTCTACGGAAAACCTGT
ATTTTCAGGGAATTGATCCCTTCACCATGAAAAAGATCGGCTTTATCGGTGCGATGGAAGAAGAAGTTGAACT
GCTGAAAGAAGCCATTGTTAACGAACTGACCATTAATCGTGCAGATATGGATTTTTTCAGCGGCATTATTAAC
GGTGTTGATGCCGTTGTTGTTAAAAGCGGTATTGGTAAAGTTAATGCAGCAATTGCAACCCAGATTCTGATCA
GCGAATTTAAAGTGGATTGCATCATTAATACCGGTGTTGCCGGTGGTCTGAAAAAAGGCATTAATGTTGGTGA
TATCGTGATCAGCAGTGATGCCATTGAACATGATTTTGATACCACCGCATTTGGTGATGAACTGGGTGTTATT
CCGCGTATGAAAACCAGCGTTTTTAAAGCGGATGAGTATCTGATTGATGTGGCATATAAAGCAGCCAACGATA
ATATTGATGGCAAAGCCTATATTGGTCGTATTGTTAGCGGTGACAAATTCATCAGCAGCAAAGATGAAGCACT
GAAACTGGGTCGTCTGTTTAATGCACTGGCAGTTGAAATGGAAGGTGCAGCCATTGCACATACCAGCTATCTG
AATAACATTCCGTTTGTGATTATTCGCAGCATTAGCGATAATGCAGATGGTAATGCAACCAAAGATTTTAGCC

Appendix A

AGTTTGTTAAAGAAGCAGCCATCGTTAGCAGCAACATTGTGAAAGAAATGATCAACCTGATCAAAGAAAATTA
A

His-tagged *Txy*MTAN Protein sequence

MHHHHHHGKPIPNPLLGLDSTENLYFQGIDPFTMKKIGFIGAMEEEVELLKEAIVNELTIN
RADMDFFSGIINGVDAVVVKSGIGKVNAAIATQILISEFKVDCIINTGVAGGLKKGINVGD
IVISSDAIEHDFDTTAFGDELGVIPRMKTSVFKADEYLIDVAYKAANDNIDGKAYIGRIVS
GDKFISSKDEALKLGRLFNALAVEMEGAAIAHTSYLNNIPFVIIRSISDNADGNATKDFSQ
FVKEAAIVSSNIVKEMINLIKEN - Stop

References

1. Knappe, J., E. Bohnert, and W. Brummer, *S-adenosyl-l-methionine, a component of the clastic dissimilation of pyruvate in Escherichia coli.* Biochimica et Biophysica Acta (BBA) - General Subjects, 1965. **107**(3): p. 603-605.

2. Broderick, W.E., B.M. Hoffman, and J.B. Broderick, *Mechanism of Radical Initiation in the Radical S-Adenosyl-l-methionine Superfamily.* Acc Chem Res, 2018. **51**(11): p. 2611-2619.

3. Chirpich, T.P., et al., *Lysine 2,3-aminomutase. Purification and properties of a pyridoxal phosphate and S-adenosylmethionine activated enzyme.* The Journal of Biological Chemistry, 1970. **245**(7): p. 1778-1789.

4. Moss, M. and P.A. Frey, *The role of S-adenosylmethionine in the lysine 2,3-aminomutase reaction.* The Journal of Biological Chemistry, 1987. **262**(31): p. 14859-14862.

5. Moss, M.L. and P.A. Frey, *Activation of lysine 2,3-aminomutase by S-adenosylmethionine.* Journal of Biological Chemistry, 1990. **265**(30): p. 18112-18115.

6. Abeles, R.H. and D. Dolphin, *The Vitamin B_{12} Coenzyme.* Accounts of Chemical Research, 1976. **9**(3): p. 114−120.

7. Petrovich, R.M., et al., *Metal Cofactors of Lysine-2,3-aminomutase.* The Journal of Biological Chemistry, 1991. **266**(12): p. 7656−7660.

8. Cheek, J. and J.B. Broderick, *Adenosylmethionine-dependent iron-sulfur enzymes: versatile clusters in a radical new role.* J Biol Inorg Chem, 2001. **6**(3): p. 209-226.

9. Sofia, H.J., et al., *Radical SAM, a novel protein superfamily linking unresolved steps in familiar biosynthetic pathways with radical mechanisms: functional characterization using new analysis and information visualization methods.* Nucleic acids research, 2001. **29**(5): p. 1097−1106.

10. Buis, J.M. and J.B. Broderick, *Pyruvate formate-lyase activating enzyme: elucidation of a novel mechanism for glycyl radical formation.* Arch Biochem Biophys, 2005. **433**(1): p. 288-96.

11. Frey, P.A., A.D. Hegeman, and F.J. Ruzicka, *The Radical SAM Superfamily.* Crit Rev Biochem Mol Biol, 2008. **43**(1): p. 63-88.

12. Broderick, J.B., et al., *Radical S-adenosylmethionine enzymes.* Chem Rev, 2014. **114**(8): p. 4229-317.

13. Hiscox, M.J., R.C. Driesener, and P.L. Roach, *Enzyme catalyzed formation of radicals from S-adenosylmethionine and inhibition of enzyme activity by the cleavage products.* Biochimica et Biophysica Acta - Proteins and Proteomics, 2012. **1824**(11): p. 1165-1177.

14. Holliday, G.L., et al., *Atlas of the Radical SAM Superfamily: Divergent Evolution of Function Using a "Plug and Play" Domain.* Methods Enzymol, 2018. **606**: p. 1-71.

15. Eisenberg, M.A., *Regulation of the Biotin Operon in E. coli.* Annals of the New York Academy of Sciences, 1985. **447**(1): p. 335-349.

16. Lotierzo, M., et al., *Biotin synthase mechanism: an overview.* Biochemical Society Transactions, 2005. **33**(4): p. 820-823.

17. Miller, J.R., et al., *Escherichia coli LipA Is a Lipoyl Synthase: In Vitro Biosynthesis of Lipoylated Pyruvate Dehydrogenase Complex from Octanoyl-Acyl Carrier Protein.* Biochemistry, 2000. **39**(49): p. 15166-15178.

18. Mahanta, N., et al., *Menaquinone biosynthesis: formation of aminofutalosine requires a unique radical SAM enzyme.* J Am Chem Soc, 2013. **135**(41): p. 15318-21.

19. Kriek, M., et al., *Thiazole synthase from Escherichia coli: an investigation of the substrates and purified proteins required for activity in vitro.* J Biol Chem, 2007. **282**(24): p. 17413-23.

20. Kriek, M., et al., *Thiamine biosynthesis in Escherichia coli: Identification of the intermediate and by-product derived from tyrosine.* Angewandte Chemie - International Edition, 2007. **46**(48): p. 9223-9226.

21. Hänzelmann, P., et al., *Characterization of MOCS1A, an oxygen-sensitive iron-sulfur protein involved in human molybdenum cofactor biosynthesis.* J Biol Chem, 2004. **279**(33): p. 34721-32.

22. Hänzelmann, P. and H. Schindelin, *Crystal structure of the S-adenosylmethionine-dependent enzyme MoaA and its implications for molybdenum cofactor deficiency in humans.* Proceedings of the National Academy of Sciences, 2004. **101**(35): p. 12870-12875.

23. Yan, F., et al., *RlmN and Cfr are Radical SAM Enzymes Involved in Methylation of Ribosomal RNA.* J Am Chem Soc, 2010. **132**(11): p. 3953–3964.

24. Grove, T.L., et al., *A Radically Different Mechanism for S-Adenosylmethionine–Dependent Methyltransferases.* Science, 2011. **332**(6029): p. 604-607.

25. LaMattina, J.W., et al., *NosN, a Radical S-Adenosylmethionine Methylase, Catalyzes Both C1 Transfer and Formation of the Ester Linkage of the Side-Ring System during the Biosynthesis of Nosiheptide.* J Am Chem Soc, 2017. **139**(48): p. 17438-17445.

26. Cheek, J. and J. Broderick, *Direct H Atom Abstraction from Spore Photoproduct C-6 Initiates DNA Repair in the Reaction Catalyzed by Spore Photoproduct Lyase: Evidence for a Reversibly Generated Adenosyl Radical Intermediate.* 2002. **124**(12): p. 2860-2861.

27. Dinis, P., B.M. Wieckowski, and P.L. Roach, *Metallocofactor assembly for [FeFe]-hydrogenases.* Current Opinion in Structural Biology, 2016. **41**: p. 90-97.

28. Nicolet, Y., et al., *X-ray structure of the [FeFe]-hydrogenase maturase HydE from Thermotoga maritima.* Journal of Biological Chemistry, 2008. **283**(27): p. 18861-18872.

29. Berkovitch, F., et al., *Crystal Structure of Biotin Synthase, an S-AdenosylmethionineDependent Radical Enzyme.* Science, 2004. **303**(5654): p. 76-79.

30. Chatterjee, A., et al., *Reconstitution of ThiC in thiamine pyrimidine biosynthesis expands the radical SAM superfamily.* Nat Chem Biol, 2008. **4**(12): p. 758-65.

31. Quitterer, F., et al., *Crystal structure of methylornithine synthase (PylB): insights into the pyrrolysine biosynthesis.* Angew Chem Int Ed Engl, 2012. **51**(6): p. 1339-42.

32. Dinis, P., et al., *X-ray crystallographic and EPR spectroscopic analysis of HydG, a maturase in [FeFe]-hydrogenase H-cluster assembly.* Proceedings of the National Academy of Sciences, 2015. **112**(5): p. 1362-1367.

33. Nicolet, Y., et al., *Crystal structure of HydG from carboxydothermus hydrogenoformans: A trifunctional [FeFe]-Hydrogenase maturase.* ChemBioChem, 2015. **16**(3): p. 397-402.

34. Vey, J.L., et al., *Structural basis for glycyl radical formation by pyruvate formate-lyase activating enzyme.* Proceedings of the National Academy of Sciences, 2008. **105**(42): p. 16137–16141.

35. Grove, T.L., et al., *Structural Insights into Thioether Bond Formation in the Biosynthesis of Sactipeptides.* J Am Chem Soc, 2017. **139**(34): p. 11734-11744.

36. Vey, J.L. and C.L. Drennan, *Structural Insights into Radical Generation by the Radical SAM Superfamily.* Chemical Reviews, 2011. **111**(4): p. 2487-2506.

37. Cosper, N.J., et al., *Direct FeS Cluster Involvement in Generation of a Radical in Lysine 2,3-Aminomutase.* Biochemistry, 2000. **39**(51): p. 15668-15673.

38. Krebs, C., et al., *Coordination of Adenosylmethionine to a Unique Iron Site of the [4Fe-4S] of Pyruvate Formate-Lyase Activating Enzyme: A Mo1ssbauer Spectroscopic Study.* J Am Chem Soc, 2002. **124**(6): p. 912-913.

39. Walsby, C.J., et al., *Electron-Nuclear Double Resonance Spectroscopic Evidence That S-Adenosylmethionine Binds in Contact with the Catalytically Active [4Fe-4S]+ Cluster of Pyruvate Formate-Lyase Activating Enzyme.* J Am Chem Soc, 2002. **124**(12): p. 3143-3151.

40. Walsby, C.J., et al., *An Anchoring Role for FeS Clusters: Chelation of the Amino Acid Moiety of S-Adenosylmethionine to the Unique Iron Site of the [4Fe-4S] Cluster of Pyruvate Formate-Lyase Activating Enzyme.* J Am Chem Soc, 2002. **124**(38): p. 11270-11271.

41. Dowling, D.P., et al., *Structural Diversity in the AdoMet Radical Enzyme Superfamily.* Biochim Biophys Acta, 2012. **1824**(11): p. 1178-1195.

42. Nicolet, Y. and C.L. Drennan, *AdoMet radical proteins--from structure to evolution--alignment of divergent protein sequences reveals strong secondary structure element conservation.* Nucleic Acids Res, 2004. **32**(13): p. 4015-25.

43. Chen, D., et al., *Coordination and Mechanism of Reversible Cleavage of S-Adenosylmethionine by the [4Fe-4S] Center in Lysine 2,3-Aminomutase.* J Am Chem Soc, 2003. **125**(39): p. 11788-11789.

44. Layer, G., et al., *Crystal structure of coproporphyrinogen III oxidase reveals cofactor geometry of Radical SAM enzymes.* The European Molecular Biology Organization Journal, 2003. **22**(23): p. 6214-6224.

45. Nicolet, Y., et al., *Unexpected electron transfer mechanism upon AdoMet cleavage in radical SAM proteins.* Proceedings of the National Academy of Sciences, 2009. **106**(35): p. 14867-14871.

46. Wang, S. and P.A. Frey, *Binding Energy in the One-Electron Reductive Cleavage of S-Adenosylmethionine in Lysine 2,3-Aminomutase, a Radical SAM Enzyme.* Biochemistry, 2007. **46**(45): p. 12889-12895.

47. Walsby, C.J., et al., *Spectroscopic Approaches to Elucidating Novel Iron−Sulfur Chemistry in the "Radical-SAM" Protein Superfamily.* 2005. **44**(4): p. 727-741.

48. Noodleman, L. and D.A. Case, *Density-Functional Theory of Spin Polarization and Spin Coupling in Iron—Sulfur Clusters*. 1992. p. 423-470.

49. Magnusson, O.T., G.H. Reed, and P.A. Frey, *Characterization of an Allylic Analogue of the 5'-Deoxyadenosyl Radical: An Intermediate in the Reaction of Lysine 2,3-Aminomutase.* Biochemistry, 2001. **40**(26): p. 7773-7782.

50. Magnusson, O.T., G.H. Reed, and P.A. Frey, *Spectroscopic Evidence for the Participation of an Allylic Analogue of the 5'-Deoxyadenosyl Radical in the Reaction of Lysine 2,3-Aminomutase.* Journal of the American Chemical Society, 1999. **121**(41): p. 9764-9765.

51. Yang, H., et al., *The Elusive 5'-Deoxyadenosyl Radical: Captured and Characterized by Electron Paramagnetic Resonance and Electron Nuclear Double Resonance Spectroscopies.* J Am Chem Soc, 2019. **141**(30): p. 12139-12146.

52. Horitani, M., et al., *Radical SAM catalysis via an organometallic intermediate with an Fe-[5'-C]-deoxyadenosyl bond.* Science, 2016. **352**(6287): p. 822-825.

53. Brown, K.L., *Chemistry and Enzymology of Vitamin B_{12}.* Chem Rev, 2005. **105**(6): p. 2075–2150.

54. Impano, S., et al., *Active-Site Controlled, Jahn-Teller Enabled Regioselectivity in Reductive S-C Bond Cleavage of S-Adenosylmethionine in Radical SAM Enzymes.* J Am Chem Soc, 2021. **143**(1): p. 335-348.

55. Vignais, P.M., B. Billoud, and J. Meyer, *Classification and phylogeny of hydrogenases.* FEMS Microbiology Reviews, 2001. **25**(4): p. 455-501.

56. Lubitz, W., et al., *Hydrogenases.* Chemical Reviews, 2014. **114**(8): p. 4081-4148.

57. Vogt, S., et al., *The exchange activities of [Fe] hydrogenase (iron-sulfur-cluster-free hydrogenase) from methanogenic archaea in comparison with the exchange activities of [FeFe] and [NiFe] hydrogenases.* Journal of Biological Inorganic Chemistry, 2008. **13**(1): p. 97-106.

58. Peters, J.W., et al., *[FeFe]- and [NiFe]-hydrogenase diversity, mechanism, and maturation.* Biochimica et Biophysica Acta - Molecular Cell Research, 2015. **1853**(6): p. 1350-1369.

59. Shafaat, H.S., et al., *[NiFe] hydrogenases: A common active site for hydrogen metabolism under diverse conditions.* Biochimica et Biophysica Acta - Bioenergetics, 2013. **1827**(8-9): p. 986-1002.

60. Britt, R.D., G. Rao, and L. Tao, *Bioassembly of complex iron–sulfur enzymes: hydrogenases and nitrogenases.* Nat Rev Chem, 2020. **4**(10): p. 542-549.

61. Britt, R.D., G. Rao, and L. Tao, *Biosynthesis of the catalytic H-cluster of [FeFe] hydrogenase: the roles of the Fe-S maturase proteins HydE, HydF, and HydG.* Chem Sci, 2020. **11**(38): p. 10313-10323.

62. Land, H., et al., *Current State of [FeFe]-Hydrogenase Research: Biodiversity and Spectroscopic Investigations.* ACS Catalysis, 2020. **10**(13): p. 7069-7086.

63. Höök, M. and X. Tang, *Depletion of fossil fuels and anthropogenic climate change—A review.* Energy Policy, 2013. **52**: p. 797-809.

64. Kalnay, E., et al., *The NCEP/NCAR 40-Year Reanalysis Project.* Bulletin of the American Meterological Society, 1996. **77**(3): p. 437-472.

65. Burton, N.A., et al., *Increasing the efficiency of hydrogen production from solar powered water electrolysis.* Renewable and Sustainable Energy Reviews, 2021. **135**.

66. Madden, C., et al., *Catalytic turnover of [FeFe]-hydrogenase based on single-molecule imaging.* J Am Chem Soc, 2012. **134**(3): p. 1577-82.

67. Pandey, K., et al., *Frequency and potential dependence of reversible electrocatalytic hydrogen interconversion by [FeFe]-hydrogenases.* Proc Natl Acad Sci U S A, 2017. **114**(15): p. 3843-3848.

68. Mersch, D., et al., *Wiring of Photosystem II to Hydrogenase for Photoelectrochemical Water Splitting.* J Am Chem Soc, 2015. **137**(26): p. 8541-9.

69. Kanygin, A., et al., *Rewiring photosynthesis: a photosystem I-hydrogenase chimera that makes H2in vivo.* Energy & Environmental Science, 2020. **13**(9): p. 2903-2914.

70. Appel, J., et al., *Cyanobacterial in vivo solar hydrogen production using a photosystem I–hydrogenase (PsaD-HoxYH) fusion complex.* Nature Energy, 2020. **5**(6): p. 458-467.

71. Mulder, D.W., et al., *Stepwise FeFe-hydrogenase H-cluster assembly revealed in the structure of HydA ΔeFG.* Nature, 2010. **465**(7295): p. 248-251.

72. Mulder, D.W., et al., *Insights into [FeFe]-hydrogenase structure, mechanism, and maturation.* Structure, 2011. **19**(8): p. 1038-52.

73. Shepard, E.M., et al., *Biosynthesis of complex iron-sulfur enzymes.* Curr Opin Chem Biol, 2011. **15**(2): p. 319-27.

74. Bortolus, M., et al., *Overview of the Maturation Machinery of the H-Cluster of [FeFe]-Hydrogenases with a Focus on HydF.* International Journal of Molecular Sciences, 2018.

75. King, P.W., et al., *Functional studies of [FeFe] hydrogenase maturation in an Escherichia coli biosynthetic system.* Journal of bacteriology, 2006. **188**(6): p. 2163-72.

76. Voordouw, G., et al., *Purification and characterization of Desulfovibrio vulgaris (Hildenborough) hydrogenase expressed in Escherichia coli.* European Journal of Biochemistry, 1987. **162**(1): p. 31-36.

77. Kuchenreuther, J., et al., *The HydG Enzyme Generates an Fe(CO)2(CN) Synthon in Assembly of the FeFe Hydrogenase H-Cluster.* Science, 2014. **343**(6169): p. 424-427.

78. Rubach, J.K., et al., *Biochemical characterization of the HydE and HydG iron-only hydrogenase maturation enzymes from Thermatoga maritima.* FEBS Letters, 2005. **579**(22): p. 5055-5060.

79. McGlynn, S.E., et al., *HydF as a scaffold protein in [FeFe] hydrogenase H-cluster biosynthesis.* FEBS Letters, 2008. **582**(15): p. 2183-2187.

80. Tao, L., et al., *Radical SAM Enzyme HydE Generates Adenosylated Fe(I) Intermediates En Route to the [FeFe]-Hydrogenase Catalytic H-Cluster.* J Am Chem Soc, 2020. **142**(24): p. 10841-10848.

81. Rohac, R., et al., *Crystal Structure of the [FeFe]-Hydrogenase Maturase HydE Bound to Complex-B.* J Am Chem Soc, 2021. **143**(22): p. 8499-8508.

82. Cendron, L., et al., *Crystal structure of HydF scaffold protein provides insights into [FeFe]-hydrogenase maturation.* Journal of Biological Chemistry, 2011. **286**(51): p. 43944-43950.

83. Kuchenreuther, J.M., R.D. Britt, and J.R. Swartz, *New insights into [FeFe] hydrogenase activation and maturase function.* PLoS One, 2012. **7**(9): p. e45850.

84. Britt, R.D. and T.B. Rauchfuss, *Biosynthesis of the [FeFe] hydrogenase H-cluster via a synthetic [Fe(II)(CN)(CO)2(cysteinate)](-) complex.* Dalton Trans, 2021. **50**(36): p. 12386-12391.

85. Rao, G., et al., *The binuclear cluster of [FeFe] hydrogenase is formed with sulfur donated by cysteine of an [Fe(Cys)(CO)2(CN)] organometallic precursor.* Proc Natl Acad Sci U S A, 2019. **116**(42): p. 20850-20855.

86. Rao, G., L. Tao, and R.D. Britt, *Serine is the molecular source of the NH(CH2)2 bridgehead moiety of the in vitro assembled [FeFe] hydrogenase H-cluster.* Chem Sci, 2019. **11**(5): p. 1241-1247.

87. Driesener, R.C., et al., *[FeFe]-hydrogenase cyanide ligands derived from S-adenosylmethionine-dependent cleavage of tyrosine.* Angew Chem Int Ed Engl, 2010. **49**(9): p. 1687-90.

88. Kuchenreuther, J.M.W.S.T.G.S.N.Y.S.J. and R. Britt, *A Radical Intermediate in Tyrosine Scission to the CO and CN- Ligands of FeFe Hydrogenase.* Science, 2013. **342**(6157): p. 472-475.

89. Chen, N., et al., *Quantum Chemical Study of a Radical Relay Mechanism for the HydG-Catalyzed Synthesis of a Fe(II)(CO)2(CN)cysteine Precursor to the H-Cluster of [FeFe] Hydrogenase.* Biochemistry, 2021. **60**(40): p. 3016-3026.

90. Pilet, E., et al., *The role of the maturase HydG in [FeFe]-hydrogenase active site synthesis and assembly.* FEBS Letters, 2009. **583**(3): p. 506-511.

91. Shepard, E.M., et al., *[FeFe]-hydrogenase maturation: HydG-catalyzed synthesis of carbon monoxide.* Journal of the American Chemical Society, 2010. **132**(27): p. 9247-9249.

92. Lanz, N.D. and S.J. Booker, *Identification and function of auxiliary iron-sulfur clusters in radical SAM enzymes.* Biochim Biophys Acta, 2012. **1824**(11): p. 1196-212.

93. Driesener, R.C., et al., *Biochemical and kinetic characterization of radical S -Adenosyl- L - Methionine enzyme HydG.* Biochemistry, 2013. **52**(48): p. 8696-8707.

94. Nicolet, Y., et al., *A glycyl free radical as the precursor in the synthesis of carbon monoxide and cyanide by the [FeFe]-hydrogenase maturase HydG.* FEBS Letters, 2010. **584**(19): p. 4197-4202.

95. Driesener, R.C., *Mechanistic and structural characterisation of HydG catalysed L-tyrosine cleavage.* PhD Thesis, 2014. **University of Southampton**.

96. Nicolet, Y., et al., *Crystal structure of tryptophan lyase (NosL): Evidence for radical formation at the amino group of tryptophan.* Angewandte Chemie - International Edition, 2014. **53**(44): p. 11840-11844.

97. Britt, R.D., et al., *Proposed Mechanism for the Biosynthesis of the [FeFe] Hydrogenase H-Cluster: Central Roles for the Radical SAM Enzymes HydG and HydE.* ACS Bio & Med Chem Au, 2021.

98. Suess, D.L.M., et al., *The Radical SAM Enzyme HydG Requires Cysteine and a Dangler Iron for Generating an Organometallic Precursor to the [FeFe]-Hydrogenase H-Cluster.* Journal of the American Chemical Society, 2016. **138**(4): p. 1146-1149.

99. Rao, G., et al., *A [4Fe-4S]-Fe(CO)(CN)-l-cysteine intermediate is the first organometallic precursor in [FeFe] hydrogenase H-cluster bioassembly.* Nature Chemistry, 2018. **10**(5): p. 555-560.

100. Broderick, W.E. and J.B. Broderick, *Radical SAM enzymes: surprises along the path to understanding mechanism.* J Biol Inorg Chem, 2019. **24**(6): p. 769-776.

101. Hannig, G. and S.C. Makrides, *Strategies for optimizing heterologous protein expression in Escherichia coli.* Trends in Biotechnology, 1998. **16**(2): p. 54-60.

102. Martins, F., *Studies on Thiamine Biosynthesis.* PhD Thesis, 2009. **University of Southampton**.

103. Johnson, D.C., et al., *Structure, Function, and Formation of Biological Iron-Sulfur Clusters.* Annual Review of Biochemistry, 2005. **74**(1): p. 247-281.

104. Fontecave, M. and S. Ollagnier-de-Choudens, *Iron-sulfur cluster biosynthesis in bacteria: Mechanisms of cluster assembly and transfer.* Archives of Biochemistry and Biophysics, 2008. **474**(2): p. 226-237.

105. Lill, R., *Function and biogenesis of iron-sulphur proteins.* Nature, 2009. **460**(7257): p. 831-838.

106. Dinis, P., *Structural analysis of proteins from the radical SAM superfamily.* PhD Thesis, 2015. **University of Southampton**.

107. Bradford, M., *A rapid and sensitive method for the quantitation of microgram quantities of protein utilizing the principle of protein-dye binding.* Analytical Biochemistry, 1976. **72**(1-2): p. 248-254.

108. Natalia B. Ugulava, Brian R. Gibney, and J.T. Jarrett, *Biotin Synthase Contains Two Distinct Iron-Sulfur Cluster Binding Sites: Chemical and Spectroelectrochemical Analysis of IronSulfur Cluster Interconversions.* Biochemistry, 2001. **40**(28): p. 8343-8351.

109. Kriek, M., et al., *Effect of iron–sulfur cluster assembly proteins on the expression of Escherichia coli lipoic acid synthase.* Protein Expression and Purification, 2003. **28**(2): p. 241-245.

110. Blanc, B., C. Gerez, and S. Ollagnier de Choudens, *Assembly of Fe/S proteins in bacterial systems: Biochemistry of the bacterial ISC system.* Biochim Biophys Acta, 2015. **1853**(6): p. 1436-47.

111. Sweeney, W.V. and J.C. Rabinowitz, *Proteins Containing 4Fe-4S Clusters: An Overview.* Annual Review of Biochemistry, 1980. **49**(1): p. 139-161.

112. Dailey., H.A., M.G. Finnegan., and M.K. Johnson., *Human Ferrochelatase Is an Iron-Sulfur Protein.* Biochemistry, 1994. **33**(2): p. 403-407.

113. Mishra, V. and D.R. Ronning, *Crystal structures of the Helicobacter pylori MTAN enzyme reveal specific interactions between S-adenosylhomocysteine and the 5'-alkylthio binding subsite.* Biochemistry, 2012. **51**(48): p. 9763-9772.

114. Choi-Rhee, E. and J.E. Cronan, *A nucleosidase required for in vivo function of the S-adenosyl-L-methionine radical enzyme, biotin synthase.* Chem Biol, 2005. **12**(5): p. 589-93.

115. North, J.A., et al., *A bifunctional salvage pathway for two distinct S-adenosylmethionine by-products that is widespread in bacteria, including pathogenic Escherichia coli.* Mol Microbiol, 2020. **113**(5): p. 923-937.

116. Challand, M.R., F.T. Martins, and P.L. Roach, *Catalytic Activity of the Anaerobic Tyrosine Lyase Required for Thiamine Biosynthesis in Escherichia coli.* Journal of Biological Chemistry, 2010. **285**(8): p. 5240-5248.

117. Cornell, K.A. and M.K. Riscoe, *Cloning and expression of Escherichia coli 5'-methylthioadenosine/S-adenosylhomocysteine nucleosidase: Identification of the pfs gene product.* Biochimica et Biophysica Acta (BBA) - Gene Structure and Expression, 1998. **1396**(1): p. 8-14.

118. Sundberg, R.J. and R.B. Martin, *Interactions of histidine and other imidazole derivatives with transition metal ions in chemical and biological systems.* Chemical Reviews, 1974. **74**(4): p. 471-517.

119. Bridwell-Rabb, J., et al., *A B12-dependent radical SAM enzyme involved in oxetanocin A biosynthesis.* Nature, 2017. **544**(7650): p. 322-326.

120. Challand, M.R., et al., *Product inhibition in the radical S-adenosylmethionine family.* FEBS Lett, 2009. **583**(8): p. 1358-62.

121. Parveen, N. and K.A. Cornell, *Methylthioadenosine/S-adenosylhomocysteine nucleosidase, a critical enzyme for bacterial metabolism.* Mol Microbiol, 2011. **79**(1): p. 7-20.

122. G. Kozianowski, et al., *Purification and characterization of thermostable pectate-lyases from a newly isolated thermophilic bacterium, Thermoanaerobacter italicus sp. nov. .* Extremophiles, 1997. **1**(4): p. 171-182.

123. Vaughn S. Cooper, Albert F. Bennett, and R.E. Lenski, *Evolution of thermal dependence of growth rate of Escherichia coli populations during 20,000 generations in a constant environment.* Evolution, 2001. **55**(5): p. 889-896.

124. Fotadar, U., P. Zaveloff, and L. Terracio, *Growth of Escherichia coli at elevated temperatures.* J Basic Microbiol, 2005. **45**(5): p. 403-404.

125. David F. Iwig and S.J. Booker, *Insight into the Polar Reactivity of the Onium Chalcogen Analogues of S-Adenosyl-l-methionine.* Biochemistry, 2004. **43**(42): p. 13496-13509.

126. Alexander P. Golovanov, G.M.H., Stuart A. Wilson, and Lu-Yun Lian, *A Simple Method for Improving Protein Solubility and Long-Term Stability.* Journal of the American Chemical Society, 2004. **29**(126): p. 8933–8939.

127. Baneyx, F., *Recombinant protein expression in Escherichia coli.* Current Opinion in Biotechnology, 1999. **10**(5): p. 411-421.

128. Della Ragione, F., Porcelli, M., Cartenì-Farina, M., Zappia, V. and Pegg, A.,, *Escherichia coli S-adenosylhomocysteine/5'-methylthioadenosine nucleosidase. Purification, substrate specificity and mechanism of action.* Biochemical Journal, 1985. **232**(2): p. 335-341.

129. Lee, J.E., et al., *Structure of Escherichia coli 5'-methylthioadenosine/ S-adenosylhomocysteine nucleosidase inhibitor complexes provide insight into the conformational changes required for substrate binding and catalysis.* J Biol Chem, 2003. **278**(10): p. 8761-70.

130. Lee, Y., Jain, M., Lee, C. and Zeikus, J., *Taxonomic Distinction of Saccharolytic Thermophilic Anaerobes: Description of Thermoanaerobacterium xylanolyticum gen. nov., sp. nov., and Thermoanaerobacterium saccharolyticum gen. nov., sp. nov.; Reclassification of Thermoanaerobium brockii, Clostridium thermosulfurogenes, and Clostridium thermohydrosulfuricum E100-69 as Thermoanaerobacter brockii comb. nov., Thermoanaerobacterium thermosulfurigenes comb. nov., and Thermoanaerobacter thermohydrosulfuricus comb. nov., Respectively; and Transfer of Clostridium thermohydrosulfuricum 39E to Thermoanaerobacter ethanolicus.* International Journal of Systematic Bacteriology 1993. **43**(1): p. 41-51.

131. Ducruix, A. and R. Giegé, *Crystallization of Nucleic Acids and Proteins: A Practical Approach*. Second ed. 1999, Oxford University Press.

132. Kam, Z., H.B. Shore, and G. Feher, *On the Crystallization of Proteins.* Journal of Molecular Biology, 1978. **123**(4): p. 539-555.

133. McPherson, A. and J.A. Gavira, *Introduction to protein crystallization.* Acta Crystallogr F Struct Biol Commun, 2014. **70**(Pt 1): p. 2-20.

134. McPherson, A., *Protein Crystallization.* Methods Mol Biol, 2017. **1607**: p. 17-50.

135. Rhodes, G., *Crystallography Made Crystal Clear - A Guide for Users of Macromolecular Models*. 1993, San Diego, Calif.: Academic Press.

136. Haas, C. and J. Drenth, *Understanding protein crystallization on the basis of the phase diagram.* Journal of Crystal Growth, 1999. **196**(2-4): p. 388-394.

137. Chayen, N.E., *Comparative Studies of Protein Crystallization by Vapour-Diffusion and Microbatch Techniques.* Acta Crystallographica Section D Biological Crystallography, 1998. **54**(1): p. 8-15.

138. Suess, D.L.M., et al., *Cysteine as a ligand platform in the biosynthesis of the FeFe hydrogenase H cluster.* Proceedings of the National Academy of Sciences, 2015. **112**(37): p. 11455-11460.

139. Dessau, M.A. and Y. Modis, *Protein crystallization for X-ray crystallography.* J Vis Exp, 2011(47).

140. Logan, S.R., *The Origin and Status of the Arrhenius Equation.* Journal of Chemical Education, 1982. **59**(4): p. 279-281.

141. Arrhenius, S., *Über die Reaktionsgeschwindigkeit bei der Inversion von Rohrzucker durch Säuren.* Zeitschrift für Physikalische Chemie, 1889. **4U**(1): p. 226-248.

142. Muller, I., *Guidelines for the successful generation of protein-ligand complex crystals.* Acta Crystallogr D Struct Biol, 2017. **73**(Pt 2): p. 79-92.

143. Monfort, B.M., *Interaction studies between the [FeFe] -hydrogenase maturation enzymes from Thermoanaerobacter italicus.* PhD Thesis, 2018. **University of Southampton**.